AD-A125 242 THERMO-MECHANICAL AND THERMAL BEHAVIOR OF HIGH-TEMPERATURE STRUCTURAL MAT.. (U) VIRGINIA POLYTECHNIC INST AND STATE UNIV BLACKSBURG COLL OF E.. 1/3

UNCLASSIFIED D P HASSELMAN ET AL. 31 DEC 82 F/G 11/2 NL

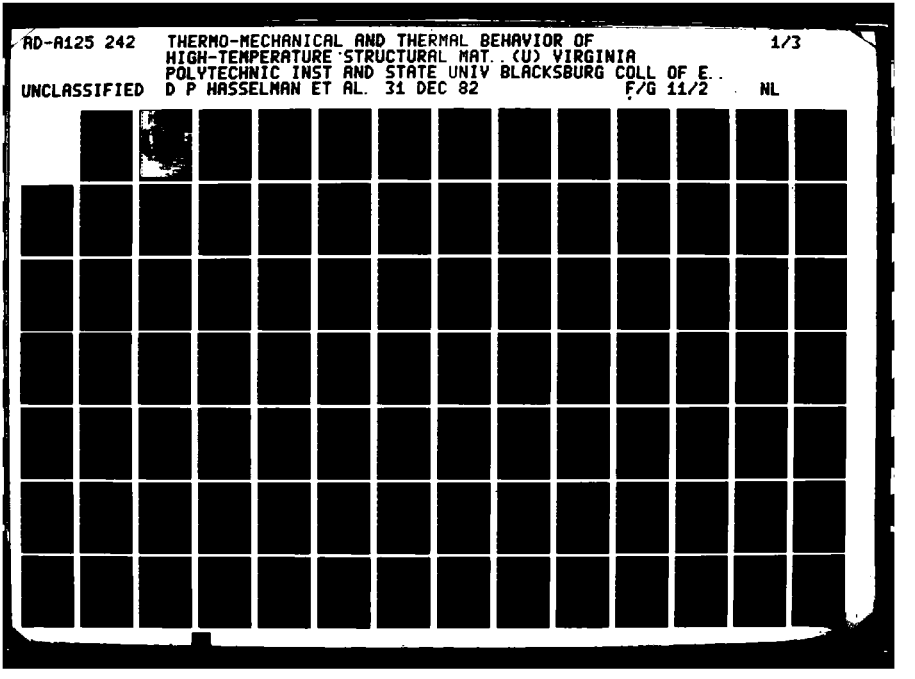

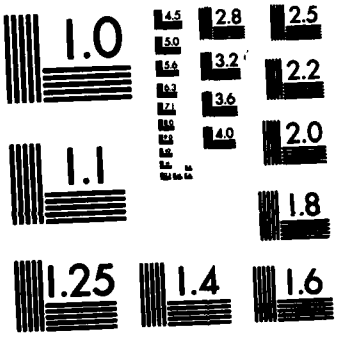

COLLEGE OF ENGINEERING

THERMO-MECHANICAL AND THERMAL

BEHAVIOR OF HIGH-TEMPERATURE STRUCTURAL MATERIALS

Interim Report to
Office of Naval Research
NR 032588
Contract No.: N00014-78-C-0431

January 1, 1982 - December 31, 1982

by

J. P. H. Hasselman
Virginia Polytechnic Institute and State University
Blacksburg, Virginia 24061

VIRGINIA POLYTECHNIC INSTITUTE AND STATE UNIVERSITY

BLACKSBURG VIRGINIA

(12)

THERMO-MECHANICAL AND THERMAL

BEHAVIOR OF HIGH-TEMPERATURE STRUCTURAL MATERIALS

Interim Report to
Office of Naval Research
NR 032588
Contract No.: N00014-78-C-0431

January 1, 1982 - December 31, 1982

by

D. P. H. Hasselman
Virginia Polytechnic Institute and State University
Blacksburg, Virginia 24061

and

M. M. Abraham, G. R. Angell, L. D. Bentsen, M. A. Bucknam
W. Chang, Y. Chen, J. I. Frankel, C. E. Knight, J. Makosey
R. G. Mitchiner, R. Ruh, J. P. Sing, J. R. Thomas, Jr.

unclassified

SECURITY CLASSIFICATION OF THIS PAGE (When Data Entered)

REPORT DOCUMENTATION PAGE		READ INSTRUCTIONS BEFORE COMPLETING FORM
1. REPORT NUMBER	2. GOVT ACCESSION NO. A125242	3. RECIPIENT'S CATALOG NUMBER
4. TITLE (and Subtitle) Thermo-Mechanical and Thermal Behavior of High-Temperature Structural Materials		5. TYPE OF REPORT & PERIOD COVERED Interim Report Jan. 1, 1982 - Dec. 31, 1982
		6. PERFORMING ORG. REPORT NUMBER
7. AUTHOR(s) D. P. H. Hasselman		8. CONTRACT OR GRANT NUMBER(s) N00014-78-C-0431
9. PERFORMING ORGANIZATION NAME AND ADDRESS Virginia Polytechnic Institute and State University, Blacksburg, Virginia 24061		10. PROGRAM ELEMENT, PROJECT, TASK AREA & WORK UNIT NUMBERS
11. CONTROLLING OFFICE NAME AND ADDRESS Office of Naval Research, Code 471 Arlington, VA 22217		12. REPORT DATE Dec. 31, 1982
		13. NUMBER OF PAGES
14. MONITORING AGENCY NAME & ADDRESS(if different from Controlling Office)		15. SECURITY CLASS. (of this report) unclassified
		15a. DECLASSIFICATION/DOWNGRADING SCHEDULE
16. DISTRIBUTION STATEMENT (of this Report) ~~See distribution list. Do not release to NTIS~~ This document has been approved for public release and sale; its distribution is unlimited.		
17. DISTRIBUTION STATEMENT (of the abstract entered in Block 20, if different from Report)		
18. SUPPLEMENTARY NOTES		
19. KEY WORDS (Continue on reverse side if necessary and identify by block number) Thermal shock, thermal stress, thermal diffusivity, thermal conductivity; refractories, composites, radiation heat transfer, cyclic heating, optical thickness, crack stability		
20. ABSTRACT (Continue on reverse side if necessary and identify by block number) This report contains preprints of studies completed during the reporting period on the thermo-mechanical and thermal behavior of high-temperature structural materials, as follows:		

DD FORM 1 JAN 73 1473 EDITION OF 1 NOV 65 IS OBSOLETE S/N 0102-LF-014-6601

unclassified

SECURITY CLASSIFICATION OF THIS PAGE (When Data Entered)

Technical Articles

I Y. Chen, M. M. Abraham, L. D. Bentsen and D. P. H. Hasselman, "Effect of Ni-Alloying on the Thermal Diffusivity/Conductivity of MgO Single Crystals."

II L. D. Bentsen, D. P. H. Hasselman and R. Ruh, "Effect of Hot-Pressing Temperature on the Thermal Diffusivity/Conductivity of SiC-AlN Composites."

III M. A. Bucknam, L. D. Bentsen and D. P. H. Hasselman, "The Measurement of the Thermal Conductivity of Refractories by the Laser-Flash Method."

IV J. R. Thomas, J. I. Frankel and D. P. H. Hasselman, "Effect of Interface Reflections and Angle of Incidence of Radiation on Thermal Stresses in Semi-Transparent Materials."

V J. P. Singh, J. R. Thomas, Jr., and D. P. H. Hasselman, "Role of Absorption Coefficient in the Frequency Dependence of the Thermal Stresses in a Partially-Absorbing Plate Subjected to Cyclic Thermal Radiation."

VI J. P. Singh, J. I. Frankel, J. R. Thomas, Jr., and D. P. H. Hasselman, "Thermal Stresses in Partially Absorbing Flat Plate Due to Sudden Interruption of Steady-State Asymmetric Radiation, I: Convective Cooling at Rear Surface."

VII J. I. Frankel, J. P. Singh, J. R. Thomas, Jr., and D. P. H. Hasselman, "Thermal Stresses in Partially Absorbing Flat Plate Due to Sudden Interruption of Steady-State Asymmetric Radiation, II: Convective Cooling at Front Surface."

VIII J. P. Singh, J. R. Thomas, Jr., and D. P. H. Hasselman, "Thermal Stresses in a Partially Absorbing Flat Plate Asymmetrically Heated by Cyclic Thermal Radiation and Cooled by Convection: Addendum."

IX W. Chang, C. E. Knight, D. P. H. Hasselman, and R. G. Mitchiner, "Analysis of Thermal Stress Failure of Segmented Refractory Structures."

Review Article

X D. P. H. Hasselman and L. D. Bentsen, "Effect of Microstructural and Compositional Heterogeneity on the Conduction of Heat in Structural Materials for High-Temperature Use."

THERMO-MECHANICAL AND THERMAL BEHAVIOR OF HIGH-TEMPERATURE STRUCTURAL MATERIALS

PREFACE

Technical ceramics because of their chemical inertness, high melting point, good wear resistance, excellent mechanical stability at high temperature and other unique properties, represent a class of materials eminently suited for many critical engineering applications. Unfortunately, because of their brittleness and unfavorable combination of pertinent material properties, technical ceramics generally are highly susceptible to catastrophic failure in non-uniform thermal environments, which give rise to thermal stresses of high magnitude.

Thermal stress failure analysis of structural materials represents a multi-disciplinary problem which involves the principles of heat transfer, mechanics and materials engineering. Over the last few decades much general understanding of the nature of thermal stress failure of brittle materials has been generated. However, due to the multi-disciplinary nature of the problem, the ability to predict thermal stress failure quantitatively for design or other purposes has lagged behind the progress made in other engineering fields. The objective of the present program is to improve the qualitative and quantitative understanding of the nature of thermal stress failure of brittle structural materials, including the experimental as well as theoretical variables. In order to achieve this objective, the participating investigators and scope of the program are organized such that full advantage is taken of the combined inputs from a number of engineering disciplines. In a similar spirit, a number of studies were conducted in cooperation with investigators at other institutions.

The effort of this program consists of four main themes, including: experimental thermal shock testing with supporting analyses, measurement of thermophysical properties relevant to thermal stress failure, the analysis of mechanisms of thermal stress failure and the dissemination of information on thermal stresses in the form of review articles, conferences, etc.

A total fifty-five (55) published, accepted or submitted technical publications have resulted from this research program since its initiation. The status of these publications is summarized in Table 1.

Studies completed within the period covered by this report are presented as individual chapters in the main body of this report. The title of these chapters within their main theme together with a brief comment are as follows:

A. Measurement of Thermophysical Properties Relevant to Thermal Stress Failure.

Chapter I: Y. Chen, M. M. Abraham, L. D. Bentsen and D. P. H. Hasselman, "Effect of Ni-Alloying on the Thermal Diffusivity/Conductivity of MgO Single Crystals"

This study showed that the thermal diffusivity/conductivity of single crystals of magnesium oxide can be affected strongly by the alloying with Ni. The relative effect was found to be a function of whether the Ni existed as a solid-solution or in the form of precipitated colloids.

Chapter II: L. D. Bentsen, D. P. H. Hasselman and R. Ruh, "Effect of Hot-Pressing Temperature on the Thermal Diffusivity/Conductivity of SiC-AlN Composites"

The results of this study show that the heat conduction of mixtures of materials depend critically on whether such mixtures exist in the form of solid solutions or as distinct composites. Specifically, it was found that the thermal conductivity/diffusivity of SiC-AlN mixtures can be controlled by varying the hot-pressing temperature which in turn controls the degree of inter-diffusion between the SiC and AlN components.

Chapter III: M. A. Bucknam, L. D. Bentsen and D. P. H. Hasselman, "The Measurement of the Thermal Conductivity of Refractories by the Laser-Flash Method"

This feasibility study showed that the laser-flash method which uses dime-sized specimens can be used successfully to measure the temperature dependence of the thermal diffusivity and conductivity of materials with relatively coarse micro-structures, as long as care is exercised in selecting a specimen with a thermal diffusivity as close as possible to the mean of the value for a batch of specimens. Data obtained for a series of refractories selected as appropriate materials for this study showed excellent agreement with the thermal conductivity obtained by two other independent methods.

B. Analyses of Role of Material Properties in Thermal Stress Resistance of Brittle Structural Ceramics

Chapters IV, V, VI, VII and VIII:

J. R. Thomas, J. I. Frankel and D. P. H. Hasselman, "Effect of Interface Reflections and Angle of Incidence of Radiation on Thermal Stresses in Semi-Transparent Materials,"

J. P. Singh, J. R. Thomas, Jr., and D. P. H. Hasselman, "Role of Absorption Coefficient in the Frequency Dependence of the Thermal Stresses in a Partially-Absorbing Plate Subjected to Cyclic Thermal Radiation,"

J. P. Singh, J. I. Frankel, J. R. Thomas, Jr., and D. P. H. Hasselman, "Thermal Stresses in Partially Absorbing Flat Plate Due to Sudden Interruption of Steady-State Asymmetric Radiation, I: Convective Cooling at Rear Surface,"

J. I. Frankel, J. P. Singh, J. R. Thomas, Jr., and D. P. H. Hasselman, "Thermal Stresses in Partially Absorbing Flat Plate Due to Sudden Interruption of Steady-State Asymmetric Radiation, II: Convective Cooling at Front Surface,"

J. P. Singh, J. R. Thomas, Jr., and D. P. H. Hasselman, "Thermal Stresses in a Partially Absorbing Flat Plate Asymmetrically Heated by Cyclic Thermal Radiation and Cooled by Convection: Addendum."

These chapters represent a continuation of the analysis of the role of the absorption coefficient in the thermal stress failure of partially absorbing ceramic materials subjected to thermal radiation for a variety of boundary conditions. In general, the analytical results show that the absorption coefficient plays a significant role in governing the magnitude of thermal stress, coupled with the frequency, angle of incidence, multiple reflections of the incoming radiation and nature of convective cooling. This phase of the program has been completed.

Chapter IX: W. Chang, C. E. Knight, D. P. H. Hasselman and R. G. Mitchiner, "Analysis of Thermal Stress Failure of Segmented Refractory Structures"

This analysis concentrated on the role of the material properties and geometry in a unique failure mode encountered in segmented high-temperature structures, which consists of crack formation perpendicular to the direction of heat flow in contrast to the more common mode of crack propagation parallel to the direction of heat flow. For other specific boundary conditions chosen, it was found that high values of thermal diffusivity are desirable if the magnitude of thermal stresses are to be minimized. Furthermore, the magnitude of the dimensions of the individual segments also are critical in governing the value of thermal stress.

C. Reviews

Chapter X: D. P. H. Hasselman and L. D. Bentsen, "Effect of Microstructural and Compositional Heterogeneity on the Conduction of Heat in Structural Materials for High-Temperature Use"

This review article represents a summary of earlier results obtained for the compositional and microstructural effects on the conduction of heat in structural ceramic materials.

Table 1. Status of Publications Submitted during Previous Reporting Periods (4/1/78 - 12/31/82)

1. D. P. H. Hasselman and W. A. Zdaniewski, "Thermal Stress Resistance Parameters of Brittle Materials Subjected to Thermal Stress Fatigue," J. Am. Ceram. Soc., 61 (7-8) 375 (1978).

2. D. P. H. Hasselman, "Effect of Cracks on Thermal Conductivity," J. Comp. Mat., 12, 403-07 (1978).

3. K. Chyung, G. E. Youngblood and D. P. H. Hasselman, "Effect of Crystallization on the Thermal Diffusivity of a Cordierite Glass-Ceramic," J. Amer. Ceram. Soc., 61, 530 (1978).

4. W. Zdaniewski, H. Knoch, J. Heinrich and D. P. H. Hasselman, "Thermal Diffusivity of Reaction-Sintered Silicon Nitride," Ceram. Bull., 58, 539 (1979).

5. G. Ziegler and D. P. H. Hasselman, "Effect of Data Scatter on Apparent Thermal Stress Failure Mode of Brittle Ceramics," Ceramurgia, 5, 126 (1979).

6. D. P. H. Hasselman, "Role of Physical Properties in the Resistance of Brittle Ceramics to Fracture in Thermal Buckling," J. Amer. Ceram. Soc., 62, 125 (1979).

7. K. Satyamurthy, J. P. Singh, M. P. Kamat and D. P. H. Hasselman, "Effect of Spatially Varying Porosity on Magnitude of Thermal Stress During Steady State Heat Flow," J. Amer. Ceram. Soc., 62, 432 (1979).

8. D. P. H. Hasselman and J. P. Singh, "Analysis of Thermal Stress Resistance of Micro-cracked Brittle Materials," Ceramic Bull., 58, 856 (1979).

9. G. E. Youngblood, L. Bentsen, J. W. McCauley and D. P. H. Hasselman, "Thermal Diffusivity of Ba-Mica/Alumina Composites," J. Amer. Ceram. Soc., 58, 620 (1979).

10. D. P. H. Hasselman and Y. Tree, "On the Thermal Fracture of Ice,"J. Mat. Sc., 14, 1499 (1979).

11. D. P. H. Hasselman, "Figures-of-Merit for the Thermal Stress Resistance of High-Temperature Brittle Materials," Ceramurgia International, 4, 147 (1979).

12. Bob R. Powell, Jr., G. E. Youngblood, D. P. H. Hasselman and Larry D. Bentsen, "Effect of Thermal Expansion Mismatch on the Thermal Diffusivity of Glass-Ni Composites," J. Amer. Ceram. Soc., 63, 581 (1980).

13. D. P. H. Hasselman, J. C. Swearengen, E. K. Beauchamp and W. A. Zdaniewski, "Effect of Alumina Dispersions on the Thermal Conductivity/Diffusivity and Thermal Stress Resistance of a Borosilicate Glass," J. Mat. Sc., 15, 518-20 (1980).

14. D. P. H. Hasselman, J. R. Thomas, Jr., M. P. Kamat and K. Satyamurthy, "Thermal Stress Analysis of Partially Absorbing Brittle Ceramics Subjected to Radiation Heating," J. Am. Ceram. Soc., 63, 21-25 (1980).

15. J. P. Singh, J. R. Thomas, Jr., and D. P. H. Hasselman, "Analysis of Effect of Heat Transfer Variables on Thermal Stress Resistance of Brittle Ceramics Measured by Quenching Experiments," J. Am. Ceram. Soc., 63, 140-44 (1980).

16. K. Satyamurthy, M. P. Kamat, J. P. Singh and D. P. H. Hasselman, "Effect of Spatially Varying Thermal Conductivity on Magnitude of Thermal Stress in Brittle Ceramics Subjected to Convective Heating," J. Am. Ceram. Soc., 63, 363 (1980).

17. D. P. H. Hasselman, P. F. Becher and K. S. Mazdiyasni, "Analysis of the Resistance of High-E, Low-E Brittle Composites to Failure by Thermal Shock," Materials Technology, 11, 82 (1980).

18. K. Satyamurthy, J. P. Singh, M. P. Kamat and D. P. H. Hasselman, "Thermal Stress Analysis of Brittle Ceramics with Density Gradients Under Conditions of Transient Convective Heat Transfer," Proc. Brit. Ceram. Soc., 80, 10 (1980).

19. N. Claussen and D. P. H. Hasselman, "Improvement of Thermal Shock Resistance of Brittle Structural Ceramics by a Dispersion Phase of Zirconia, "Proceedings of Conference on Thermal Stresses in Materials and Structures in Severe Thermal Environments, Plenum Press (1980).

20. J. P. Singh, J. R. Thomas and D. P. H. Hasselman, "Thermal Stresses in Partially Absorbing Flat Plate Symmetrically Heated by Thermal Radiation and Cooled by Convection," J. of Thermal Stresses, 3, 341 (1980).

21. K. Satyamurthy, D. P. H. Hasselman and J. P. Singh, "Effect of Nature of Concavity of Temperature Distribution on Position and Sign of Maximum Thermal Stress," J. Thermal Stresses, 3, 551 (1980).

22. C. Shih, J. P. Singh and D. P. H. Hasselman, "Effect of Crack Interaction on the Fracture Initiation and Crack Propagation in Brittle Ceramics Subjected to Severe Thermal Shock," High Temp-High Pressures, 12, 477 (1980).

23. J. P. Singh, J. R. Thomas, Jr. and D. P. H. Hasselman, "Stresses Due to Thermal Trapping in Semi-Absorbing Materials Subjected to Intense Radiation," Proc. Conf. Thermal Stresses in Materials and Structures in Severe Thermal Environments, Plenum Press (1980).

24. K. Satyamurthy, D. P. H. Hasselman, J. P. Singh, and M. P. Kamat, "Effect of Spatial Variation of Thermal Conductivity on Magnitude of Tensile Thermal Stresses in Brittle Materials Subjected to Convective Heating," Proc. Conf. Thermal Stresses in Materials and Structures in Severe Thermal Environments, Plenum Press, (1980).

25. Proc. Conf. Thermal Stresses in Materials and Structures in Severe Thermal Environments. Co-edited by D. P. H. Hasselman and R. A. Heller, by Plenum Press (1980).

26. K. Satyamurthy, J. P. Singh, D. P. H. Hasselman and M. P. Kamat, "Transient Thermal Stresses in Cylinders with Square Cross-Section Under Conditions of Convective Heat Transfer," J. Amer. Ceram. Soc., 63 (11-12) 694-98 (1980).

27. G. Ziegler, L. D. Bentsen and D. P. H. Hasselman, "Orientation Effects on the Thermal Diffusivity of Hot-Pressed Silicon Nitride," Comm. Amer. Ceram. Soc., 64, 35 (1981).

28. J. P. Singh, C. Shih and D. P. H. Hasselman, "Analysis of Role of Crack Interaction on Nature of Strength Loss of Brittle Ceramics Subjected to Thermal Shock," Comm. Am. Ceram. Soc., 64 (8) (1981).

29. K. Niihara, L. D. Bentsen, K. Mazdiyasni and D. P. H. Hasselman, "Anisotropy Effects in the Thermal Diffusivity of Si_3N_4-BN Composites," Comm. Am. Ceram. Soc., 64 (9) C117-18 (1981).

30. J. R. Thomas, Jr., J. P. Singh and D. P. H. Hasselman, "Analysis of Thermal Stress Resistance of Partially Absorbing Ceramic Plate Subjected to Asymmetric Radiation, I: Convective Cooling at Rear Surface," J. Am. Ceram. Soc., 64, 163 (1981).

31. J. P. Singh, K. Satyamurthy, J. R. Thomas and D. P. H. Hasselman, "Analysis of Thermal Stress Resistance of Partially Absorbing Ceramic Plate Subjected to Asymmetric Radiation II: Convective Cooling at Front Surface," J. Amer. Ceram. Soc., 64, 169 (1981).

32. J. P. Singh, D. P. H. Hasselman, W. M. Su, J. A. Rubin and R. Palicka, "Observations on the Nature of Micro-Cracking in Brittle Composites," J. Mat. Sc., 16, 141 (1981).

33. G. Ziegler and D. P. H. Hasselman, "Effect of Phase Composition and Microstructure on the Thermal Diffusivity of Silicon Nitride," J. Mat. Sc., 16, 495 (1981).

34. J. P. Singh, Y. Tree and D. P. H. Hasselman, "Effect of Bath and Specimen Temperature on the Thermal Stress Resistance of Brittle Ceramics Subjected to Thermal Quenching," J. Mat. Sc., 16 (8) 2109-2118 (1981).

35. K. Niihara, J. P. Singh, L. D. Bentsen and D. P. H. Hasselman, "Observation on the Sub-Critical Growth and Healing of Micro-Cracks in Brittle Ceramics," Proceedings of Conference in Surface and Interfaces in Ceramics and Ceramic-Metal Systems, Plenum Press, (1981).

36. L. D. Bentsen, N. Claussen and D. P. H. Hasselman, "Effect of Micro-cracking on the Conduction of Heat in Brittle Composites," pp. 369-82 in Proc. Conf. Degradation of Engineering Materials, (VPI Press) (1981).

37. J. P. Singh, K. Niihara and D. P. Hasselman, "Analysis of Thermal Fatigue Behavior of Brittle Structural Materials," M. Mat. Sc., 16, 2789-97 (1981).

38. J. R. Thomas, Jr., J. P. Singh and D. P. H. Hasselman, "Thermal Stress in Materials Heated Internally by Radiation Absorption," J. of Nuclear Materials, 103-104, 167 (1981).

39. J. R. Thomas, J. P. Singh and D. P. H. Hasselman, "Role of Thermal Expansion in the Thermal Stress Resistance of Semi-Absorbing Brittle Materials Subjected to Severe Thermal Radiation," Proc. 7th Thermal Expansion Symposium, Plenum Press (1982).

40. Y. Chen, M. M. Abraham, L. D. Bentsen and D. P. H. Hasselman, "Effect of Ni-Alloying on the Thermal Diffusivity/Conductivity of MgO Single Crystals," Comm. Amer. Ceram. Soc., 65 (7) C104-05 (1982).

41. J. J. Brennan, L. D. Bentsen and D. P. H. Hasselman, "Measurement of the Thermal Conductivity and Diffusivity of Fine Silicon Carbide Fibers by the Composite Technique," J. Mat. Sc., 17, 2337 (1982).

42. K. Niihara, J. P. Singh and D. P. H. Hasselman, "Observations on the Characteristics of a Fluidized Bed for the Thermal Shock Testing of Brittle Ceramics," J. Mat. Sc., 17, 2553-59 (1982).

43. D. P. H. Hasselman, "Effect of Micro-cracking on Thermal Conductivity: Analysis and Experiment," Proc. 16th Int. Conf. Thermal Conductivity (in press).

44. M. Srinivasan, L. D. Bentsen and D. P. H. Hasselman, "Thermal Diffusivity of Silicon-Carbide-Silicon Composites," Proc. 17th Int. Thermal Conductivity Conference (in press).

45. J. R. Thomas, Jr., J. P. Singh and D. P. H. Hasselman, "Thermal Stresses in a Partially Absorbing Flat Plate Asymmetrically Heated by Cyclic Thermal Radiation and Cooled by Convection," J. Thermal Stresses (in press).

46. T. Ozyener, K. Satyamurthy, C. E. Knight, G. Ziegler, J. P. Singh and D. P. H. Hasselman, "Effect of ΔT- and Spatially Varying Heat Transfer Coefficient on Thermal Stress Resistance of Brittle Ceramics Measured by the Quenching Method," J. Amer. Ceram. Soc., (in press).

47. D. P. H. Hasselman and L. D. Bentsen, "Effect of Microstructural and Compositional Heterogeneity on the Conduction of Heat in Structural Materials for High-Temperature Use," Proc. on Thermomechanical Behavior of High-Temperature Materials. J. of Thermal Insulation (in press).

48. M. Bucknam, L. D. Bentsen and D. P. H. Hasselman, "The Measurement of the Thermal Conductivity of Refractories by the Laser-Flash Method," Proc. and Trans. Brit. Ceram. Soc., (in press).

49. J. R. Thomas, J. I. Frankel and D. P. H. Hasselman, "Effect of Interface Reflections and Angle of Incidence of Radiation on Thermal Stresses in Semi-Transparent Materials," J. Thermal Stresses (in press).

50. J. R. Thomas, J. P. Singh and D. P. H. Hasselman, "Thermal Stresses in a Partially Absorbing Flat Plate Asymmetrically Heated by Cyclic Thermal Radiation and Cooled by Convection; Addendum," J. Thermal Stresses (in press).

51. J. P. Singh, J. I. Frankel, J. R. Thomas, Jr., and D. P. H. Hasselman, "Thermal Stresses in Partially Absorbing Flat Plate Due to Sudden Interruption of Steady-State Asymmetric Radiation, I: Convective Cooling at Rear Surface," J. Thermal Stresses (in press).

52. J. I. Frankel, J. P. Singh, J. R. Thomas, Jr., and D. P. H. Hasselman, "Thermal Stresses in Partially Absorbing Flat Plate Due to Sudden Interruption of Steady-State Asymmetric Radiation, II: Convective Cooling at Front Surface," J. Thermal Stress (in press).

53. J. P. Singh, J. R. Thomas, Jr., and D. P. H. Hasselman, "Role of Absorption Coefficient in the Frequency Dependence of the Thermal Stresses in a Partially-Absorbing Plate Subjected to Cyclic Thermal Radiation," J. Thermal Stress (in review).

54. L. D. Bentsen, D. P. H. Hasselman and R. Ruh, "Effect of Hot-Pressing Temperature on the Thermal Diffusivity/Conductivity of SiC-AlN Composites," J. Amer. Ceram. Soc. (in press).

55. W. Chang, C. E. Knight, D. P. H. Hasselman and R. G. Mitchiner," Analysis of Thermal Stress Failure of Segmented Refractory Structures," J. Amer. Ceram. Soc. (in review).

CHAPTER I

EFFECT OF Ni-ALLOYING ON THE THERMAL DIFFUSIVITY/CONDUCTIVITY OF MgO SINGLE CRYSTALS

Y. Chen*, M. M. Abraham*, L. D. Bentsen+, D. P. H. Hasselman+

*Solid State Division, Oak Ridge National Laboratories
Oak Ridge, TN 37830 USA

+Department of Materials Engineering
Virginia Polytechnic Institute and State University
Blacksburg, VA 24061 USA

EFFECT OF Ni-ALLOYING ON THE THERMAL DIFFUSIVITY/CONDUCTIVITY OF MgO SINGLE CRYSTALS

Y. Chen, M. M. Abraham, L. D. Bentsen, D. P. H. Hasselman

The thermal diffusivity/conductivity of Ni-doped MgO single crystals was measured as a function of temperature by the laser-flash method. The Ni in the form of Ni^{2+} substitutional solid solution has a much greater effect on the thermal diffusivity/conductivity than precipitated Ni colloids. These results are discussed in terms of phonon and photon scattering effects.

The conduction of heat through solids can be affected significantly by the presence of other elements and is particularly sensitive to their size and distribution. Isolated point defects reduce the thermal conductivity significantly due to increased phonon scattering[1-3]. Larger colloids produce a similar effect but the reduction in thermal conductivity is not as great as for point defects. Still larger particles require that composite theory be used to describe the overall thermal conductivity which may be higher or lower than that of the host matrix[4].

Studies of the effect of metallic colloids on thermal conductivity have concentrated mostly on the halides due to the ease by which they can be synthesized[5,6]. For refractory oxides, Li, Na and k atoms have been introduced by ion implantation[8,9], however, these elements were limited to the surface regions. Such materials were therefore not suitable for measurement

ment of the effect of alloying elements on the heat conduction behavior of refractory oxides. Recently a method which produces a more uniform distribution of the alloying element was developed and applied to the alloying of magnesium oxide with Ni.[10,11,12] The aim of the present study was to determine the effect of the distribution of the Ni atoms on the thermal diffusivity/conductivity of MgO single crystals.

The Ni-doped MgO crystals were grown by the arc-fusion technique[13] from high-purity MgO powder with 5 wt.% NiO. The as-grown crystals exhibited a slightly greenish color associated with Ni^{2+} in substitutional sites[14,15]. Atomic emission spectroscopy showed the nickel concentration to be $\sim$ 0.4 wt.%. Transmission electron microscopy and optical absorption measurements confirmed that the nickel consisted primarily of Ni^{2+} ions[16]. Precipitation of the nickel was achieved by heating the Ni-doped crystals at 2100K in a reducing atmosphere of magnesium vapor at $\sim$ 6 atmospheres for periods of 2 or 20 hours. Following reduction the Ni-doped crystals appeared to be black.

Optical absorption spectra at 77K before and after reduction of a typical specimen is shown in Fig. 1. The absorption spectrum before reduction results from the Ni^{2+} ions. The large absorption coefficient of $\sim$ 600 cm^{-1} in the visible region is indicative of the high opacity after reduction. The broad band of high absorption coefficient near 2 eV is attributed to the formation of the Ni colloids.

Figure 2a shows the EPR spectrum at 80K of an "as-grown" MgO:Ni crystal with the magnetic field ranging from 0 to 500 Gauss oriented along the <100> axis. The single isotropic line is due to the Ni^{2+} species. Figure 2b shows the corresponding spectrum of a sample with the same volume, but

reduced for 2 hours. The Ni^{2+} signal is markedly reduced in intensity and a large broad background signal has appeared. The latter is attributed to the metallic nickel colloids which grew at the expense of the substitutional nickel ions. The sample reduced for 20 hours exhibited the broad spectrum due to the colloidal nickel without evidence for the presence of Ni^{2+} ions.

Figure 3 shows the data for the thermal diffusivity measured by the laser-flash method[17] for a pure MgO single crystal and the single crystals doped with Ni and heat-treated as described above. The pure crystal generally exhibits the highest values for the thermal diffusivity, whereas the crystal with nickel in solid solution exhibits the lowest values. Precipitation of the Ni leads to an increase of the thermal diffusivity with the heat-treatment for 20 hours resulting in values nearly identical to that of the undoped crystal. Similar trends are apparent in the data for the thermal conductivity, shown in Fig. 4 as a function of 1/T, calculated from the experimental data for the thermal diffusivity, the density of the crystals and handbook data for the specific heat of magnesium oxide and nickel[18]. The linear dependence of the thermal conductivity on 1/T for the Ni-doped crystals indicates that heat transfer through the crystals occurs primarily by phonon transport. The positive deviation at higher temperatures for the undoped crystal suggests that heat transfer by radiation makes a significant contribution to the total conductivity.

In order to provide an explanation for the present observations it may be noted that the phonon conductivity (K_L) can be expressed as:

$$K_L = 1/3 \int c(\omega) v \ell(\omega) d\omega \qquad (1)$$

where c is the specific heat per unit volume, v is the average velocity

of the phonons, ℓ is the phonon mean free path, and ω is the phonon frequency. The total mean free path is composed of an intrinsic term (ℓ_i) resulting from anharmonic processes and a term (ℓ_d) resulting from various defects with:

$$1/\ell = 1/\ell_i + 1/\ell_d \tag{2}$$

For the present samples the defect mean free path is governed by the Ni^{2+} point defects and the nickel colloids. For the same number of Ni atoms, the probability of phonon scattering with corresponding value of $1/\ell_d$ is much higher for Ni atoms in solid solution than the corresponding value for extended Ni colloids. For this reason, the value for the thermal conductivity of MgO with Ni^{2+} atoms is expected to be well below the corresponding value for the MgO with Ni colloids, in general agreement with the present data.

It may be noted that the pure MgO crystal has a thermal conductivity somewhat below the value for the MgO with Ni colloids. Possibly this observation is attributable to a small contribution of heat transfer by electron transport within the Ni colloids. However, this contribution is sufficiently small that the overall conductivity is controlled by phonon transport within the MgO as indicated by the 1/T dependence. This latter observation also indicates that the radiative component of the total conductivity is also very small. The thermal conductivity due to radiation can be expressed as either[19]:

$$K_R = \frac{16}{3}\,\sigma n^2 T^3 \ell \tag{3}$$

or

$$K_R = \left(\frac{e}{2-e}\right) 4\sigma n^2 T^3 d \tag{4}$$

where σ, n, T, ℓ, d and e are the Stefan-Boltzman constant, index of refraction, temperature, photon mean free path, sample thickness, and the

emissivity of the specimen surfaces, respectively. Equation 3 is applicable when ℓ, which is equal to the reciprocal of the absorption coefficient, is small compared to the thickness of the sample. Such is the case for the Ni colloid containing crystal with an absorption coefficient of $\approx 600\ cm^{-1}$ in which less than 1% of the total conductivity may be attributed to photon transfer. Equation 4 may be used when $\ell >> d$; however, since the laser-flash method employs very small samples ($d \approx 2$ mm) the radiative conductivity is also small even for the pure MgO crystal, except at very high temperatures, in agreement with the present data.

The data and discussion presented thus confirm the critical role of the distribution of alloying elements on the conduction of heat through solids.

ACKNOWLEDGMENT

The present study was supported by the Office of Naval Research under contract N00014-78-C-0431.

REFERENCES

1. P. G. Klemens, Seventh Symposium on Thermophysical Properties, Ed. A. Cezairliyan, ASME (1977).
2. R. Berman, Thermal Conduction in Solids (Clarendon Press, Oxford, 1976).
3. J. Callaway and H. C. von Baeyer, Phys. Rev., 120, 1149 (1960).
4. A. E. Powers, Conductivity in Aggregates, Rept. KAPL-2145, Knolls Atomic Power Plant (1961).
5. A. E. Hughes and S. C. Jain, Adv. in Phys. 28, 717 (1979).
6. S. Amelinckx, The Direct Observation of Dislocations, Suppl. to Solid State Phys, ed. F. Seitz and D. Turnbull, Academic Press (1964).
7. C. Childs and L. Slifkin, J. Phys. Chem. Solids, 12, 119 (1959).
8. M. Treilleux, P. Thevenard, G. Chussagne and L. W. Hobbs, Phys. Status Solidi A 48, 425 (1978).
9. M. Treilleux and G. Chassagne, J. Phys. Lett., Paris, 40, L-161 (1979).
10. F. A. Modine, L. A. Boatner, M. M. Abraham, W. P. Unruh and R. Bunch, Bull. Am. Phys. Soc. 24, 413 (1979).
11. J. Narayan, Y. Chen and R. Moon, Phys. Rev. Lett. (in press).
12. Y. Chen, J. Narayan and K. L. Tsaug, Bull. Am. Phys. Soc. 26, 268 (1981).
13. M. M. Abraham, C. T. Butler and Y. Chen, J. Chem. Phys. 55, 3752 (1971).
14. J. E. Ralph and M. G. Towsen, J. Chem. Phys., 48, 149 (1968).
15. M. V. Iverson, J. C. Windscheif and W. A. Sibley, Appl. Phys. Lett., 36, 183 (1980).
16. J. Narayan and Y. Chen, J. Appl. Phys., 51, 1242 (1980).
17. W. J. Parker, R. J. Jenkins, C. P. Butler, and G. L. Abbott, J. Appl. Phys. 32, 1679 (1961).

18. Y. S. Touloukian, et. al., Specific Heat-Nonmetallic Solids, Thermophysical Properties of Matter, Vol. 5., IFI/Plenum (1973).

19. D. W. Lee and W. D. Kingery, J. Am. Ceram. Soc., 43, 594 (1960).

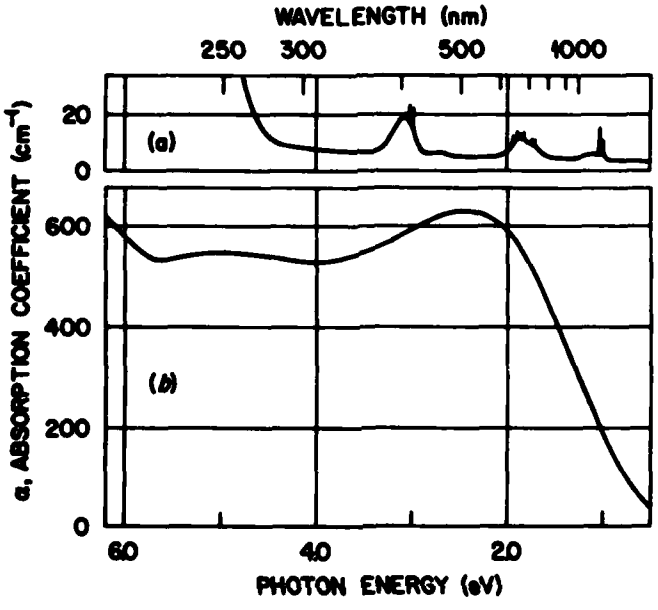

Fig. 1. Optical absorption spectra at 77K of Ni-doped MgO crystals (a) before and (b) after reduction.

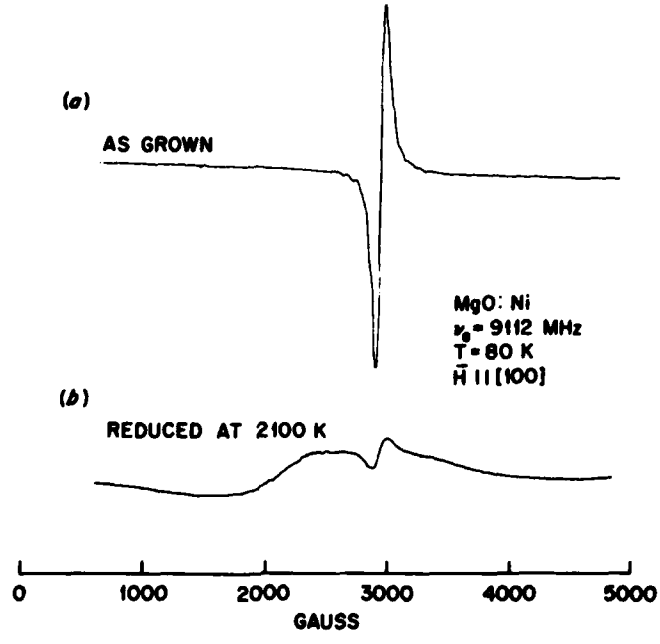

Fig. 2. EPR spectrum of Ni-doped MgO crystal (a) before and (b) after being reduced for 2 hours.

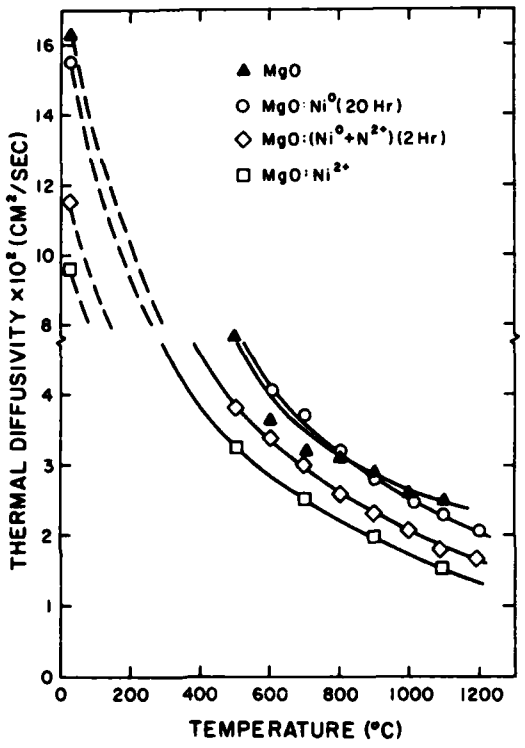

Fig. 3. Measured thermal diffusivity of a pure MgO and the Ni-doped single crystals reduced for various lengths of time.

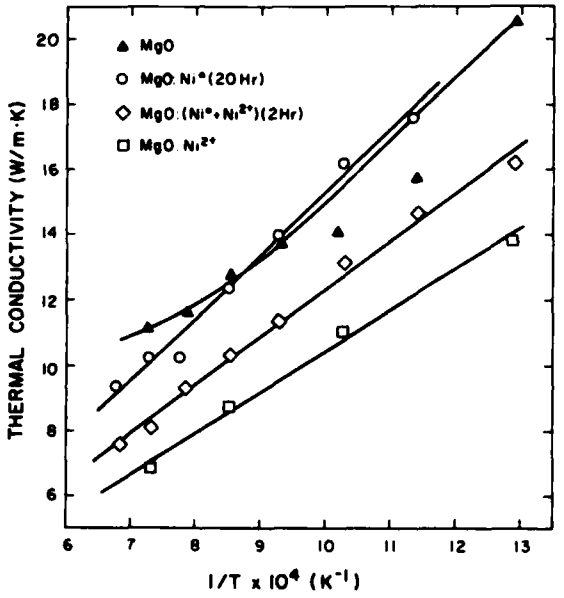

Fig. 4. Thermal conductivity calculated from the experimental data for the thermal diffusivity of a pure MgO and Ni-doped single crystals given in Fig. 3.

CHAPTER II

EFFECT OF HOT-PRESSING TEMPERATURE ON THE THERMAL DIFFUSIVITY/CONDUCTIVITY OF SiC-AlN COMPOSITES

by

L. D. Bentsen*, D. P. H. Hasselman*, R. Ruh§

*Department of Materials Engineering
Virginia Polytechnic Institute and State University
Blacksburg, Virginia 24061

§Air Force Wright Aeronautical Laboratories
Wright-Patterson Air Force Base, Ohio 45433

EFFECT OF HOT-PRESSING TEMPERATURE ON THE THERMAL DIFFUSIVITY/CONDUCTIVITY OF SiC-AlN COMPOSITES

L. D. Bentsen*, D. P. H. Hasselman*, R. Ruh§

*Department of Materials Engineering
Virginia Polytechnic Institute and State University
Blacksburg, Virginia 24061

Air Force Wright Aeronautical Laboratories
Wright-Patterson Air Force Base, Ohio 45433

ABSTRACT

Data are presented for the thermal diffusivity/conductivity of hot-pressed mixtures of SiC and AlN. The results indicate that hot-pressing at higher temperatures, which permits solid-solution formation, results in significantly lower thermal diffusivity/conductivity than obtained by hot-pressing at lower temperatures, at which the SiC-AlN exists as discrete phases.

The thermal conductivity of solids can be affected significantly by the presence of foreign elements and is particularly sensitive to their size and distribution. Due to increased phonon scattering, isolated point defects can significantly reduce the thermal conductivity (1-3). In contrast, particles which are large enough to retain their individual bulk properties may cause an increase or decrease in overall thermal conductivity, depending on their thermal conductivity relative to the host matrix. In this case, thermal conductivity can be calculated by means of composite theory (4). Th. important role of the distribution of a foreign element on heat conduction was demonstrated recently by experimental data (5) for MgO single crystals alloyed with Ni, which existed in either solid solution or in the form of precipitates.

Because of its high sensitivity on the distribution of foreign elements, the thermal conductivity of solids can be controlled by modifying the processing conditions which affect the distribution of the alloying elements. The feasibility of this approach is demonstrated by experimental data for the effect of aluminum nitride additions on the thermal diffusivity of silicon carbide.

The specimens used for this study were prepared for an earlier investigation of the crystallographic, compositional and microstructural analysis of SiC-AlN solid solutions and two-phase mixtures (6). These samples were hot-pressed from mixtures of

SiC and AlN powders at temperatures ranging from 1700 to 2200°C. The specimens hot-pressed at the lower temperatures consisted of mixtures of SiC and AlN grains with only slight inter-diffusion between the SiC and AlN. Those specimens prepared at the highest temperatures consisted of solid-solutions due to inter-diffusion between the two components. Although some of these solid-solutions consisted of a single polymorph, the distribution of the individual atomic species was found to be highly non-uniform. For details the reader is referred to the original study (6).

The thermal diffusivity of the samples was measured by the flash method (7) using a glass-Nd laser as the flash source, with an estimated accuracy of $\sim$ 3%. Figure 1 shows the experimental data for the thermal diffusivity at room temperature as a function of AlN content and a range of hot-pressing temperatures. It is evident that the AlN-SiC mixtures hot-pressed at the higher temperatures exhibit a thermal diffusivity significantly lower than those hot-pressed at the lower temperatures. The differences in the thermal diffusivity for the two AlN samples without SiC at least in part are due in part to differences in density which was 95.3% for the sample hot-pressed at 1700°C and 94.4% for the sample prepared at 2100°C. Undoubtedly other variables may have contributed to these differences as well. For the SiC samples without AlN the values for the thermal diffusivity are appreciably lower than the value near 0.8 cm^2s^{-1} observed in this laboratory (8) for other samples of SiC from other sources. The lower values of this study are thought to be due to the rela-

tively high boron content of the two starting powders used for their preparation. This hypothesis is based on preliminary data obtained during another study (8) which showed that a 15% porous SiC without boron exhibited a thermal diffusivity higher than fully dense SiC with boron.

Figure 2 shows the values of the thermal conductivity calculated from the data for the thermal diffusivity given in Fig. 1 by multiplication with the product of density and specific heat. Also included in Fig. 2 are the data for the thermal conductivity reported by Rafaniello et al (9) for SiC-AlN solid solutions made by carbothermal reduction of silica and alumina followed by hot-pressing at 1950 to 2200°C. These latter data show quite good agreement with the samples of the present study hot-pressed at the two highest temperatures of 2100 and 2200°C. Included in Fig. 2 is the expected dependence of the thermal conductivity calculated from composite theory on the assumption that the AlN-SiC consists of a mixture of AlN and SiC without any inter-diffusion or interfacial resistance to the flow of heat. For clarity, the composite thermal conductivity was calculated from the data for SiC and AlN hot-pressed at 2100°C. Clearly, the composite behavior will vary with the choice of the particular end-point data. Comparison of the calculated data for composite behavior with the experimental data, especially those for the highest hot-pressing temperatures, clearly shows that the formation of a solid solution results in a dramatic decrease of the thermal conductivity.

The thermal conductivity of the AlN-SiC mixtures hot-pressed at temperatures ranging from 1850 to 2000°C is significantly higher than that of the samples prepared at 2100 or 2200°C. This difference indicates the absence of complete solid solution. Presumably, at these lower temperatures the rate of inter-diffusion is too low for solid-solutions to form so that in these samples the SiC and AlN have retained their original form. It is of interest to note, however, that the data for the thermal conductivity of these samples falls below the calculated behavior if the SiC-AlN mixtures were true composites. This suggests the existence of either a barrier to heat flow at the SiC-AlN interface due to less than perfect atomic bonding, or alternatively, and perhaps more likely, solid solution formation occurred at the interfacial zone over a thickness sufficient to affect the thermal conductivity significantly. In fact, such a thin zone of inter-diffusion was detected by XRD in TEM.

At higher temperatures, where phonon scattering is greater, the effect of the distribution of other elements on thermal conductivity becomes less significant (2). This behavior is exhibited by the present samples as shown in Fig. 3 which compares the temperature dependence of the thermal diffusivity of two samples containing 50% AlN. These samples were hot-pressed at 1900 and 2100°C and constitute a two-phase mixture and a solid solution respectively. The relative difference in thermal diffusivity decreases with increasing temperature. The same effect is also shown in Fig. 4 for two samples with 24.8 and 34% AlN hot-pressed

at 1950 and 2100°C, respectively. Nevertheless, even at the higher temperatures, significant differences in the thermal diffusivity of the mixtures and solid-solutions still exist.

The results of the present study clearly indicate that by modifying processing conditions (temperature in this case), a significant measure of control can be exerted over the thermal transport behavior of composites that form solid solutions.

ACKNOWLEDGMENTS

This study was conducted as part of a research program on the thermal and thermo-mechanical behavior of structural ceramics for high-temperature purposes under contract N00014-78-C-0431. The specimens were made at the Air Force Wright Aeronautical Laboratories, Wright-Patterson Air Force Base, Ohio 45433.

REFERENCES

1. P. G. Klemens, Seventh Symposium on Thermo-Physical Properties. Edited by A. Cezairliyan. The American Society of Mechanical Engineers, 1977.

2. R. Berman, Thermal Conduction in Solids, Clarendon, Oxford, 1976.

3. J. Callaway and H. C. Von Baeyer, "Effect of Point Imperfections on Lattice Thermal Conductivity," Phys. Rev., 120 (4) 1149-54 (1960).

4. A. E. Powers, "Conductivity in Aggregates," Knolls Atomic Power Tech., Rept. KAPL-2145, General Electric Co., March 6, 1961.

5. Y. Chen, M. M. Abraham, L. D. Bentsen and D. P. H. Hasselman, "Effect of Nickel Alloying on the Thermal Diffusivity/Conductivity of MgO Single Crystals", J. Amer. Ceram. Soc. 65 (7) C104-05 (1982).

6. R. Ruh and A. Zangvil, "Composition and Properties of Hot-Pressed SiC-AlN Solid Solutions", J. Amer. Ceram. Soc., 65 (5) 260-65 (1982).

7. W. J. Parker, R. J. Jenkins, C. P. Butler and G. L. Abbott, "Flash Method of Determining Thermal Diffusivity, Heat Capacity, and Thermal Conductivity", J. Appl. Phys., 32 (9) 1679-84 (1961).

8. L. D. Bentsen and D. P. H. Hasselman, research in progress.

9. W. Rafaniello, K. Cho, and A. Virkar, "Fabrication and Characterization of SiC-AlN Alloys", J. Mater. Sci., 16 (1981) 3479-88.

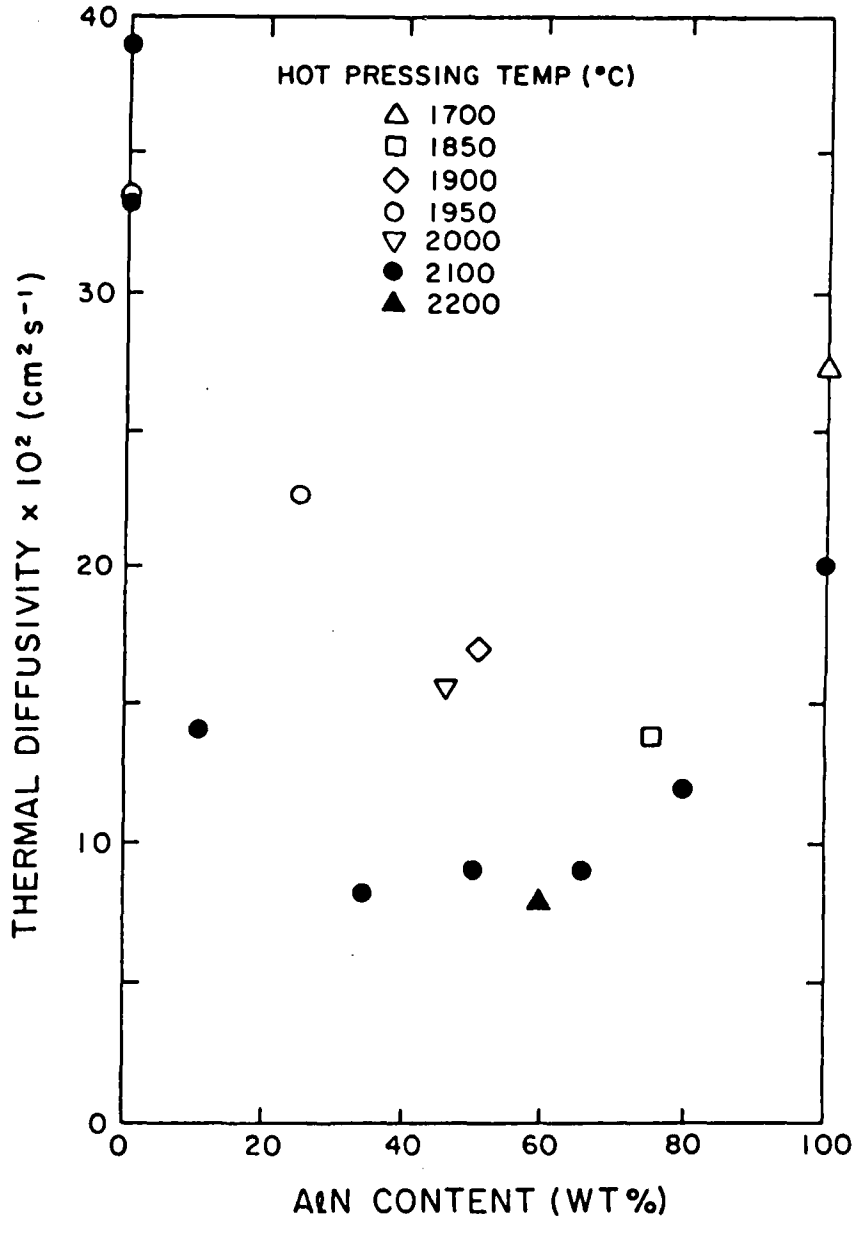

Fig. 1. Room temperature thermal diffusivity of SiC-AlN composites hot-pressed over a range of temperatures.

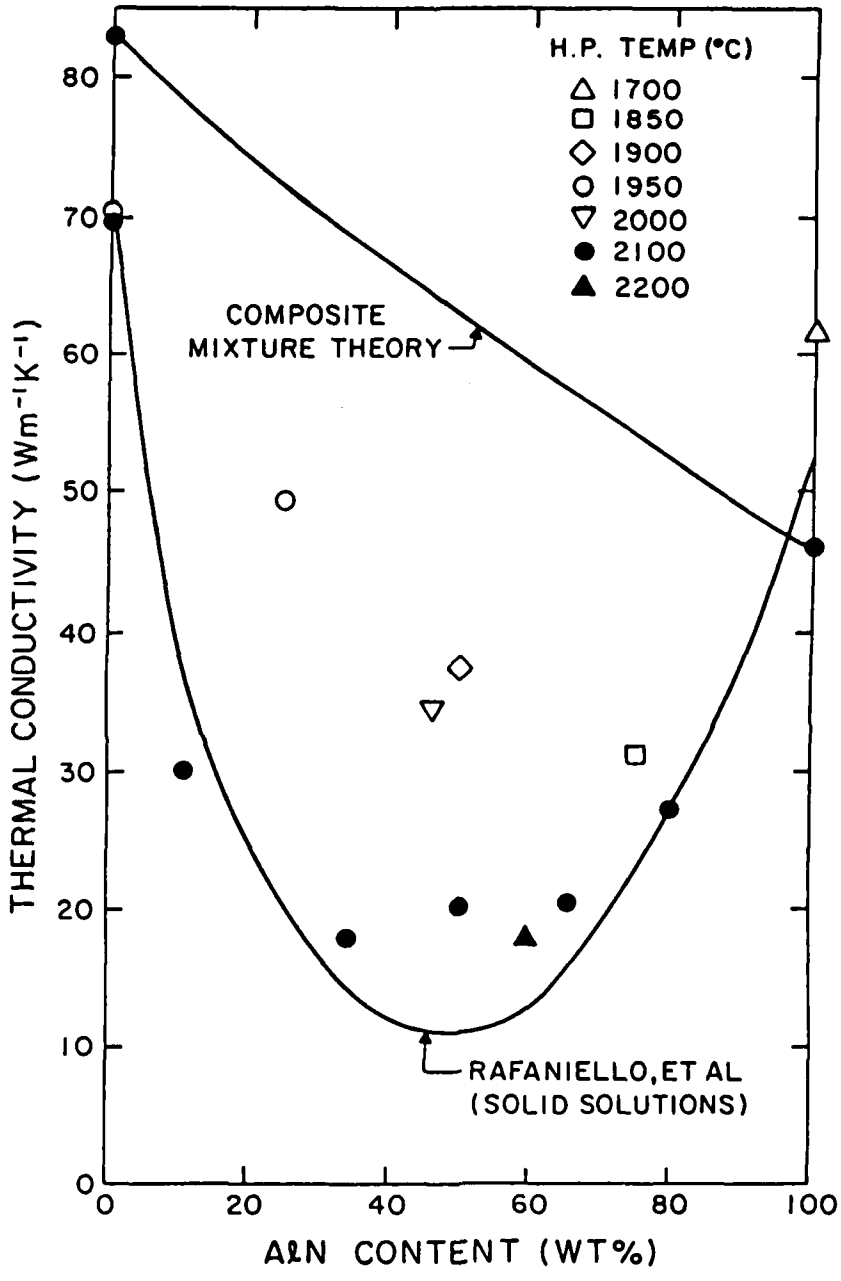

Fig. 2. Calculated values of the thermal conductivity of SiC-AlN composites hot-pressed over a range of temperature, compared with literature data.

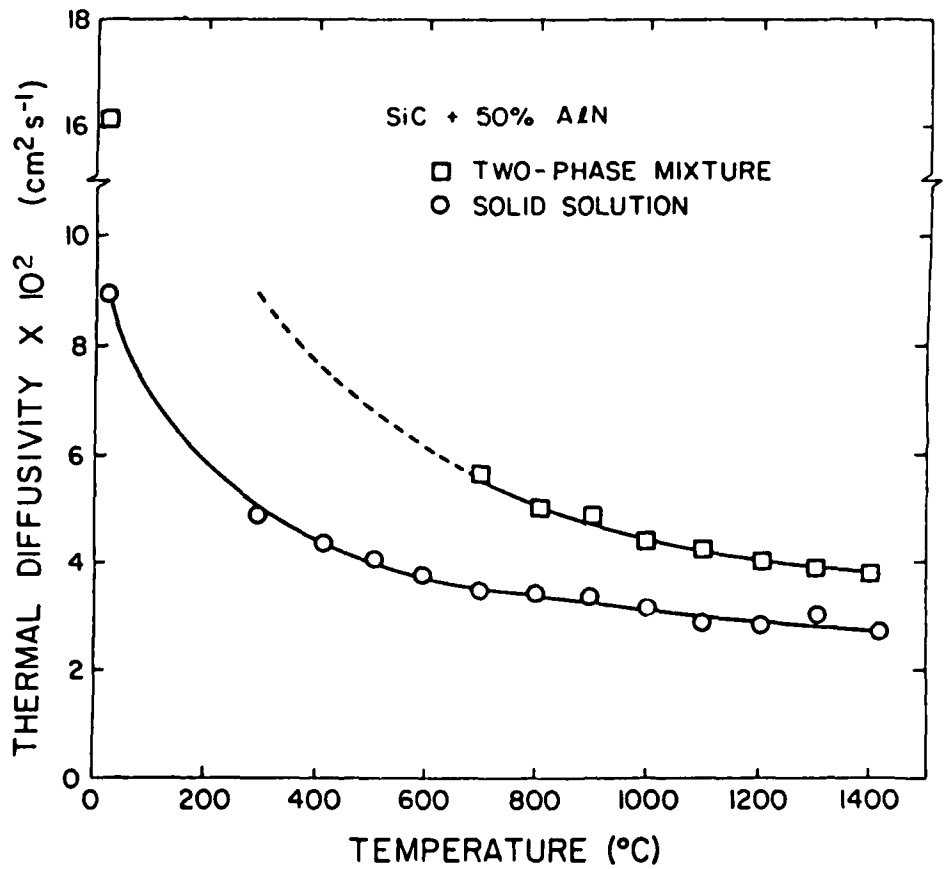

Fig. 3. Temperature dependence of the thermal diffusivity of SiC-AlN mixtures with 50 wt.% AlN, hot-pressed at 1900 and 2100°C.

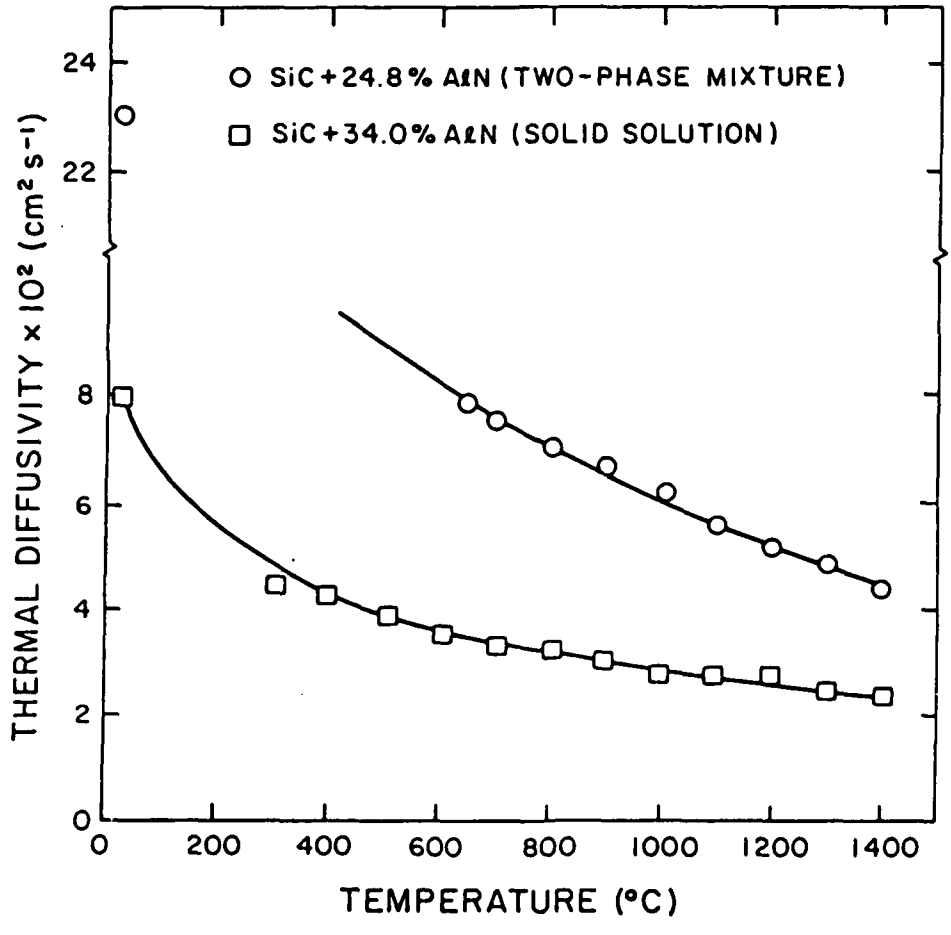

Fig. 4. Temperature dependence of the thermal diffusivity of SiC-AlN mixtures with 24.8 and 34.0 wt.% AlN hot-pressed at 1950 and 2100°C, respectively.

CHAPTER III

THE MEASUREMENT OF THE THERMAL CONDUCTIVITY OF REFRACTORIES BY THE LASER-FLASH METHOD

by

M. A. Bucknam*, L. D. Bentsen*, James Makosey[§],
G. R. Angell**, D. P. H. Hasselman*

*Department of Materials Engineering
Virginia Polytechnic Institute and State University
Blacksburg, Virginia 24061

[§]Harbison-Walker Refractories
Dresser Industries, Inc.
Garber Research Center
Box 98037
Pittsburgh, PA 15227

**Kaiser Aluminum and Chemical Corporation
Center for Technology
P.O. Box 887
Pleasanton, CA 94566

ABSTRACT

A study was conducted to determine the feasibility of the laser-flash diffusivity method for determining the thermal conductivity of refractories. Considerable specimen-to-specimen variation in the values of thermal diffusivity at room temperature was found for a set of specimens cut from eleven different refractories. The specimen with the value of thermal diffusivity closest to the mean was taken to be representative of the bulk material and was used for measurements at higher temperatures. For the dense refractories the thermal conductivity at elevated temperatures obtained by the laser-flash method agreed quite well with the corresponding data obtained by the guarded-plate and hot-wire methods. For a relatively porous insulating refractory the thermal conductivity obtained by the laser-flash method was found to exceed the data obtained by the guarded-plate method. This observation was thought to be due to penetration of the laser-flash into the specimen interior. The thermal conductivity near room temperature obtained by the laser-flash method exceeded the data obtained by the guarded-plate or hot-wire methods. Further research is needed in order to establish the reasons for this effect. In general, the results of this study indicate that, provided care is taken in selecting the appropriate test

specimen, the laser-flash method represents a valuable, convenient, and rapid tool for measuring the thermal conductivity of refractories at elevated temperatures.

1. INTRODUCTION

Thermal conductivity plays a critical role in the performance of refractory materials in structures such as high temperature process vessels, furnaces, kilns, retorts, and recuperators to name just a few. Low values of thermal conductivity are required if heat losses are to be kept to a minimum. On the other hand, heat transfer through brickwork (desirable in certain heating operations) and control of hot-face temperatures is obtained most easily by using refractories of higher thermal conductivity (1). This latter characteristic is also desirable, if not critical, in avoiding the incidence of failure by thermal shock. For these reasons, reliable thermal conductivity data are essential for the selection of a refractory which will perform optimally in a given application.

The measurement of the thermal conductivity of refractories at this time relies primarily on the guarded-plate and hot-wire methods (2,3,4). An increasingly popular method for measuring the conduction of heat through solids is the laser-flash method, pioneered by Parker, et. al. (5). In general, this method consists of subjecting one side of a small, thin, disc-shaped specimen to a uniform laser pulse (or other suitable instantaneous heat source). The heat absorbed at the irradiated surface will diffuse through the specimen. The transient temperature response at the opposite face, recorded by an appropriate method, allows calculation of the thermal diffusivity. Thermal conductivity can be calculated by multiplying the thermal diffusivity with independently obtained values of density and specific heat.

The specimen required for the laser-flash method is of simple geometry, with dimensions of the order of 2mm in thickness by 10mm in diameter or diagonal, for specimens of circular or square geometry. One essential requirement for the measurement of thermal conductivity (or any property) by any method is that the test specimen used for the measurement must be representative of the bulk of the material under investigation. For specimens of the dimensions given above for the laser-flash method, this requirement is certainly met if the test material is homogeneous and consists of a single solid phase with grain and pore sizes of a few microns.

Refractories are usually highly heterogeneous, both chemically as well as structurally. Furthermore, refractories possess a relatively coarse microstructure with a wide distribution of pore and grain sizes, perhaps as large as a few millimeters. This latter dimension is of the same order as the thickness of the laser flash specimens. Thus, the data obtained by the laser-flash method may depend critically on the location in a refractory brick from which the specimen was cut. Considerable specimen to specimen variation is expected and may pose a limitation on the use of the laser-flash method for determining the thermal diffusivity/conductivity of refractories. The purpose of this study was to resolve this question by comparing data for the thermal conductivity of a number of refractories measured by the laser-flash method with corresponding data obtained by the guarded-plate or hot-wire method.

2. EXPERIMENTAL

2.1 MATERIALS AND SAMPLE PREPARATION

Table 1 lists the eleven refractory compositions selected for this study. The listed value of density represents the mean of the range of density reported by the manufacturers.

In preparing the disc-shaped specimens required for the laser-flash method, cores approximately 12.5mm in diameter by approximately 50mm long were cut from the larger samples by means of a diamond core drill. Because of possible preferred alignment of the grains and/or pores, the heat conduction of refractories could exhibit anisotropic behavior. In order to assure a valid comparison of the data, the cores from the refractory samples provided by manufacturer A were drilled in the direction of heat flow used in the guarded plate method. Since the hot-wire method involves radial heat flow, the cores cut from the samples provided by manufacturer B were cut in two mutually perpendicular directions, each in turn perpendicular to the length of the wire in the hot-wire method. The cores were then sliced into a number of circular discs approximately 2mm in thickness with a low-speed diamond bench-saw. The disc samples were then cleaned in acetone to remove the saw lubricant and cutting debris, followed by drying for at least 24 hours.

2.2 EXPERIMENTAL PROCEDURE

2.2.1 Laser-Flash Method

Figure 1 schematically illustrates the principle components of the experimental equipment used for this study. The laser-flash source consists of a Nd-glass laser* with a laser rod having a diameter of approximately 12.5mm. The wavelength of the laser pulse was 1.06 μm with a pulse-width of about 800 μsec. The energy per pulse was a maximum of approximately 70 Joules at the 5kV peak voltage of the laser power supply. The latter voltage was kept at approximately 4.1kV in order to extend the life of the flash-lamp. At this voltage, the intensity of the beam was highly uniform, as verified by the flash imprint on photographic film.

For measurement of the thermal diffusivity at elevated temperatures the sample rested upon a graphite specimen holder which consisted of a graphite ring 6mm thick with an outer and inner diameter of 24 and 6mm, respectively. The specimen was centered on a circular knife-edge machined at the edge of the center hole. The specimen holder and sample were held within a carbon resistance furnace** which was capable of reaching temperatures as high as 2500°C in an inert atmosphere. Nitrogen gas was used throughout this study. The furnace was oriented vertically with the specimen lying horizontally within the holder. The flash from the laser entered the top of the furnace via a first-surface

---

* Model K-1,Compulaser, Canoga Park, California
**Model 1000A, Astro Industries, Santa Barbara, California.

gold mirror through a fused quartz window. Because of a slight divergence of the laser beam, specimens with the same nominal diameter as the laser rod were irradiated uniformly over their entire surface, also verified by the flash imprint on photographic film.

The transient temperatures of the lower face of the specimen induced by the laser pulse at the top surface were monitored by remote optical sensors. An InSb infrared-detector* was used for specimen temperatures ranging from about 300°C to 600°C. For temperatures in excess of 600°C the transient temperature response of the specimens was measured by a silicon photodiode detector.** These two detectors were placed underneath the furnace and focused through a sapphire window at the bottom of the furnace onto the lower surface of the specimen. It should be pointed out that the furnace provided the ambient temperature of the specimen. The mean temperature rise of the specimen due to the laser flash is less than five degrees.

A side-viewing liquid nitrogen cooled InSb detector*** was used for measurements of thermal diffusivity at room temperature. For this purpose the specimens, contained in a thermally insulated holder, were placed directly in the path of the laser pulse and immediately in front of the detector window. For measurements at all temperatures, the specimens were coated with a thin

---

* 12-8722 InSb, Barnes Industry, Stamford, Conn., USA.
** Built for this purpose at VPI & SU for this laboratory.
*** Type TI-ISV381 InSb, Texas Instruments, Dallas, Texas.

layer of graphite* in order to prevent direct transmission of the laser flash through the samples.

The signal from an optical detector can be recorded with an appropriate data acquisition system such as the storage oscilloscope** used for the present study. (A computerized data acquisition and analysis system is being constructed at this time.) The oscilloscope was triggered at the instant the laser fired by a signal from a photodiode mounted at the back of the laser from which approximately 1% of the total flash energy is emitted. By appropriately biasing the signal from the detectors corresponding to the temperature of the specimen prior to the laser-flashing, only the transient temperature rise is recorded. This transient temperature rise is shown schematically in Figure 2. The pertinent value to be measured is $t_{1/2}$, which represents the time required for the lower face of the specimen to reach one half of the maximum temperature change. The absolute temperature rise need not be known quantitatively for the determination of the thermal diffusivity.

For unidirectional heat flow, uniform radiation of the specimen, and no heat losses following laser flashing, the thermal diffusivity (κ), the half-rise time ($t_{1/2}$), and the specimen thickness (L) are related by:

$$\kappa = 1.37\ L^2/\pi^2 t_{1/2} \qquad (1)$$

---

* dgf 123 Dry Graphite Film, Miracle Power Products Corp., Cleveland, Ohio.
**Tektronix 5111 storage oscilloscope.

At higher temperatures where heat losses may be appreciable during the time of the specimen's transient temperature response, equation 1 must be modified. In this study the rate of specimen cooling was determined by measuring the relative temperature rises and times at the point of T_{max} and 10 $t_{1/2}$. Equation 1 then was readily corrected by the use of tables compiled by Heckman (6). The precision of the thermal diffusivity due to measurement errors is about 2.5%. Data obtained on Armco iron using the equipment of this study was accurate to within 4% of literature values (7).

The thermal conductivity (λ) was calculated from:

$$\lambda = \kappa \rho c_p \qquad (2)$$

where ρ and c_p are the density and specific heat, respectively. The values of density used were those listed in Table 1, whereas the data for the specific heat (1) are listed in Table 2. Above room temperature, changes in the specimen thickness and density with temperature were taken into account in the evaluation of the thermal diffusivity and conductivity.

The laser-flash specimens cut from a given refractory composition were measured at room temperature. A total of four separate readings of $t_{1/2}$ were taken for each specimen and averaged. This average $t_{1/2}$ was used to calculate the thermal diffusivity of the specimen at room temperature. The specimen with the value of thermal diffusivity closest to the mean value of all the specimens cut from the same refractory was judged to be representative of the bulk material and was selected for measurement of

thermal diffusivity as a function of temperature. Equation (2) was then used to calculate the thermal conductivity from each thermal diffusivity data point.

2.2.2 Measurement of Thermal Conductivity

Values for the thermal conductivity of the samples provided by manufacturers A and B were obtained by the guarded-plate and hot-wire methods, respectively. The data obtained by the guarded plate method used equipment identical to that designated for the ASTM test (4). The bricks used for these measurements were nominally identical in composition and microstructure to those used for the laser-flash measurements.

Measurement of the thermal conductivity by the hot-wire method (3) was based on the accurate measurement of the change in resistance of a pure platinum wire connected to a constant current source. The wire is located between two 22.5 cm straights held at temperatures ranging from room temperature to 1500°C. A fully computerized data acquisition and analysis system* was used. Five seperate measurements were made at each of seven different test temperatures. Specimens for the laser-flash measurements were cut from one of the identical bricks used for the hot wire measurements.

---

* Hewlett-Packard 3052A Data Acquisition System.

3. RESULTS, DISCUSSION AND CONCLUSIONS

Tables 3 and 4 list the thermal diffusivity data for room temperature measurements of the individual specimens from those refractories which exhibited the smallest and largest specimen-to-specimen variations, respectively. It can be seen from the scatter in the data that any one single specimen cannot be considered as representative of the bulk material. Accordingly, in order to obtain reliable thermal diffusivity and conductivity data, care must be taken in selecting a specimen which can be considered representative of the bulk material. For this study, as few as six and as many as seventeen individual specimens were cut from each refractory brick for each direction of heat flow where appropriate. Measurement of the thermal diffusivity of twenty specimens at room temperature requires no more than a couple of hours, depending on the number of measurements made for any one specimen. Measurement at elevated temperatures, on the other hand, is more time consuming and thus impractical for all specimens. As an aside, it should be noted that, in principle, specimen-to-specimen variation can be reduced by the use of larger and thicker samples. This, however, would require much larger lasers, with prohibitive cost and is therefore less practical.

Figures 3 to 13 show the experimental data for the thermal diffusivity and calculated values of thermal conductivity, as a function of temperature, obtained by the laser-flash method for all eleven refractory compositions. Also included in these fig-

ures are the data for the thermal conductivity obtained by the guarded-plate or hot-wire method. Comparison of the data shows that at elevated temperatures, with the exception of refractory 4, the agreement between the laser-flash data and those obtained by the guarded-plate or hot-wire method is quite good.

For refractory 4, which is a rather porous refractory, the laser-flash data exceed those obtained by the guarded-plate method by 20 to 30%. It is suggested here that for this refractory the laser-flash data are too high. This effect most likely arises from the presence of the pores in the surface of the specimen. These pores permit the absorption of the laser radiation within the interior of the specimen rather than at a planar surface assumed in the development of the underlying theory. The same effect arises at the opposite surface, where pores permit detection of temperature changes in regions within the specimen. Both effects combine to reduce the effective specimen thickness which tends to increase the value of the thermal diffusivity calculated from $t_{1/2}$. This effect, which is expected to be a function of the pore volume fraction as well as pore size, may in principle, be accounted for theoretically. However, this would require information on the surface pore configuration for any pertinent material to be tested, coupled with a transient heat flow analysis of the spatially non-uniform absorption of the laser radiation. An analysis of this type is beyond the scope of the present study.

Near room temperature, the data for the thermal conductivity obtained by the laser-flash method generally exceed those obtained by the guarded-plate and hot-wire methods. It is thought that this effect does not arise from some systematic error in the flash method because good agreement was found between data obtained by this method and data for thermal conductivity standards such as Armco iron. In the guarded-plate method the temperature of the specimen is reported in terms of the linear average of the two temperatures recorded by the thermocouples. This, however, tends to over and under estimate the spacial average of the temperature and thermal conductivity, respectively, for materials with a negatively temperature dependent thermal conductivity. Possibly, similar effects are operative during measurements by the hot-wire method.

In conclusion the results of this study indicate that for appropriately chosen specimens, the laser-flash method is a useful tool for obtaining the thermal diffusivity and conductivity of dense refractories.

ACKNOWLEDGEMENT

The measurement of the thermal diffusivity was conducted as part of a research program on the thermophysical and thermomechanical behavior of structural materials funded by the Office of Naval Research under contract N00014-78-C-0431. Special thanks are extended to Leigh Brooks for experimental assistance and review of the manuscripts.

REFERENCES

1. Modern Refractory Practice, Harbison-Walker Refractories, Pittsburgh, Pa. (1961).

2. Y. S. Touloukian, R. W. Powell, C. Y. Ho, and P. G. Klemens, Thermal Conductivity: Nonmetallic Solids (Thermophysical, Properties of Matter, Vol. 2), IFI/Plenum (1970).

3. W. R. Davis and A. Downs, Trans. J. British Ceramic Society, Vol. 79, No. 2 (1980), 44-52.

4. ASTM, 1980, Annual Book of ASTM Standards, Part 17, (1980).

5. W. J. Parker, R. J. Jenkins, C. P. Butler, and G. L. Abbot, J. Appl. Phys., Vol. 32, No. 9, (1961), 1679-1684.

6. R. C. Heckman, J. Appl. Phys., Vol. 44, No. 4, (1973), 1455-1460.

7. H. R. Shanks, A. H. Klein, and G. C. Danielson, J. Appl. Phys., Vol. 38, No. 7 (1967) 2885-2892.

Table 1. REFRACTORY TYPE AND DESCRIPTION

Manufacturer	Brick	Lab No.	Refractory Type	Density (gm/cm^3)	Chemical Composition (wt %) Al_2O_3	MgO	SiO_2	CaO	TiO_2	Fe_2O_3	Other
A	1	299	High Alumina	2.47	70.5	0.2	24.2	0.2	2.9	1.6	0.4
	2	298	High Alumina	2.38	50.5	0.4	44.5	0.2	2.3	1.3	0.8
	3	292	High Alumina	2.84	88.5	-	11.0	-	0.1	0.1	0.3
	4	315	Alumina-Silica (Insulating)	1.37	40.1	0.2	53.8	0.3	2.1	1.4	2.1
	5	314	Magnesite	2.96	-	95.7	-	2.4	-	-	1.9
	6	302	Carbon-Magnesite (Tar Impregnated)	3.10	0.2	96.0	1.2	2.4	-	0.2	-
	7	304	Carbon-Magnesite (Tar Bonded)	3.03	0.2	96.5	0.8	2.3	-	0.2	-
B	8	344	Magnesite	2.95	0.5	95.5	2.1	1.0	-	0.5	6.4
	9	343	Magnesite	2.83	8.2	90.2	0.8	0.6	-	0.2	-
	10	342	High Alumina	2.96	91.6	-	8.0	-	-	0.2	0.2
	11	345	Alumina-Chromia	3.27	89.6	-	0.1	-	0.2	0.1	(10.0 Cr_2O_3)

TABLE 2. SPECIFIC HEAT VALUES USED TO DETERMINE THE THERMAL CONDUCTIVITY

Temperature °C	Specific Heat (cal/g.C)			
	Refractory 1,2	Refractory 3,10,11	Refractory 4	Refractory 5-9
0	0.193	0.171	0.184	0.208
93	0.199	0.196	0.192	0.219
204	0.206	0.214	0.214	0.232
316	0.212	0.226	0.223	0.242
427	0.220	0.235	0.229	0.251
538	0.227	0.242	0.233	0.258
649	0.234	0.248	0.237	0.263
760	0.241	0.252	0.240	0.268
871	0.248	0.257	0.242	0.273
982	0.253	0.260	0.245	0.278
1093	0.258	0.264	0.247	0.283
1204	0.262	0.267	0.249	0.288
1316	0.266	0.270	0.251	0.293
1427	0.269	0.273	0.253	0.297
1538		0.276	0.255	
1649		0.279	0.256	
1760		0.282	0.258	

Table # 3

Thermal Diffusivity of Adjacent Samples in Refractory # 4 at Room Temperature Parallel to the Pressing Direction.

Sample Number	Thickness (10^{-1} cm)	$t_{1/2}$ (10^{-1} sec)	Th. Diff. (10^{-3} cm^2/sec)
1	2.11	8.80	7.19
2	2.33	11.0	6.85
3	2.12	8.50	7.34
4	2.10	8.15	7.51
5	2.20	9.50	7.07
6	2.33	10.5	7.18
7 *	2.08	8.40	7.15
8	2.12	8.80	7.09

AVERAGE DIFFUSIVITY = 0.00717 cm^2/sec

AVERAGE CONDUCTIVITY = 0.764 W/m·K

* Denotes specimen used for high temperature measurements

Table #4

Thermal Diffusivity of Adjacent Samples in Refractory #7 at Room Temperature Parallel to the Pressing Direction.

Sample Number	Thickness (10^{-1}cm)	$t_{1/2}$ (10^{-1}sec)	Th. Diff. ($10^{-2}cm^2/sec$)
1	2.11	2.18	2.83
2	2.23	1.16	5.95
3	2.22	1.44	4.75
4	2.20	2.20	3.05
5*	2.21	-	-
6	2.17	1.38	4.74
7	2.20	2.00	3.36
8	2.19	1.75	3.80
9	2.07	1.30	4.57
10	2.12	2.50	2.50

* Specimen damaged, not suitable for testing.

(table continued on next page)

Table # 4
(continued)
Thermal Diffusivity of Adjacent Samples in Refractory # 7
at Room Temperature Parallel to the Pressing Direction .

Sample Number	Thickness (10^{-1}cm)	$t_{1/2}$ (10^{-1}sec)	Th. Diff. (10^{-2}cm^2/sec)
11 **	2.18	1.78	3.71
12	2.22	2.60	2.63
13	2.11	2.53	2.44
14	2.23	2.50	2.76
15	2.26	2.80	2.53
16	2.22	2.05	3.34
17*	2.18	-	-
18	2.31	1.95	3.80
19	2.15	1.50	4.28

AVERAGE DIFFUSIVITY = 0.0359 cm^2/sec

AVERAGE CONDUCTIVITY = 9.60 W/m·K

* Specimen not suitable for testing.

** Denotes specimen used for high temperature measurements

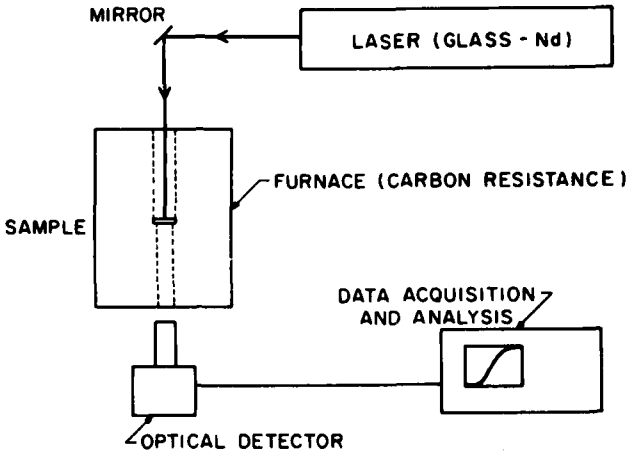

Fig. 1. Principal components of laser-flash diffusivity apparatus used in this study.

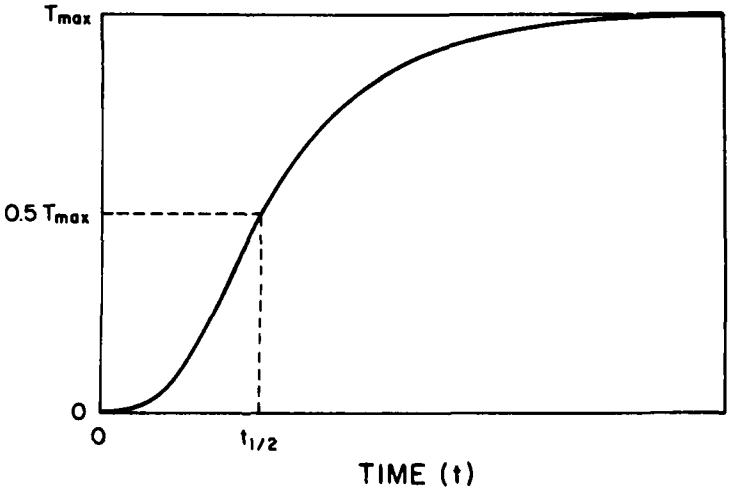

Fig. 2. Transient temperature response at back-surface of specimen following absorption of laser-flash at front surface.

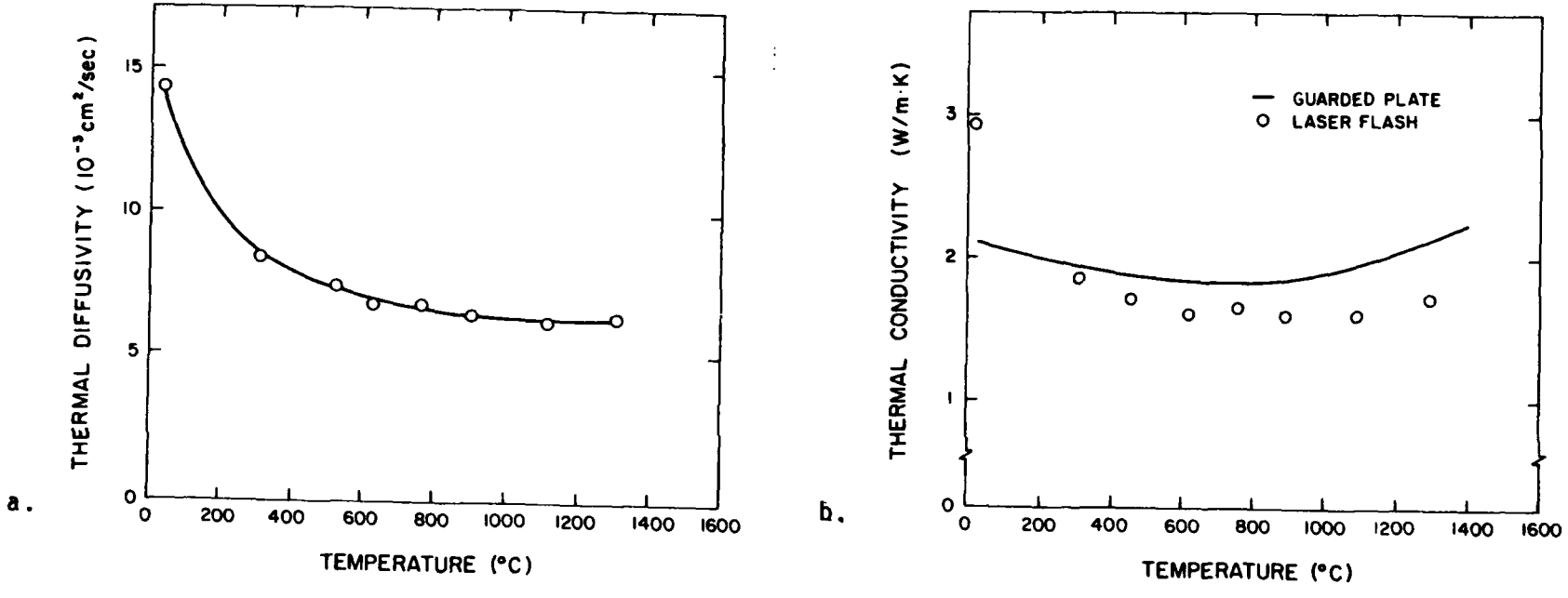

Fig. 3. Thermal diffusivity (a) and thermal conductivity (b) for high-alumina refractory (#1).

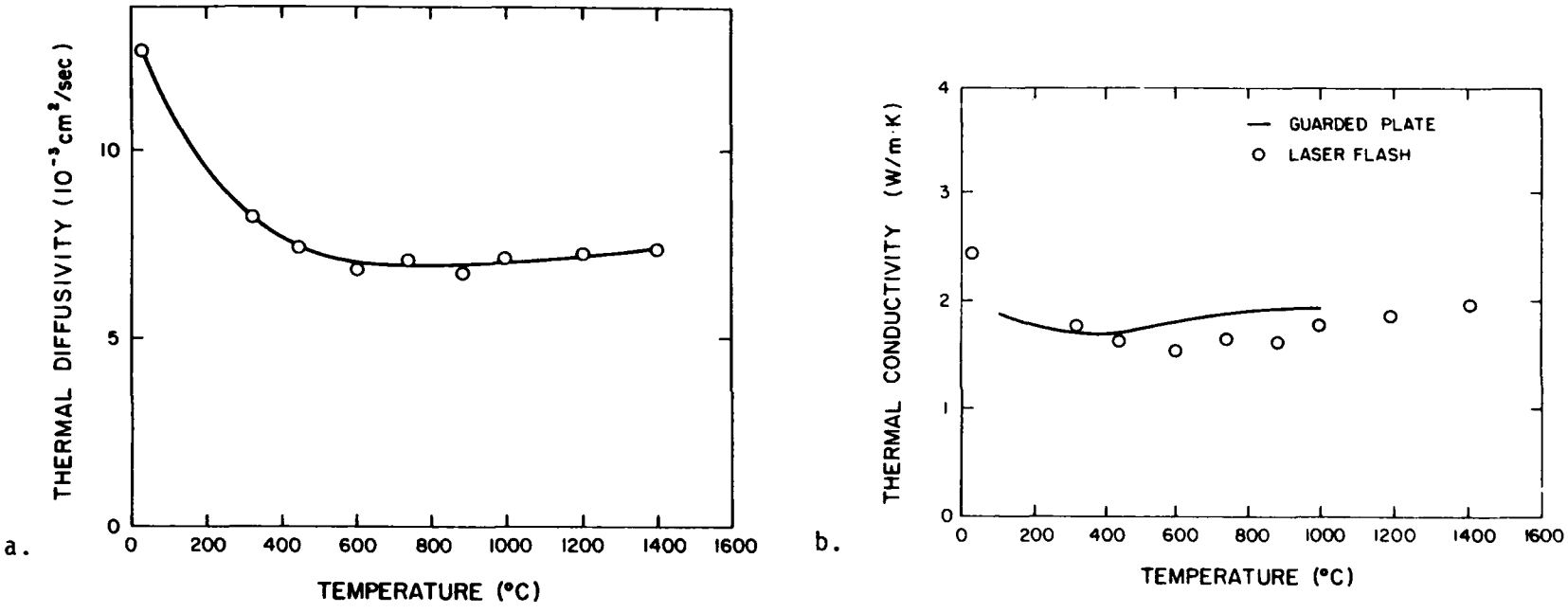

Fig. 4. Thermal diffusivity (a) and thermal conductivity (b) for high-alumina refractory (#2).

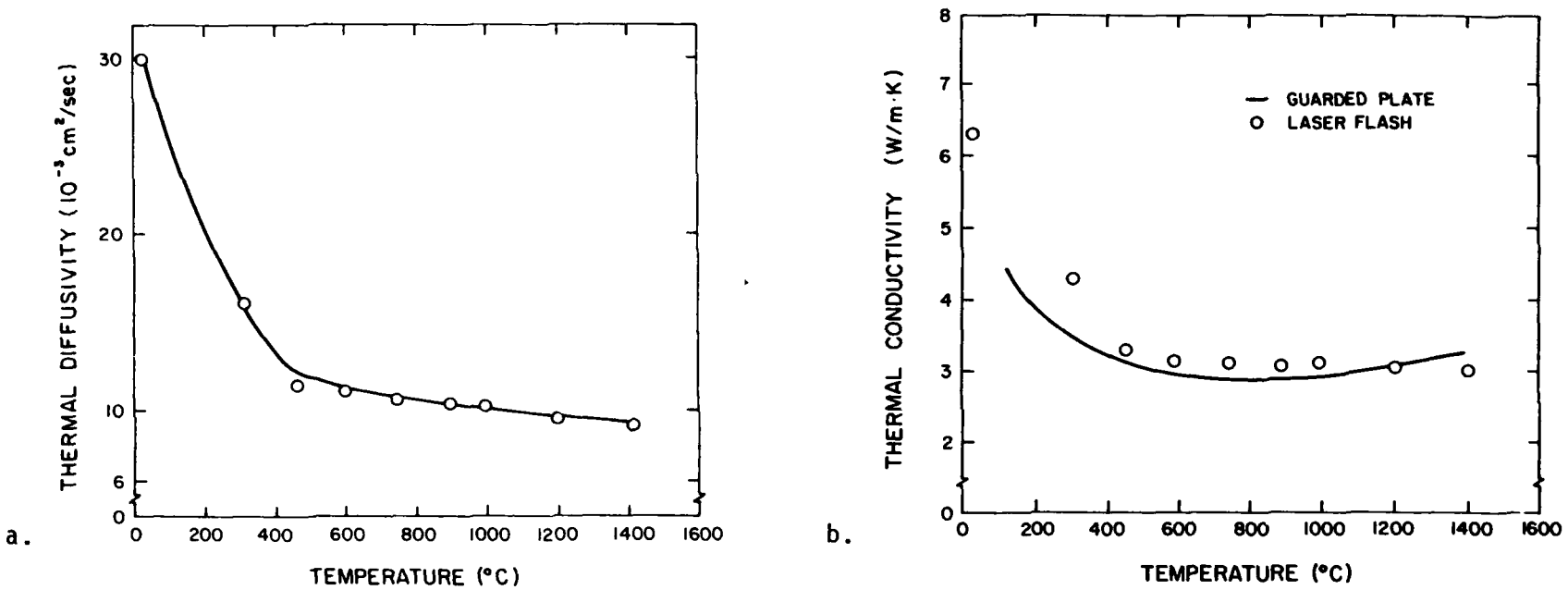

Fig. 5. Thermal diffusivity (a) and thermal conductivity (b) for high-alumina refractory (#3).

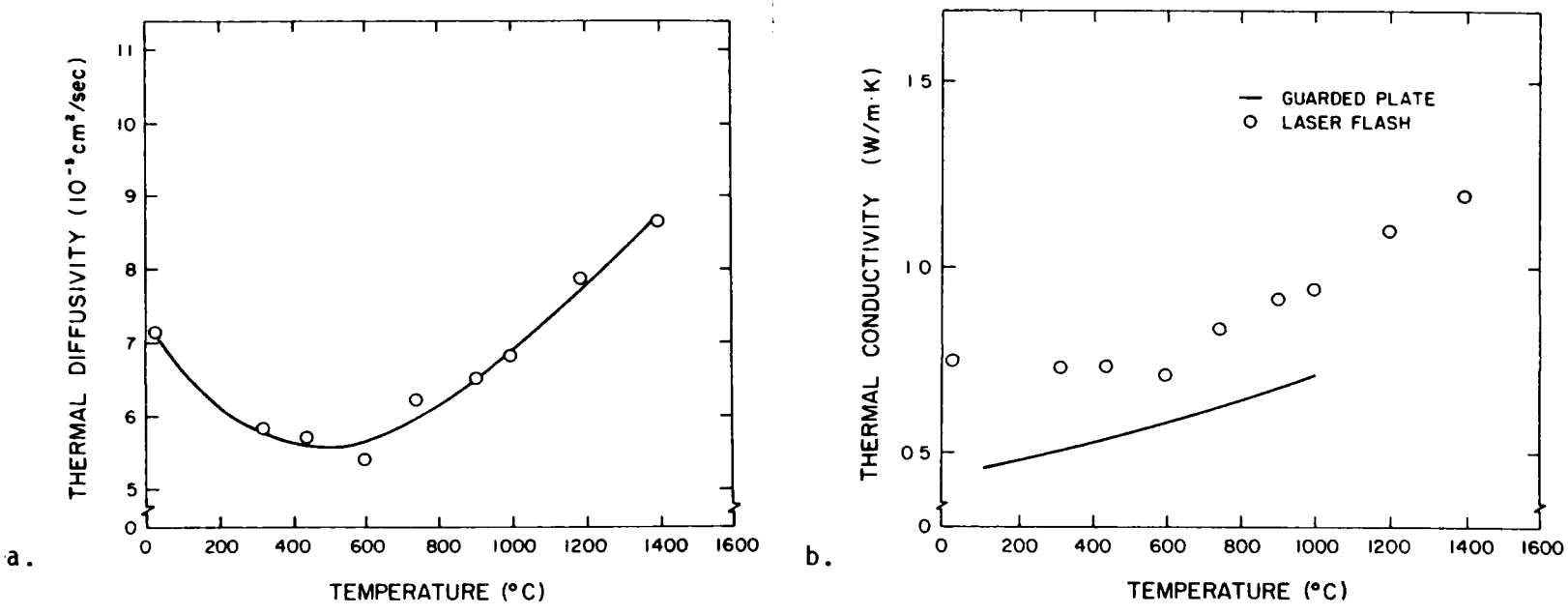

Fig. 6. Thermal diffusivity (a) and thermal conductivity (b) for porous alumina-silica refractory (#4).

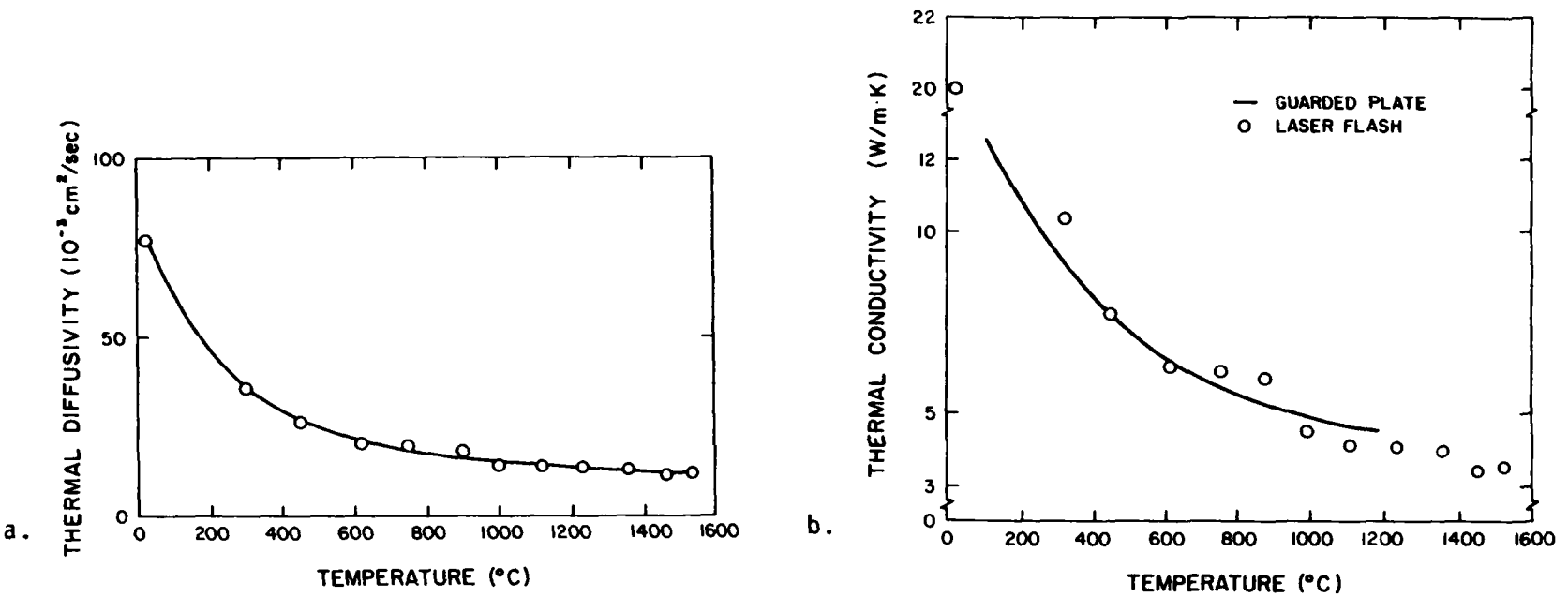

Fig. 7. Thermal diffusivity (a) and thermal conductivity (b) for magnesite refractory (#5).

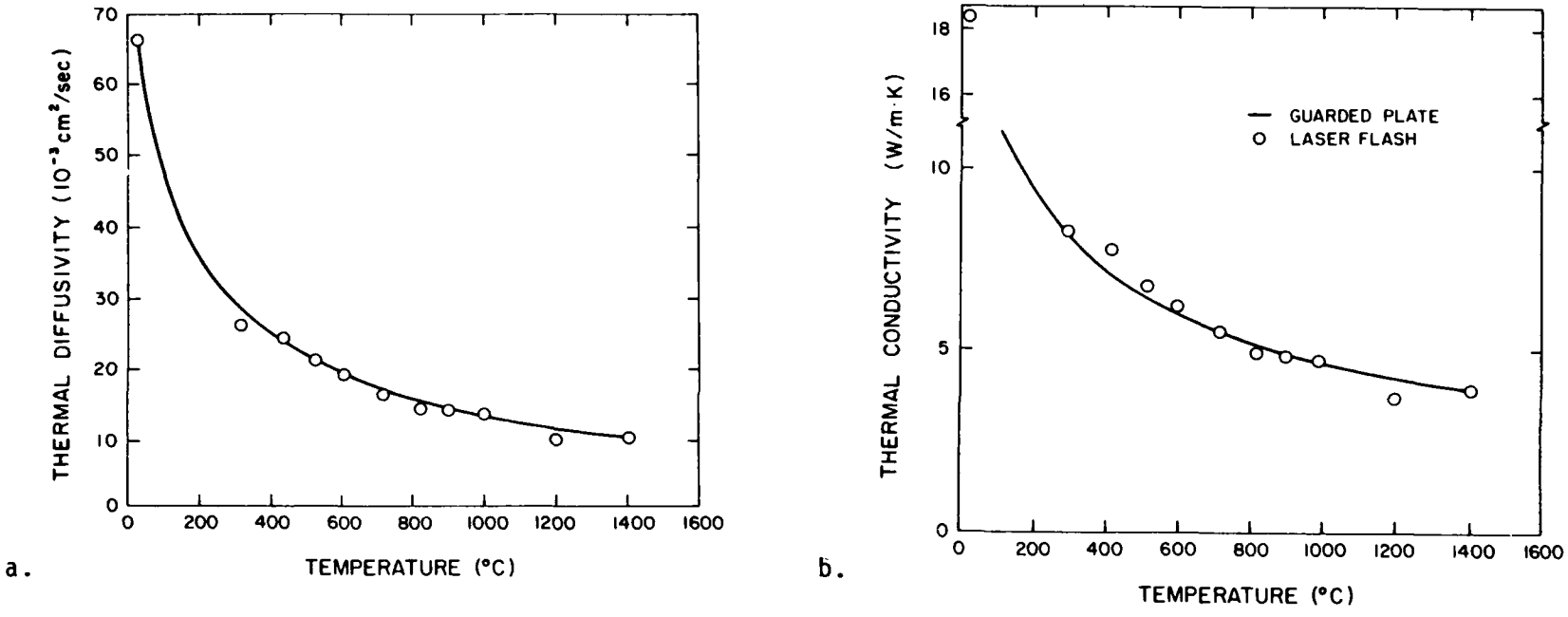

Fig. 8. Thermal diffusivity (a) and thermal conductivity (b) for tar-impregnated magnesite refractory (#6).

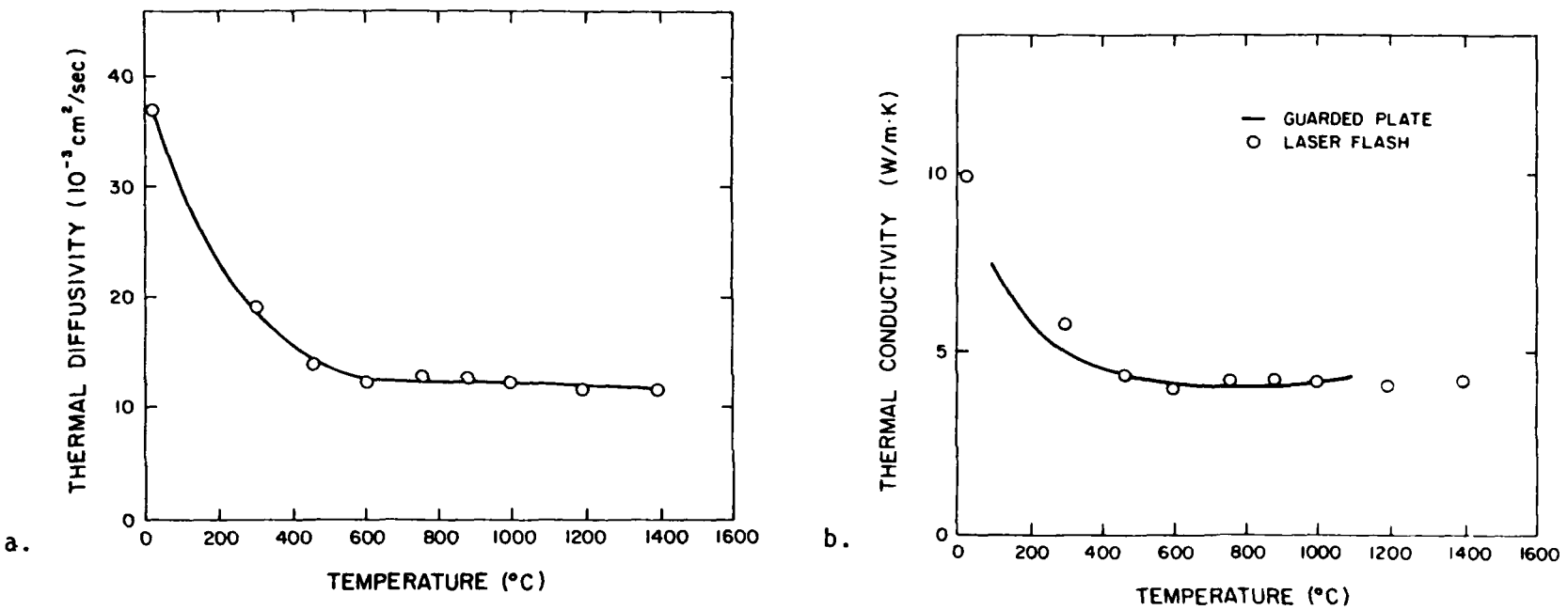

Fig. 9. Thermal diffusivity (a) and thermal conductivity (b) for tar-bonded magnesite refractory (#7).

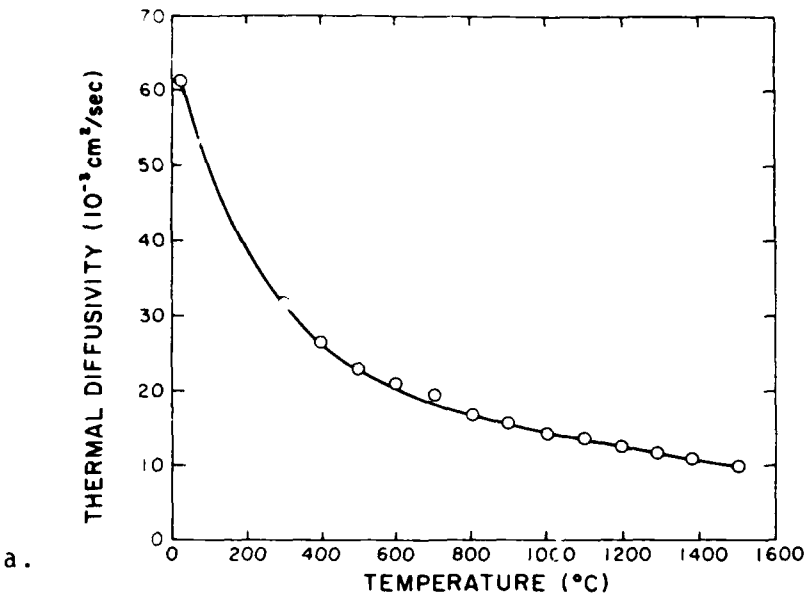

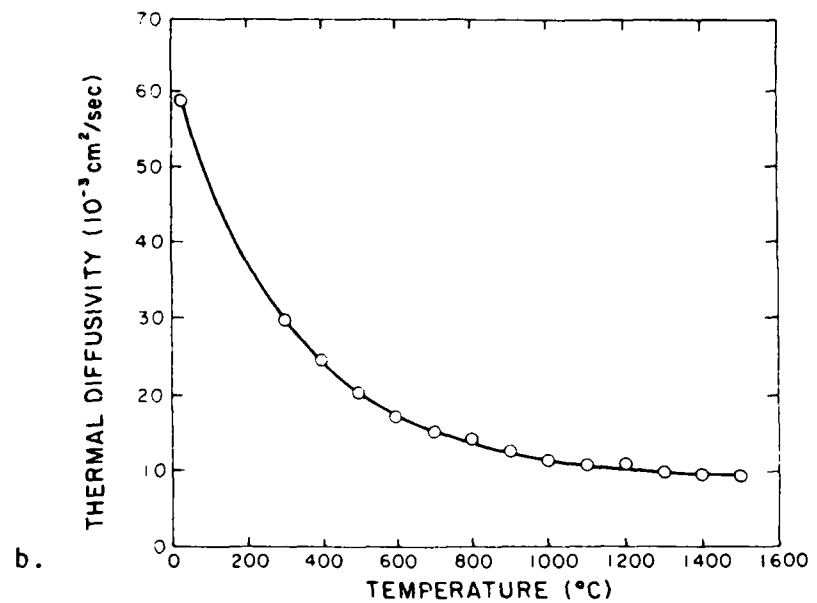

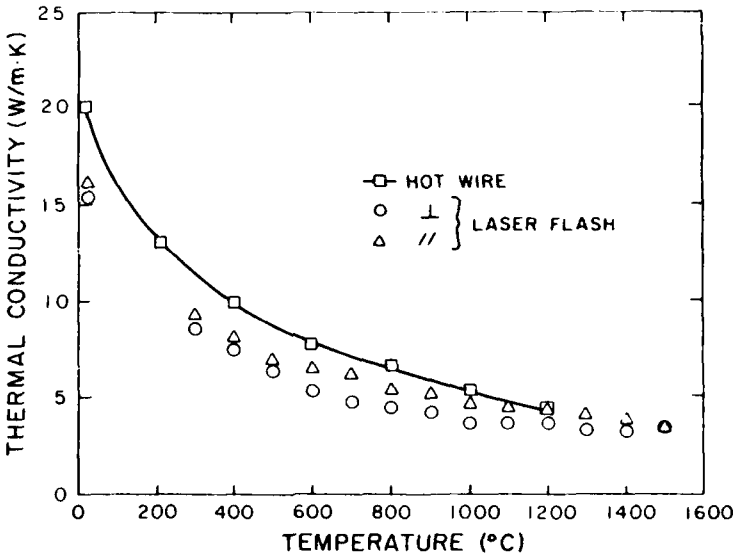

Fig. 10. Thermal diffusivity perpendicular (a) and parallel (b) to wide face magnesite refractory brick (#8) and corresponding thermal conductivity (c).

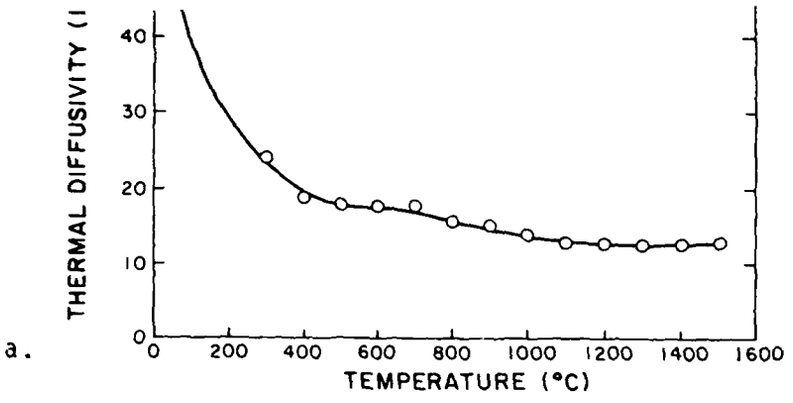

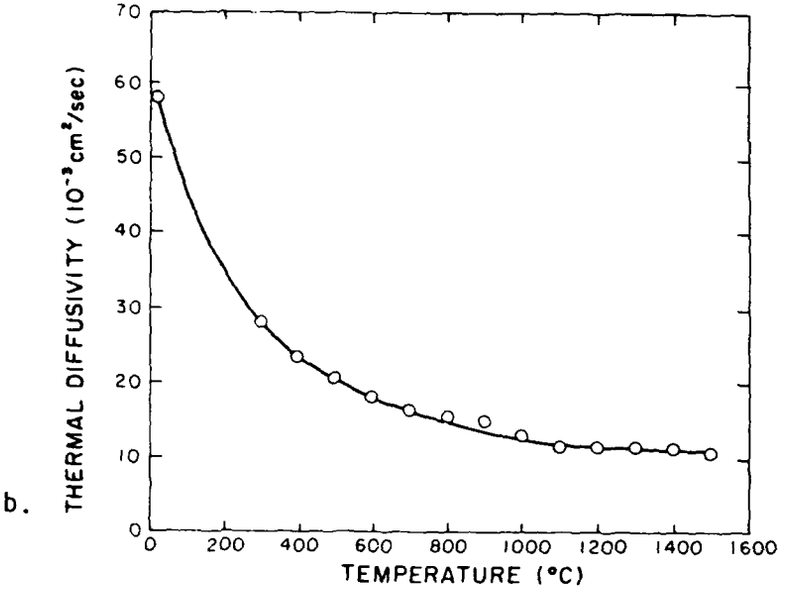

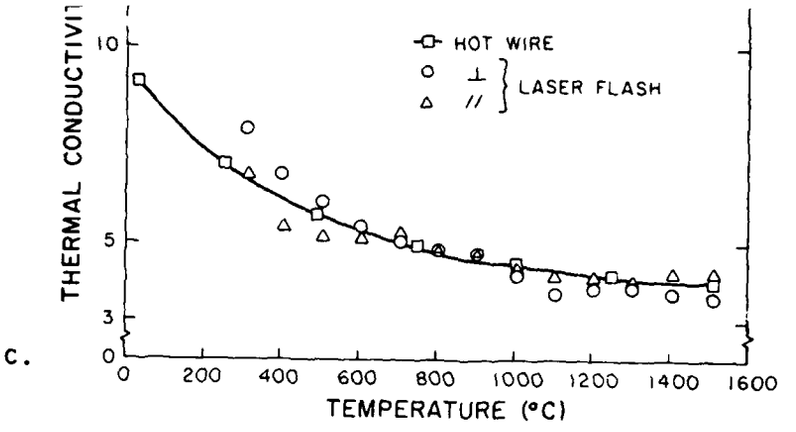

Fig. 11. Thermal diffusivity perpendicular (a) and parallel (b) to wide face of magnesite refractory #9 and corresponding values for the thermal conductivity (c).

a.

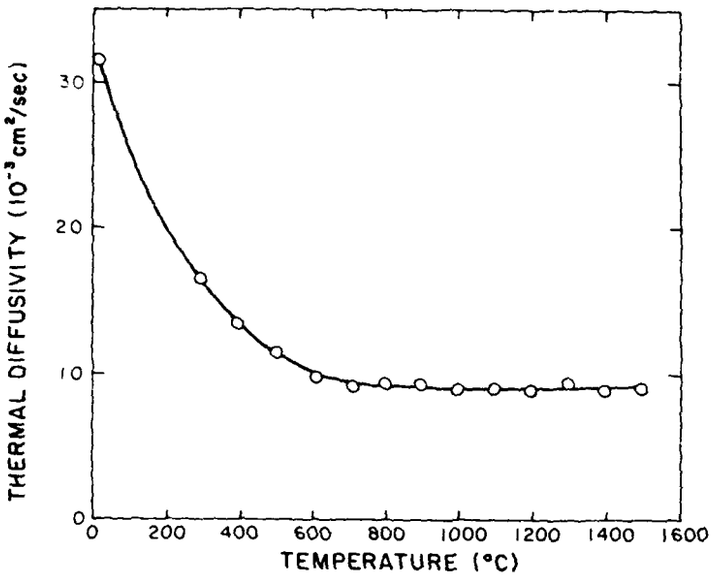

b.

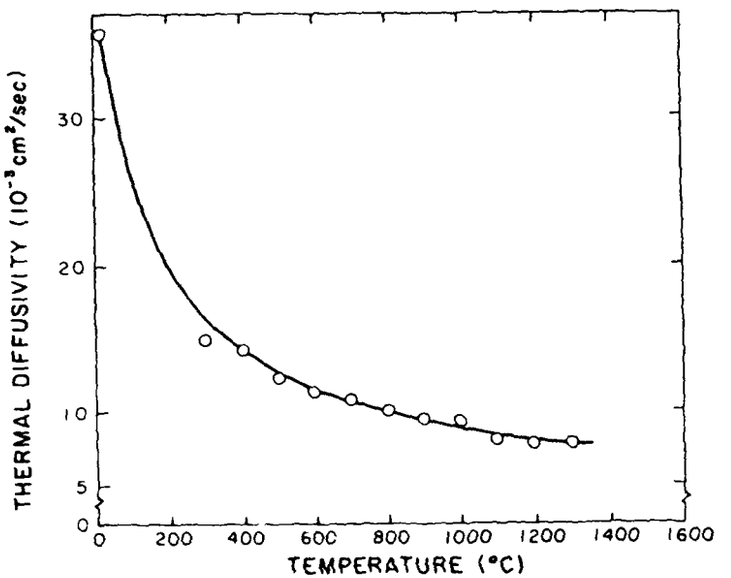

c.

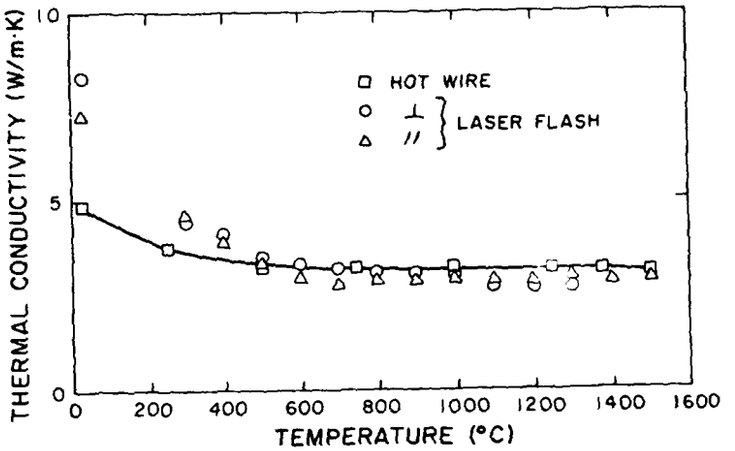

Fig. 12. Thermal diffusivity perpendicular (a) and parallel (b) to wide face of high-alumina refractory brick (#10) and corresponding thermal conductivity (c).

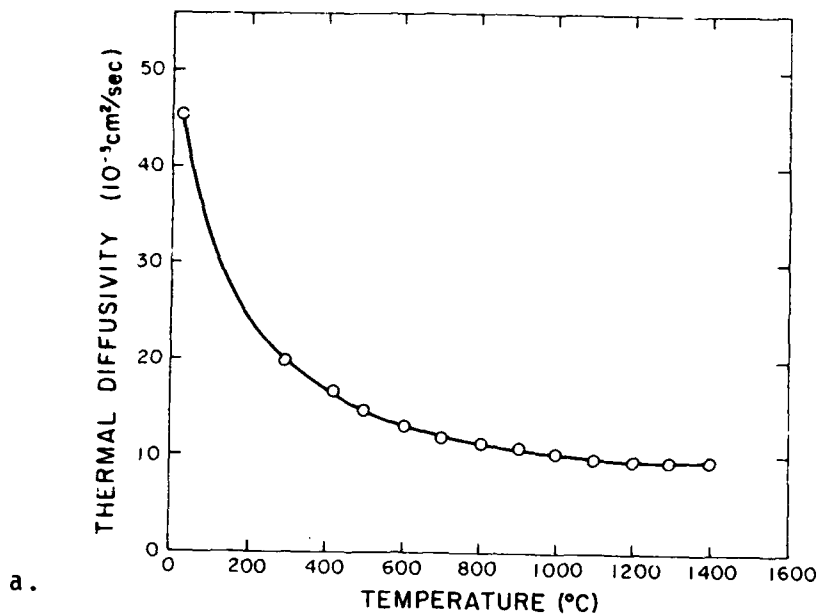

a.

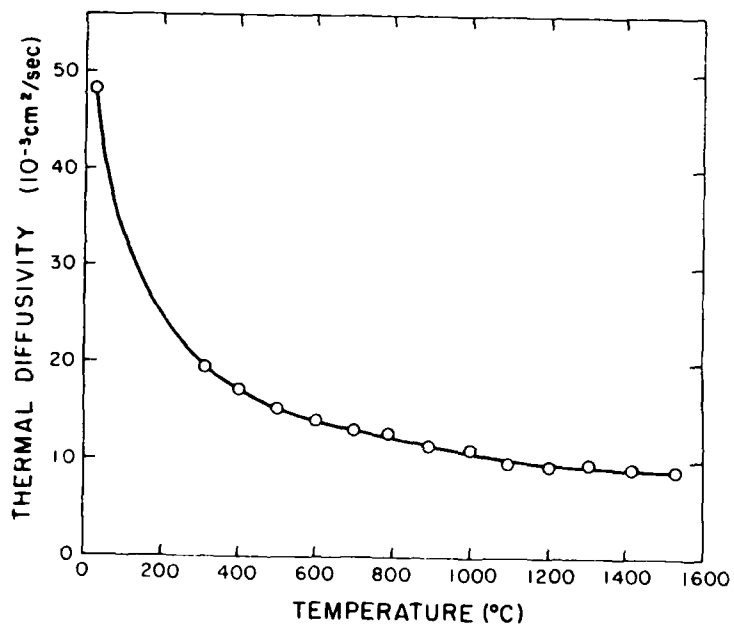

b.

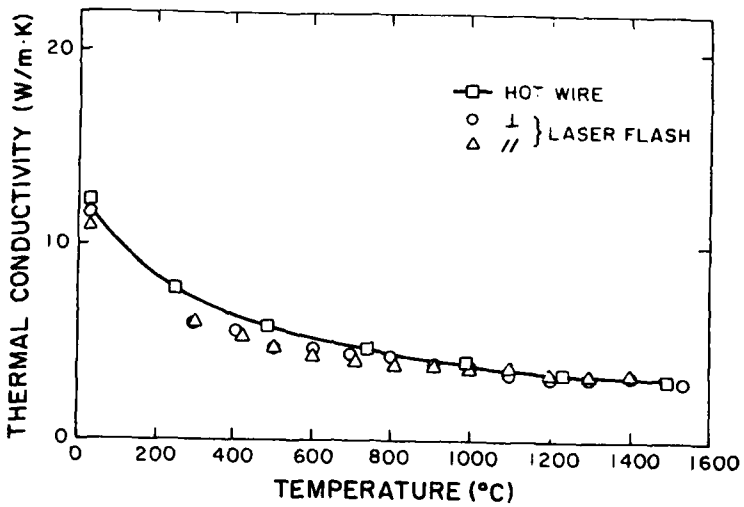

c.

Fig. 13. Thermal diffusivity perpendicular (a) and parallel (b) to wide face of alumina-chromia refractory (#11) and corresponding thermal conductivity (c).

CHAPTER IV

Effect of Interface Reflections and Angle of Incidence of Radiation on Thermal Stresses in Semi-transparent Materials

by

J. R. Thomas, Jr.
J. I. Frankel
Department of Mechanical Engineering

and

D. P. H. Hasselman
Department of Materials Engineering

Virginia Polytechnic Institute and State University
Blacksburg, Virginia 24061

Background and Objectives

In several previous papers [1-7] the present authors and co-workers have presented the results of studies on the thermal stresses produced by suddenly applied [1-5] or suddenly removed [6-7] radiation heating of semi-transparent material. In all cases we assumed well-collimated incident radiation striking a flat plate of the material in question and being absorbed through-the-thickness of the plate. We also assumed normal incidence of the radiation, and ignored internal reflections. In the case of nuclear radiation, no surface reflections occur and if the material is either purely absorbing or optically thin, these assumptions lead to a realistic model of the heat generation. If the heating is produced by thermal radiation, on the other hand, even in a purely absorbing medium some reflection occurs at the material interfaces due to the different indices of refraction, and this would be further complicated by non-normal incidence. It is then natural to ask if such reflections significantly alter the heat generation and thermal stress, and what the effect of varying the angle of incidence would be. In the work reported here we provide answers to some of these questions.

Our objectives here are to determine the effects of interface reflections on the thermal stresses generated by radiation absorption in a semi-transparent flat plate, and to study the effect of varying the angle of incidence. We consider both suddenly applied radiation, and a sudden interruption of radiation from an established steady-state condition. Reflections at the surface of the plate should result in "trapping" more of the radiation within the plate, and thus to a larger volumetric heat source. Whether or not this leads to increased thermal

stress can only be determined by analysis. However, varying the angle of incidence away from normal increases the surface reflection from the plate, but it also increases the path length of the radiation within the plate, changes which should have opposite effects on the heat generation. Again, only analysis can determine the net result, as we shall see.

Method of Analysis

Consider a flat plate of thickness $w = 2a$ (See Fig. 1) insulated on the front face ($x = 0$) and cooled on the rear face ($x = w$) by a convective medium at temperature T_∞ and heat transfer coefficient h. The plate is assumed to be initially in equilibrium at temperature T_∞; at time $t = 0$, a collimated beam of thermal radiation of intensity I_o is applied to the surface at $x = 0$ at an incidence angle ϕ. This radiation originates in a medium of refractive index n_o, while the plate has index of refraction n_1 and the convective medium n_2. To determine the thermal stresses generated by absorption of the radiation, we must (a) formulate the appropriate volumetric-heat-source term for the conduction equation; (b) solve the conduction equation for the unsteady temperature profile $T(x,t)$; and (c) compute the thermal stress $\sigma_{yz}(x,t)$ from the temperature profile. Since we want to compute the thermal stresses both for suddenly applied and suddenly removed incident radiation, the analysis in parts (b) and (c) must be performed for both of these cases.

We first derive an expression for the heat source $g'''(x,\phi)$ by summing the contributions from each pass of the radiation through the plate resulting from successive reflections at the plate surfaces, as shown in Fig. 2. We assume a purely absorbing medium with absorption (extinction) coefficient μ. The angle of incidence ϕ and the refracted

angle θ are related through the complex refractive indices of the two materials [8]. At a given depth x into the medium, it is necessary to add heat generation due to radiation absorption at points 1, 2, 3, .. . A fraction ρ_1 is reflected at the first interface, so that at point 1, the radiation intensity is

$$I_0 (1 - \rho_1) \exp (- \mu L_1),$$

where

$$L_1 = x/\cos\theta . \tag{1}$$

Similarly at point 2, the intensity is

$$I_0 (1 - \rho_1) \rho_2 \exp [- (L + L_2)],$$

where

$$L_2 = (w - x)/\cos\theta, \tag{2}$$

and

$$L = L_1 + L_2. \tag{3}$$

Thus, in general, the intensity at x is

$$I(x) = I_0 (1 - \rho_1) \left\{ e^{-\mu L_1} [1 + \rho_1\rho_2 e^{-2\mu L} + \left(\rho_1\rho_2 e^{-2\mu L}\right)^2 + \left(\rho_1\rho_2 e^{-2\mu L}\right)^3 + \ldots] + \rho_2 e^{-\mu(L + L_2)} [1 + \rho_1\rho_2 e^{-2\mu L} + \left(\rho_1\rho_2 e^{-2\mu L}\right)^2 + \left(\rho_1\rho_2 e^{-2\mu L}\right)^3 + \ldots] \right\} . \tag{4}$$

Summing the geometric series, we find

$$I(x) = I_0 (1 - \rho_1) \left[\frac{e^{-\mu L_1} + \rho_2 e^{-\mu(L + L_2)}}{1 - \rho_1 \rho_2 e^{-2\mu L}} \right] , \tag{5}$$

or explicitly in terms of x, w, and θ,

$$I(x) = I_0(1 - \rho_1) \left[\frac{e^{-\mu x/\cos\theta} + \rho_2 e^{-\mu(2w - x)/\cos\theta}}{1 - \rho_1 \rho_2 e^{-2\mu w/\cos\theta}} \right]. \tag{6}$$

The volumetric heat source at location x is then

$$g'''(x,\phi) = \mu I(x), \tag{7}$$

i.e. the rate of absorption of the radiation at x with I(x) given by Eq. (6). It must be recognized in Eq. (6) that the reflectivities ρ_1 and ρ_2 also depend on θ (and thus ϕ) through the refractive indexes n_0, n_1, and n_2 [8].

(a) Suddenly applied radiation

We seek a solution of the heat conduction equation

$$k \frac{\partial^2 T}{\partial x^2} (x,t) + g'''(x) = \rho c \frac{\partial T}{\partial t} , \quad t > 0, \tag{8}$$

where T(x,t) represents the temperature at location x at time t, k the thermal conductivity, ρ the density, and c the specific heat capacity. The appropriate boundary conditions for this case are

$$\frac{\partial T}{\partial x} (0,t) = 0 , \tag{9}$$

$$- k\frac{\partial T}{\partial x}(w,t) = h\,[T(w,t) - T_\infty], \tag{10}$$

with initial condition

$$T(x,0) = T_\infty. \tag{11}$$

Using standard techniques [9] we find the solution to be

$$T_1(x,t) = T_\infty + \sum_{n=0}^{\infty} B_n(t) \cos(\lambda_n x),\ 0 \le x \le w,\ t > 0, \tag{12}$$

where

$$B_n(t) = (\Omega_{1n} + \Omega_{2n})\,(1 - e^{-\kappa\lambda_n^2 t})/\lambda_n^2 N_n. \tag{13}$$

In Eq. (13),

$$N_n = \frac{w}{2} + \frac{\sin(2\lambda_n w)}{4\lambda_n}, \tag{14}$$

$$\Omega_{1n} = \frac{\phi_1}{\mu^2 + \lambda_n^2 \cos^2\theta}\left\{e^{-\mu w/\cos\theta}[-\mu\cos\theta\cos(\lambda_n w) + \lambda_n \sin(\lambda_n w) \cdot \cos^2\theta] + \mu\cos\theta\right\}, \tag{15}$$

$$\Omega_{2n} = \frac{\phi_2}{\mu^2 + \lambda_n^2 \cos^2\theta}\left\{e^{\mu w/\cos\theta}[\mu\cos\theta\cos(\lambda_n w) + \lambda_n \sin(\lambda_n w) \cos^2\theta] - \mu\cos\theta\right\}, \tag{16}$$

where

$$\phi_1 = \frac{1}{k}\left[\frac{\mu I_0 (1-\rho_1)}{1-\rho_1\rho_2 \exp(-2\mu w/\cos\theta)}\right], \tag{17}$$

and

$$\phi_2 = \phi_1 \rho_2 \exp(-2\mu w/\cos\theta) . \tag{18}$$

The eigenvalues λ_n are the roots of the transcendental equation

$$\lambda_n \tan(\lambda_n w) = \frac{h}{k} . \tag{19}$$

The thermal stresses are computed from the well-known equation for an unconstrained flat plate [10],

$$\sigma_{yz}(x,t) = \frac{\alpha E}{1-\nu}\left[-T(x,t) + \frac{1}{2a}\int_{-a}^{a} T(\xi,t)d\xi + \frac{3x}{2a^3}\right.$$
$$\left.\cdot \int_{-a}^{a} \xi T(\xi,t)d\xi\right] \tag{20}$$

where, for convenience, we have now shifted the origin of coordinates to the center of the plate such that $-a \leq x \leq a$. Substituting Eq. (12) into Eq. (20) and performing the indicated integrations, we find

$$\sigma_{yz}(x,t) = \frac{\alpha E}{1-\nu}\sum_{n=1}^{\infty} B_n(t) F_n(x) , \tag{21}$$

where

$$F_n(x) = \left[-\cos \lambda_n (x + a) + \frac{\sin 2\lambda_n a}{2\lambda_n a} - \frac{3x}{2a^3} \left(\frac{2 \sin^2 \lambda_n a}{\lambda_n^2} - \frac{a \sin 2\lambda_n a}{\lambda_n} \right) \right], \quad -a \leq x \leq a, \; t \geq 0. \tag{22}$$

We will study this result in more detail in a future section.

(b) Suddenly interrupted radiation

For generality, we assume that the incident radiation is interrupted after a time interval τ; $\tau \to \infty$ corresponds to equilibrium conditions and can easily be recovered from the following general result. We thus seek a solution to Eq. (8) subject to boundary conditions (9) and (10), but with initial condition

$$T(x,0) = T_\infty + \sum_{n=0}^{\infty} B_n (\tau) \cos \lambda_n x, \quad 0 \leq x \leq w . \tag{23}$$

The solution is easily shown to be

$$T(x,t) = T_\infty + \sum_{n=0}^{\infty} B_n (t) e^{-\kappa \lambda_n^2 t} \cos \lambda_n x, \; 0 \leq x \leq w , \tag{24}$$

with corresponding thermal stress distribution

$$\sigma_{yz} (x,t) = \frac{\alpha E}{1-\nu} \sum_{n=0}^{\infty} B_n (t) e^{-\kappa \lambda_n^2 t} F_n (x) , \quad -a \leq x \leq a . \tag{25}$$

In the following section we display computed results from these equations, and in particular, we examine the effect of varying the incidence angle ϕ and the role of multiple surface reflections. It is clear from Eqs. (15-19) that ϕ enters in a rather complicated fashion, particularly since ρ_1 and ρ_2 also depend on θ and ϕ through the complex refractive indices for absorbing media [8].

Numerical Results

To illustrate the effects of interest to this investigation we use a particular example of a glass with wavelength dependence of transmittance as shown in Fig. (3) [11]. This introduces another variable to be considered, but it does help show the role of the extinction coefficient μ, since we exhibit results for 2.6 and 3.5 μm, respectively, where the absorption coefficients are quite different.

In Figs. (4) and (5) we display the non-dimensional temperature and the stress distributions as computed from Eqs. (12) and (22) immediately after the radiation begins. The non-dimensional temperature is defined as

$$T^*(x,t) = \frac{T(x,t) - T_\infty}{T_F - T_\infty} \tag{26}$$

where T_F is the temperature at which the material fails. It is clear that the greater temperature rise occurs at normal incidence ($\phi = 0°$). However, the stresses are greatest for a 60° incidence angle. This is illustrated more clearly in Fig. (6), where we plot the maximum tensile stress as a function of incidence angle for two different wavelengths. Both curves show a broad maximum in the region near $\phi = 60°$. Thus, apparently at this incidence angle, the competing effects of increased reflection at the surface and greater path length in the plate are just balanced. The overall stress levels are higher at 2.6 μm because the absorption coefficient μ is much larger at this wavelength.

We would like to assess the effect of ignoring multiple surface reflections on the temperature and stress profiles. In Fig. (7) we have plotted the non-dimensional temperature profile immediately after

application of the radiation at normal incidence. The two curves represent temperature profiles resulting from the heat source distribution $g'''(x,0°)$, which includes reflections, and the heat source $g'''(x)$, which does not. Figure (8) shows the corresponding stress distributions. It is seen that the temperature profile shows a miximum difference of about 20% at the right face, away from the incident radiation. The maximum difference in the stress distributions occurs at the center of the plate, and is of the order of 5%.

The stress levels predicted in our analysis are still well below the failure stress for the material considered [11] because this material has a very low thermal expansion coefficient. A radiation source of the intensity used in these calculations ($5 \times 10^6 W/cm^2$) would melt the material before it would fracture. Many other brittle materials, however, have much larger values of thermal expansion coefficient and the stresses will be correspondingly higher. In these cases, the structure could will fail by thermal stress fracture.

If the radiation is incident for a time interval of sufficient length to allow an equilibrium temperature distribution to be established, and the heat source is then suddenly removed, the rapid collapse of the temperature profile can again produce large stresses. The resulting stress distribution will depend on the angle of incidence of the radiation through the initial temperature profile. This is illustrated in Fig. (9) where we have plotted the maximum tensile stress at several times during the cooling phase vs. angle of incidence. It is seen that at early times the maximum stresses still occur for an incidence angle near 60°, but as time passes this effect is gradually lost. After

out 10 seconds, for this case, all history of the incidence angle has disappeared.

The evolution of the temperature and stress profiles during the cooldown phase is clearly apparent from Figs. (10) and (11). In these figures I show temperature and stress distributions at several times after the eat source is removed, with time displayed on a third axis. With the ft face no longer receiving radiation, the temperature there drops most pidly, and the profile changes from concave-up to concave-down. The ress distribution (Fig. 11) thus shifts from concave-down to concave-. At intermediate times, however, the stress distribution shows two cal minima which can be correlated with inflection points in the mperature profiles. Thus it appears that the stress profile always splays concavity opposite to that of the temperature profile.

nclusions

It is clear from the above that multiple surface reflections and n-normal incidence angles can be accounted for quite straightewardly in studies of thermal stresses generated by radiation heat-g. Temperatures throughout the medium decrease monotonically as angle of incidence increases, whereas the largest thermal stress ses through a broad maximum near an incidence angle of 60°. Thus would be advantageous in design of structures exposed to transient iation heating to avoid incidence angles near 60°. Upon sudden intertion of the radiation, this same effect appears during the early ges of the cooldown, but gradually disappears as the history of original heating pattern is lost.

For radiation at normal incidence, ignoring surface reflections leads to a maximum error of approximately + 20% in the temperature distribution, but no more than + 10% in the thermal stress.

References

1. D. P. H. Hasselman, J. R. Thomas, Jr., M. P. Kamat, and M. Satyamurthy, Thermal Stress Analysis of Partially Absorbing Brittle Ceramics Subjected to Symmetric Radiation Heating, J. Am. Ceram. Soc., Vol. 63, pp. 169-173, 1980.

2. J. P. Singh, J. R. Thomas, Jr., and D. P. H. Hasselman, Thermal Stresses in a Partially Absorbing Flat Plate Asymmetrically Heated by Thermal Radiation and Cooled by Convection, J. Therm. Stresses, Vol. 3, pp. 341-349, 1980.

3. J. R. Thomas, Jr., J. P. Singh, and D. P. H. Hasselman, Analysis of Thermal Stress Resistance of Partially Absorbing Ceramic Plate Subjected to Asymmetric Radiation, I: Convective Cooling at Rear Surface, J. Am. Ceram. Soc., Vol. 64, pp. 163-169, 1981.

4. J. P. Singh, K. Satyamurthy, J. R. Thomas, Jr., and D. P. H. Hasselman, Analysis of Thermal Stress Resistance of Partially Absorbing Ceramic Plate Subjected to Asymmetric Radiation, II: Convective Cooling at Front Surface, J. Am. Ceram. Soc., Vol. 63, pp. 21-25, 1980.

5. J. R. Thomas, Jr., J. P. Singh, and D. P. H. Hasselman, Thermal Stresses in a Partially Absorbing Flat Plate Asymmetrically Heated by Cyclic Thermal Radiation and Cooled by Convection, (In press).

6. J. I. Frankel, J. P. Singh, J. R. Thomas, Jr., and D. P. H. Hasselman, Thermal Stresses in Partially Absorbing Flat Plate Due to Sudden Interruption of Steady-State Asymmetric Radiation, I: Convective Cooling at Rear Surface, J. Therm. Stresses, (in press).

7. J. P. Singh, J. I. Frankel, J. R. Thomas, Jr., and D. P. H. Hasselman, Thermal Stresses in Partially ABsorbing Flate Plate Due to Sudden Interruption of Steady-State Asymmetric Radiation, II: Convective Cooling at Front Surface, J. Therm. Stresses, (in press)

8. R. Siegel, and J. R. Howell, Thermal Radiation Heat Transfer, 2nd ed., McGraw-Hill Book Co, New York, 1981.

9. V. S. Arpaci, Conduction Heat Transfer, Addison-Wesley, Reading, Mass., 1966.

10. B. A. Boley, and J. H. Weiner, Theory of Thermal Stresses, John Wiley & Sons, Inc., New York, 1960.

11. Corning Premium-quality Fused Silica Low-expansion Material Code 7940, FS 7940/9-78(A), Corning Glass Works, Corning, N.Y.

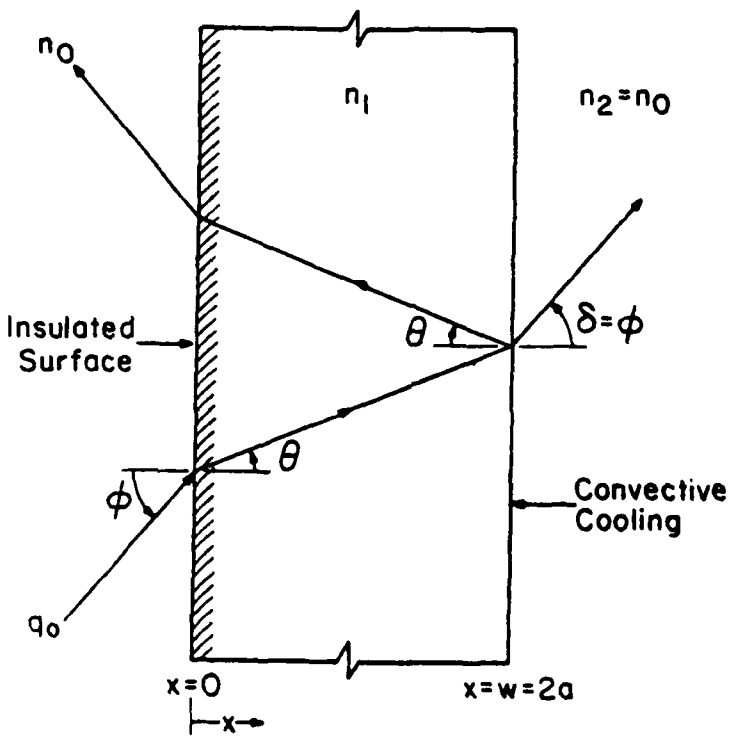

Figure 1. Problem Geometry

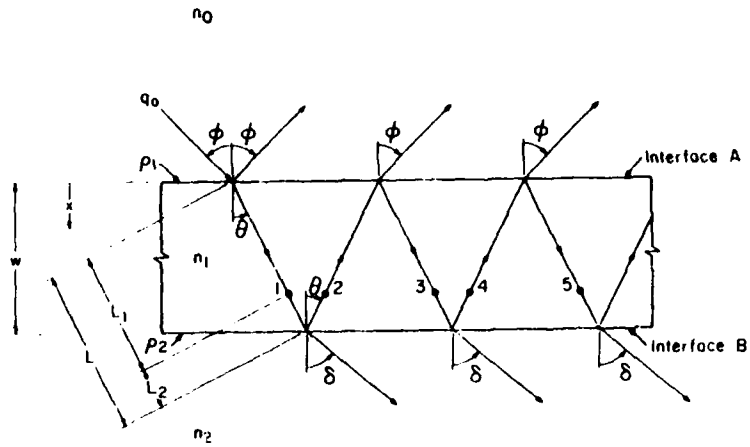

Figure 2. Ray tracing to determine the total energy absorption rate

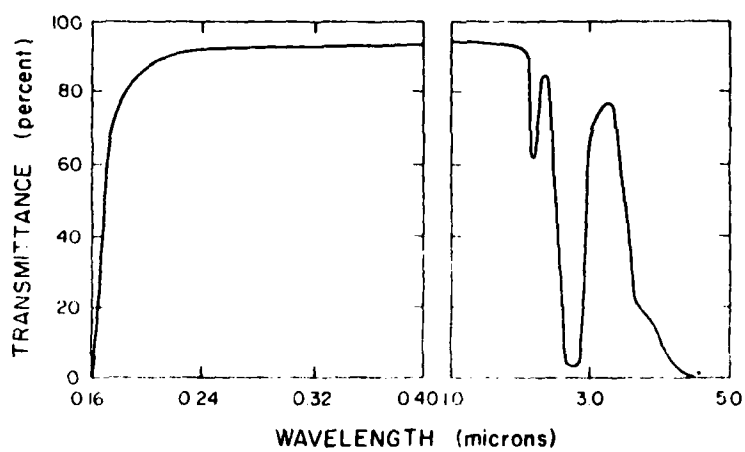

Figure 3. Wavelength dependence of transmittance for a 1 cm. thick Fused Silica #7940 glass plate at 20°C (from Ref. 11).

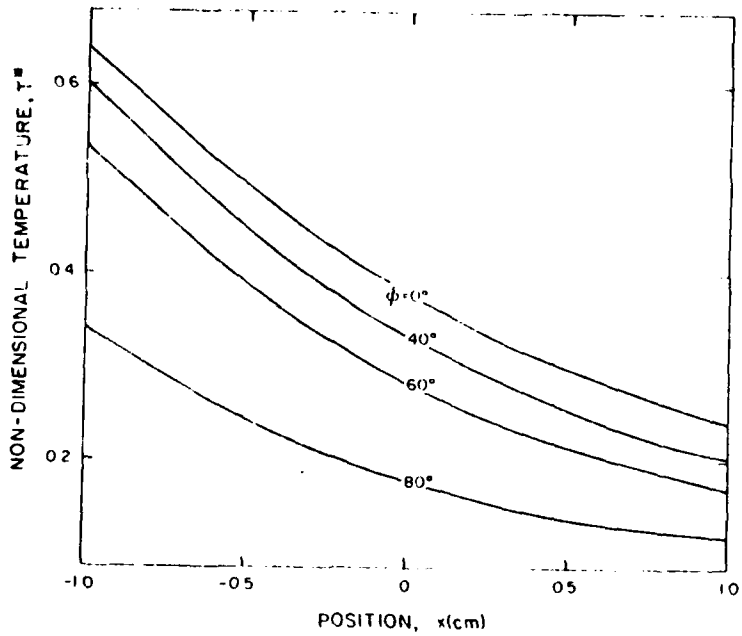

Figure 4. Non-dimensional temperature distribution for the heated plate at $t = 10^{-6}$ seconds for various incidence angles ϕ.

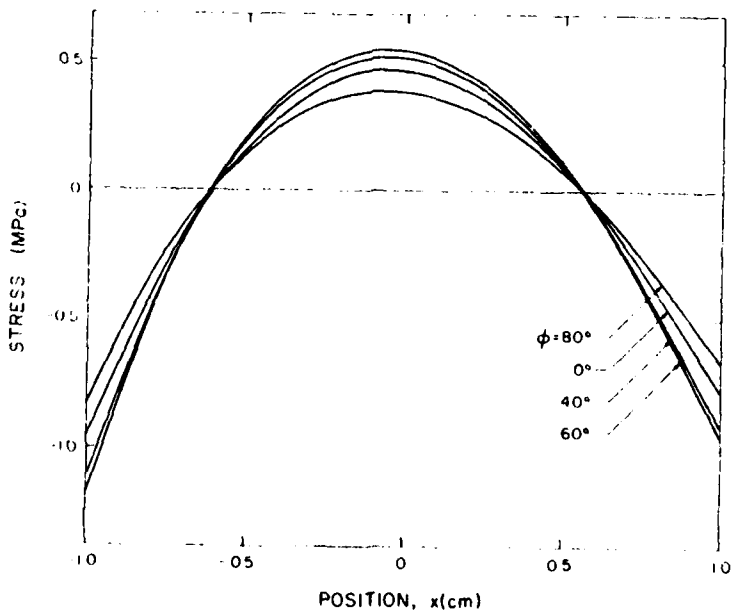

Figure 5. Stress distribution for the heated plate at 10^{-6} seconds for various incidence angles.

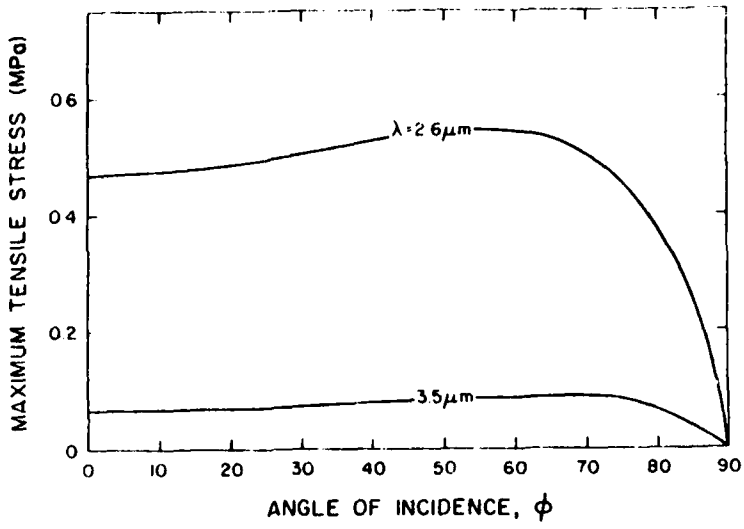

Figure 6. Maximum tensile stress in the heated plate at $t = 10^{-3}$ seconds as a function of incidence angle for two different wavelengths.

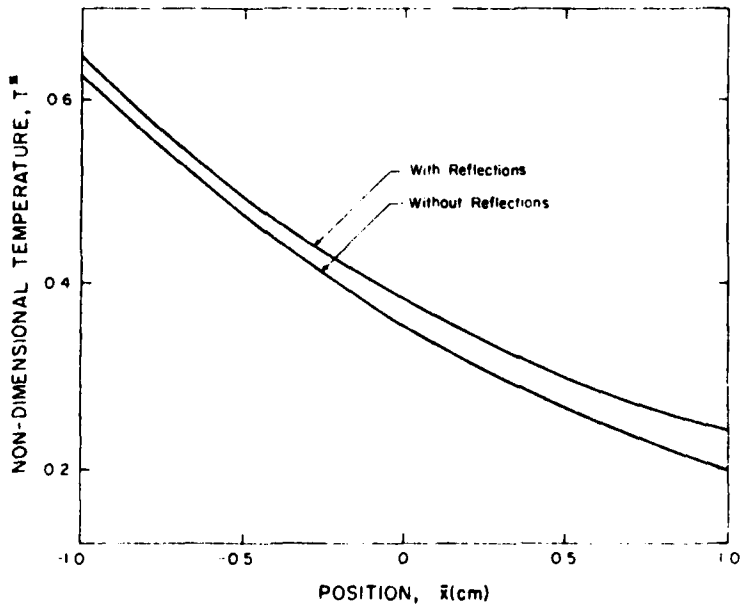

Figure 7. Effect of interface reflections on the non-dimensional temperature distribution in a heated flat plate at $t = 10^{-2}$ seconds, normal incidence, $\lambda = 2.6$ μm.

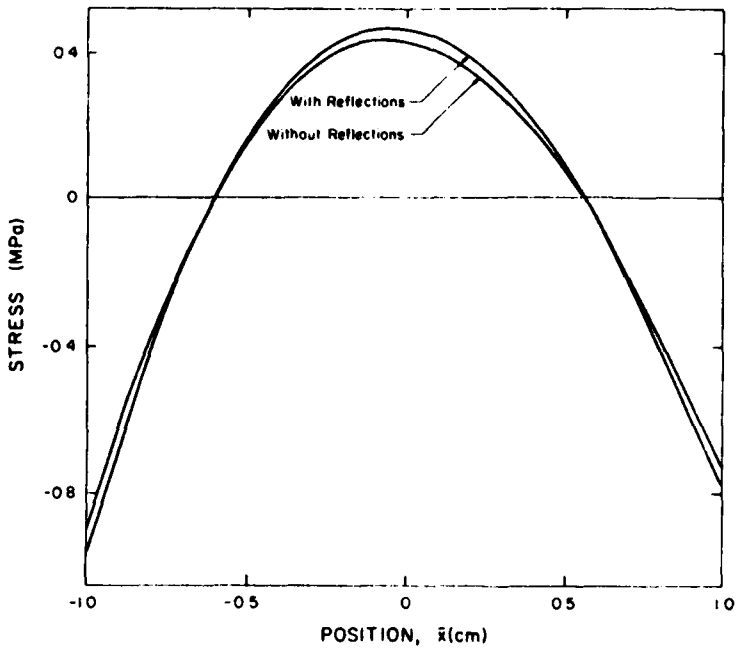

Figure 8. Effect of interface reflections on the stress distribution in a heated flat plate at $t = 10^{-2}$ seconds, normal incidence, $\lambda = 2.6$ μm.

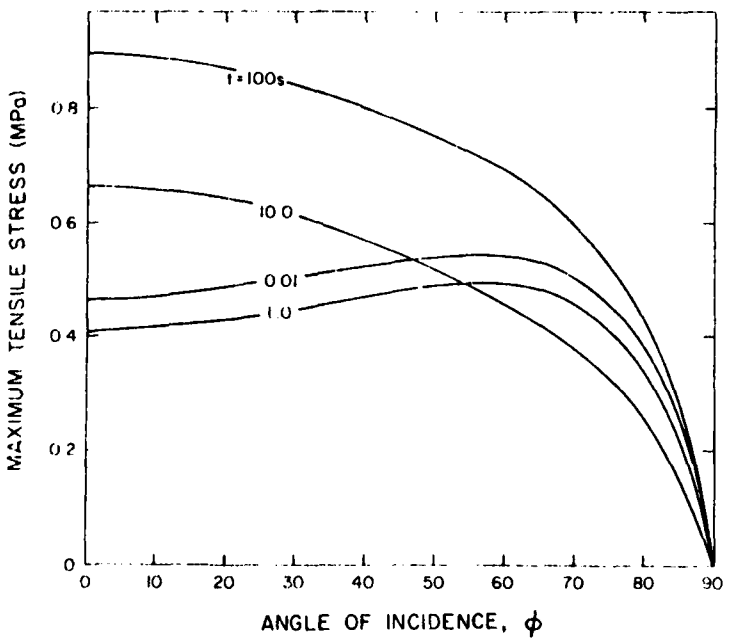

Figure 9. Maximum tensile stress at various times during the cooling of the radiatively heated plate as a function of the incidence angle of the radiation, $\lambda = 2.6$ μm.

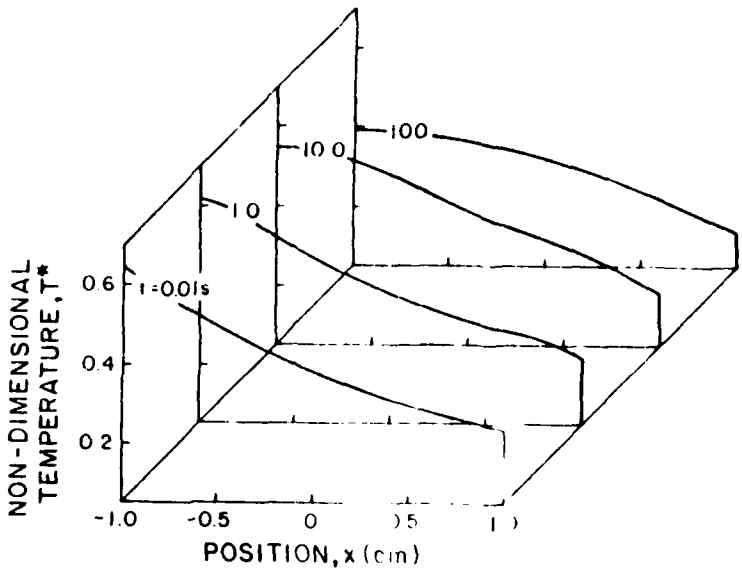

Figure 10. Three-dimensional portrayal of the non-dimensional temperature distribution during the cooling of the radiatively heated plate, normal incidence, λ = 2.6 μm.

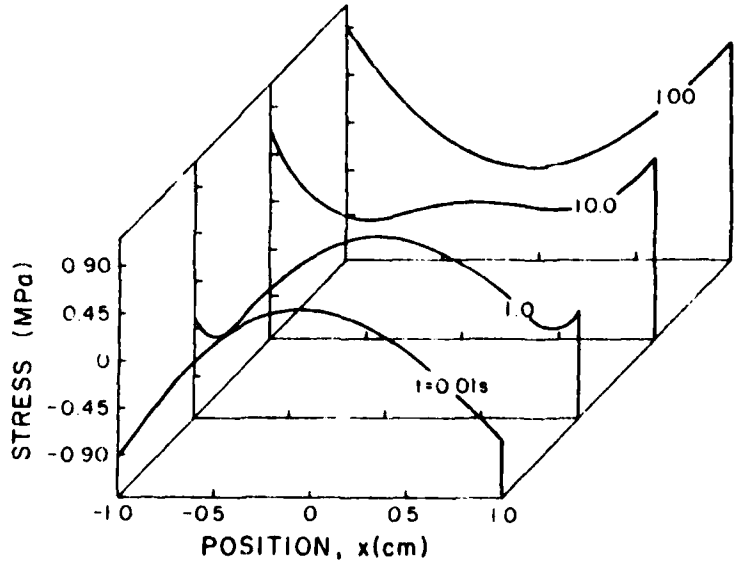

Figure 11. Three-dimensional portrayal of the stress distribution during the cooling of the radiatively heated plate, normal incidence, λ = 2.6 μm.

CHAPTER V

ROLE OF ABSORPTION COEFFICIENT IN THE FREQUENCY DEPENDENCE OF THE THERMAL STRESSES IN A PARTIALLY-ABSORBING PLATE SUBJECTED TO CYCLIC THERMAL RADIATION

J. P. Singh, J. R. Thomas, Jr. and D. P. H. Hasselman
Departments of Materials and Mechanical Engineering
Virginia Polytechnic Institute and State University
Blacksburg, Virginia 24061 USA

ABSTRACT

The frequency dependence of the thermal stresses in a partially absorbing plate subjected to cyclic thermal radiation is shown to be a function of the optical thickness.

INTRODUCTION

Earlier reports in this series of analytical studies of the thermal stresses in partially absorbing plates subjected to radiation heating concentrated on a series of boundary conditions including symmetric [1,2] or asymmetric steady-state radiation [3,4] combined with convective cooling, sudden loss of radiation following long-term steady-state radiation [5,6] and cyclic radiation combined with convective cooling [8,9]. These latter two studies concentrated on the frequency dependence of the thermal stresses for a single value of optical thickness near the value which under steady-state radiation resulted in the highest value of thermal stress.

The purpose of this paper is to present an analysis and numerical result for the effect of optical thickness on the frequency dependence of the thermal stresses in a partially absorbing plate subjected to cyclic radiation.

ANALYSIS

Boundary and Initial Conditions

The flat plate, infinite in extent, is located in the yz-plane and $-a \leq x \leq a$. At time $t=0$ the front face of the plate ($x = -a$) is subjected

to normally incident spatially uniform cyclic radiation and cooled by Newtonian convection. The back face of the plate (x = a) is fully insulated. The reflectivity of the material of the plate is assumed to be sufficiently low that multiple reflections within the plate can be neglected. For the effect of non-normal incidence and multiple reflections under conditions of steady-state radiation the reader is referred to the study of Thomas et al. [7]. The material properties which affect the temperature and stress such as the emissivity (absorptivity), absorption coefficient, coefficient of thermal expansion, Young's modulus of elasticity, Poisson's ratio, thermal conductivity and the thermal diffusivity are assumed to be independent of temperature. The optical properties of the material of the plate were assumed to be "grey", i.e. independent of wavelength. The temperature of the plate over its total thermal history is assumed to be sufficiently low that the intensity of the re-emitted radiation can be considered negligible compared to the magnitude of the incident radiative heat flux.

The flux q(t) of the normally incident radiation at x = -a was taken to be of the form:

$$q(t) = q_o[1 + \delta \sin(\omega t)] \tag{1}$$

where q_o is the value of heat flux at t = 0, ω is the angular frequency and $0 \leq \delta \leq 1$. For the numerical example to be presented later δ was taken to be identically equal to unity, so that the intensity of the incident radiation varies between 0 and $2q_o$.

The heat flux q at any position x within the plate due to thermal radiation entering at x = -a is:

$$q(x,t) = \varepsilon q_o e^{-\mu(a+x)}[1 + \delta \sin(\omega t)] \tag{2}$$

where $\varepsilon = 1 - r$ with r being the reflectivity and μ the absorption coefficient. The rate of internal heat absorption per unit volume (g''') within the plate at x is:

$$g'''(x,t) = \mu\varepsilon q_o e^{-\mu(a+x)}[1 + \delta \sin(\omega t)] \tag{3}$$

Solutions for the transient temperature T(x,t) are obtained by solving the heat conduction equation [10]:

$$\frac{\partial^2 T}{\partial x^2} + \frac{g'''(x,t)}{k} = \frac{1}{\kappa}\frac{\partial T}{\partial t} \tag{4}$$

where k is the thermal conductivity and κ is the thermal diffusivity.

For the given heating and cooling conditions, the initial and boundary conditions are:

$$T(x,0) = T_o \tag{5}$$

$$\frac{\partial T}{\partial x}(a,t) = 0 \tag{6}$$

$$\frac{\partial T}{\partial x}(-a,t) = -\frac{h}{k}[T(-a,t)-T_o] \tag{7}$$

Solutions for the transient temperatures were obtained using standard techniques [10].

$$T(x,t) = T_o + \sum_{n=1}^{\infty} B_n(t)\cos(\lambda_n x) \tag{8}$$

where the λ_n are the roots of the transcendental equation

$$\lambda_n \tan(2\lambda_n a) = \frac{h}{k} \tag{9}$$

and

$$B_n(t) = \frac{G_n \delta}{\omega^2 + (\kappa\lambda_n^2)^2}\left[\kappa\lambda_n^2 \sin(\omega t) - \omega\cos\omega t + \omega e^{-\kappa\lambda_n^2 t}\right] + \frac{G_n}{\kappa\lambda_n^2}(1-e^{-\kappa\lambda_n^2 t}) \tag{10}$$

with

$$G_n = \frac{\kappa q_o \varepsilon \mu}{k N_n}\left[\frac{\lambda_n \sin(2\lambda_n a)+\mu\cos(2\lambda_n a)-\mu e^{-2\mu a}}{\mu^2+\lambda_n^2}\right] \tag{11}$$

and

$$N_n = a + \frac{h}{2k\lambda_n^2}\cos^2(2\lambda_n a) \tag{12}$$

THERMAL STRESSES

Thermal stresses $\sigma_{y,z}(x,t)$ are obtained by substituting for T from equation (8) into [11]

$$\sigma_{y,s} = \frac{\alpha E}{1-\nu}\left[-T + \frac{1}{2a}\int_{-a}^{a} T dx' + \frac{3x}{2a^3}\int_{-a}^{a} Tx' dx'\right] \tag{13}$$

which yields:

$$\sigma_{y,z} = -\frac{\alpha E}{1-\nu}\sum_{n=1}^{\infty} B_n \cos\lambda_n(x-a)$$

$$+\frac{\alpha E}{2(1-\nu)a}\sum_{n=1}^{\infty}\frac{B_n}{\lambda_n}\sin 2\lambda_n a$$

$$+\frac{3\alpha E x}{2(1-\nu)a^3}\sum_{n=1}^{\infty} B_n(t)\left[-\frac{a}{\lambda_n}\sin(2\lambda_n a)+\frac{1}{\lambda_n^2}-\frac{1}{\lambda_n^2}\cos(2\lambda_n a)\right] \tag{14}$$

For convenience, the numerical results are reported in terms of the non-dimensional temperature

$$T^* = \frac{(T - T_o)k}{\varepsilon q_o a}$$

the non-dimensional stress

$$\sigma^* = \frac{\sigma(1-\nu)k}{\alpha E q_o \varepsilon a}$$

the non-dimensional time, $t^* = \kappa t/a^2$ and the non-dimensional distance, x/a.

NUMERICAL RESULTS AND DISCUSSION

The analytical results for the temperatures and stresses obtained above can be demonstrated most conveniently by means of numerical examples. With the exception of numerical values for the optical thickness, μa, and the angular frequency, ω, for convenience the other relevant parameters were chosen to have constant values as follows: heat transfer coefficient $h = 0.006$ W.cm^{-2}°C^{-1}; thermal conductivity $k = 0.3$ W cm^{-1}°C^{-1}; thermal diffusivity $\kappa = 0.1$ cm^{2}s^{-1}; and plate half-thickness $a = 1$ cm. The amplitude factor, δ, is assumed equal to be unity throughout.

For the specific case of $\mu a = 3$ and $\omega = 0.21$ rad.s^{-1}, Figs. 1 and 2 show the temperatures and stresses, respectively, at the front face ($x = -1$ cm), center ($x = 0$ cm) and back face ($x = 1$ cm) for a number of cycles corresponding to: (a) the initiation of radiation at $t = 0$; (b) after a number of cycles at which the plate has reached an intermediate level of temperature and, (c) after sufficient cycles that no signicant cycle-to-cycle variation in the magnitude of temperature and thermal stresses occurs. For all three cases, the cyclic variation of the temperature decreases from the front to the back face. Of course, this is expected from the specific boundary conditions chosen for this analysis. Also, as expected, the cyclic temperature variation at the center and back face lag in time behind that at the front face. Also note that for this value of angular frequency (0.21 rad.s^{-1}) for the data in Figs. 1 and 2, the cyclic variation of temperature within any one cycle is small compared to the mean temperature rise of the plate.

The magnitude of thermal stresses at the front and back face become increasingly more positive (i.e., tensile) as the plate is subjected to an increasing number of cycles, whereas the stresses at the center become increasingly more negative. This latter effect arises because as time progresses the plate develops a temperature distribution which is generally concave downward on which the cyclic variation is superimposed. As pointed out elsewhere [12] such a concave downward temperature distribution will result in thermal stresses which are tensile in the front and back surface of the plate, in spite of the fact that after long periods of time the mean temperatures at the back surface and center are higher than those in front.

The magnitude of the thermal stresses shown in Fig. 2 can be compared with those obtained in the earlier study for identical values of all relevant parameters, but with convective cooling of the plate at the back face [8]. It is easily noted that the values of the stresses for front or back face cooling are almost identical. Such near equality for the stresses for front and back face cooling was also noted for steady-state radiation [3,4]. More recently it was pointed out [5,6] that as the plate thickness $a \to 0$, the stresses for convective cooling at the front or back become identical. For $a = 10$ cm, differences were noted for these cooling conditions for

in a plate due to the sudden interruption of long-term steady-
diation [5,6].

a very low value of angular frequency, $\omega = 10^{-4}$ rad.s^{-1}, and $\mu a = 3$,
and 3b show the temperature and thermal stresses, respectively,
ction of time over the duration of the first cycle from the
of the initiation of radiation at $t = 0$ at a value $q = q_o$ to the
of time within the cycle at which the magnitude of heat flux $q = 0$.
3a the magnitude of the temperatures at the front, center and back
close together to be plotted separately for the relatively large
ed for the temperature axis. The time at which the temperature
its maximum corresponds exactly to the time at which the heat flux
a value of $2q_o$. This implies that at sufficiently low frequenc es,
ed out also in an earlier study [9], that following a brief initial
t, the temperature and stresses in the plate cycle along with the
neous value of heat flux, with a corresponding value for a constant
κ equal to the instantaneous value of cyclic heat flux. Confirmation
conclusion is given by Fig. 3b which shows that after a brief
transient which is complete at $\kappa t/a^2 \approx 2x10^2$ (or $2x10^3$s), the stresses
ctly proportional t. the instantaneous heat flux. Furthermore, the
ıe of stress corresponds to twice the value found for the steady-
ress encountered for steady-state radiation of magnitude q_o [3,4].
ıre 4 shows the magnitude of the thermal stress in the front face
ldentical value of frequency (10^{-4} rad.s^{-1}) and time period within
: cycle as for the data shown in Fig. 3b, but for a range of values
ıl thickness. The value of peak stress for any value of μa is
: value for radiation of constant intensity [3,4]; again, this
the earlier statement that at low frequency, for purposes of evaluating
ıeratures and stresses, the plate can be regarded to be subjected to
state heat flux.

re 5 shows the frequency dependence of the maximum stresses during
t the front face ($x = -a$) after a sufficient time period such
ycle-to-cycle variation in the magnitude of temperature or stresses
These results clearly indicate that the relative frequency dependence
ermal stresses is a function of the optical thickness. As the

AD-A125 242 THERMO-MECHANICAL AND THERMAL BEHAVIOR OF HIGH-TEMPERATURE STRUCTURAL MAT..(U) VIRGINIA POLYTECHNIC INST AND STATE UNIV BLACKSBURG COLL OF E.. 2/3

UNCLASSIFIED D P HASSELMAN ET AL. 31 DEC 82 F/G 11/2 NL

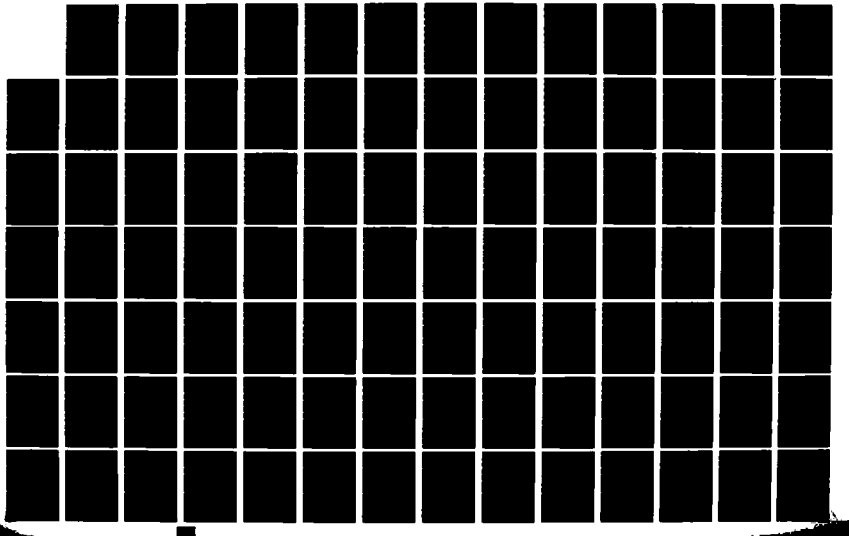

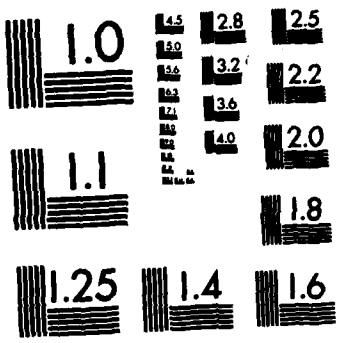

frequency $\omega \to \infty$ the magnitude of stress approaches the value for the stresses after long-term radiation with intensity q_o. As $\omega \to 0$ (but not $\omega = 0$) the magnitude of maximum stress within the cycle approaches the value for long-term steady-state radiation of intensity $2q_o$. At $\omega = 0$, the intensity of radiation remains constant at a value q_o with stresses corresponding to steady-state radiation of intensity q_o. For this reason, the magnitude of stress displays a discontinuity at $\omega = 0$, with a value of stress as $\omega \to 0$, which is twice the value for $\omega = 0$.

ACKNOWLEDGMENT

This study was supported by the Office of Naval Research under Contract No. N00014-78-C-0431.

REFERENCES

1. D.P.H. Hasselman, J.R. Thomas, Jr., M.P. Kamat and K. Satyamurthy, Thermal Stress Analysis of Partially Absorbing Brittle Ceramics Subjected to Symmetric Radiation Heating, J. Am. Ceram. Soc., Vol. 63, pp. 21-25, 1980.

2. J.P. Singh, J.R. Thomas, Jr., and D.P.H. Hasselman, Thermal Stresses in Partially Absorbing Flat Plate Symmetrically Heated by Thermal Radiation and Cooled by Convection, J. of Thermal Stresses, Vol. 3, pp. 341-349 (1980).

3. J.R. Thomas, Jr., J.P. Singh and D.P.H. Hasselman, Analysis of Thermal Stress Resistance of Partially Absorbing Ceramic Plate Subjected to Asymmetric Radiation, I: Convective Cooling at Rear Surface, J. Am. Ceram. Soc., Vol. 64, pp. 163-169, 1981.

4. J.P. Singh, K. Satyamurthy, J.R. Thomas, Jr., and D.P.H. Hasselman Analysis of Thermal Stress Resistance of Partially Absorbing Ceramic Plate Subjected to Asymmetric Radiation, II: Convective Cooling at Front Surface, J. Am. Ceram. Soc., 64, pp. 169-173, 1981.

5. J.I. Frankel, J.P. Singh, J.R. Thomas, Jr., and D.P.H. Hasselman, Thermal Stresses in Partially Absorbing Flat Plate Due to Sudden Interruption of Steady-State Asymmetric Radiation, I: Convective Cooling at Rear Surface, J. Thermal Stresses (in press).

6. J.P. Singh, J.I. Frankel, J. R. Thomas, Jr., and D.P.H. Hasselman, Thermal Stress in Partially Absorbing Flat Plate Due to Sudden Interruption of Steady-State Asymmetric Radiation, II: Convective Cooling at Front Surface, J. Thermal Stresses (in press).

7. J.R. Thomas, Jr., J. I. Frankel and D.P.H. Hasselman, Effect of Interface Reflections and Angle of Incidence of Radiation on Thermal Stresses in Semi-Transparent Materials, J. of Thermal Stresses (in review).

8. J.R. Thomas, Jr., J.P. Singh and D.P.H. Hasselman, Thermal Stresses in a Partially Absorbing Flat Plate Asymmetrically Heated by Cyclic Thermal Radiation and Cooled by Convection, J. Thermal Stresses (in press).

9. J.P. Singh, J. R. Thomas, Jr., and D.P.H. Hasselman, Thermal Stresses in a Partially Absorbing Flat Plate Asymmetrically Heated by Cyclic Thermal Radiation and Cooled by Convection, Addendum, J. Thermal Stresses (in press).

10. H.S. Carslaw and J.C. Jaeger, Conduction of Heat in Solids, 2nd ed., Clarendon Press, Oxford, 1960.

11. B.A. Boley and J. H. Wiener, Theory of Thermal Stresses, Wiley, New York, 1960.

12. K. Satyamurthy, D.P.H. Hasselman and J.P. Singh, Effect of Nature of Concavity of Temperature Distribution on Position and Sign of Maximum Thermal Stress: A Short Note, J. Thermal Stresses, Vol. 3, pp. 551-553, 1980.

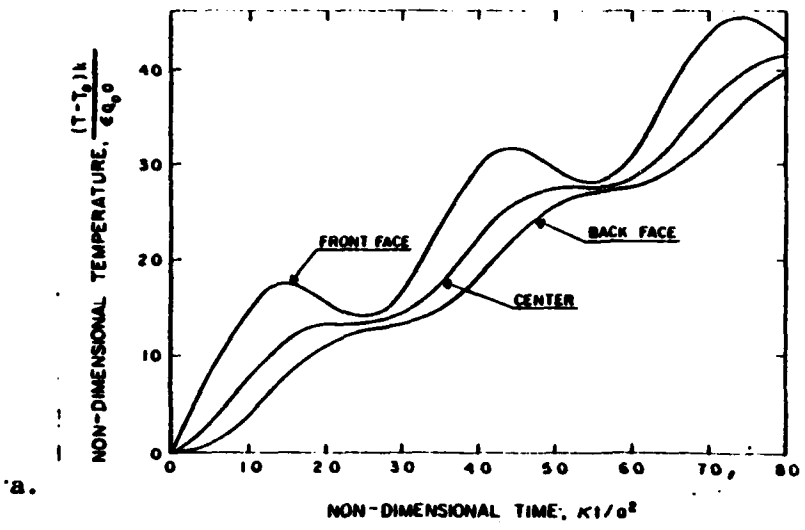

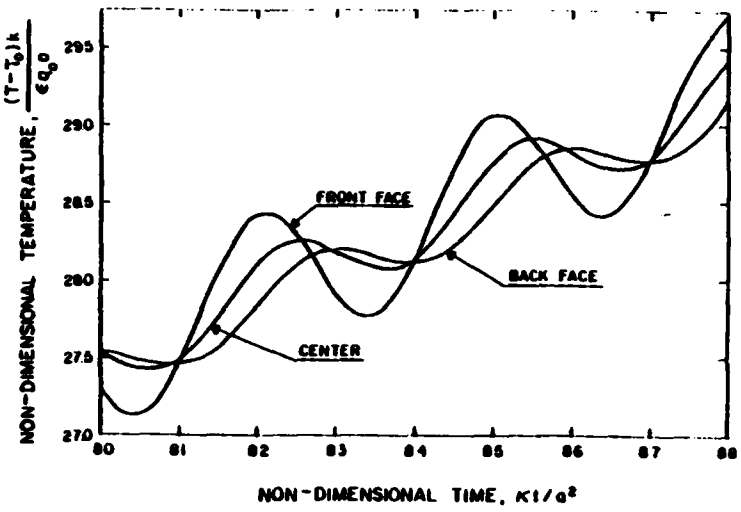

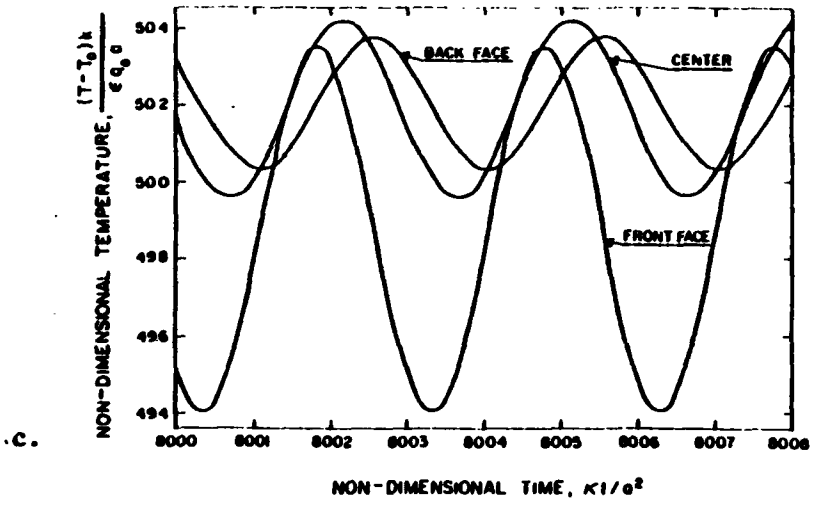

Fig. 1. Transient temperatures in a partially absorbing flat plate heated in front by normally incident cyclic thermal radiation and cooled by convection for three different time intervals, for values of the parameters: $h = 0.006$ W.cm.$^{-2}$°C^{-1}; $k = 0.3$ W cm^{-1}°C^{-1}; $\kappa = 0.1$ cm.^{2}s^{-1}; $\omega = 0.21$s^{-1}; $a = 1$ cm and $\mu a = 3$.

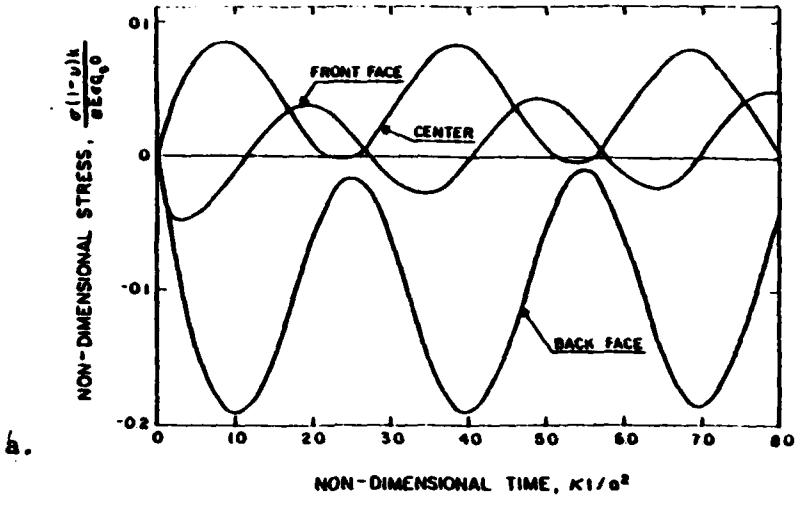

a.

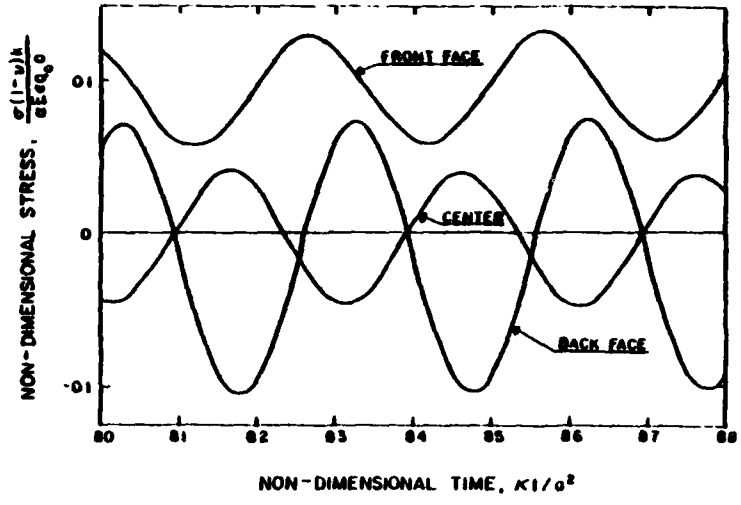

b.

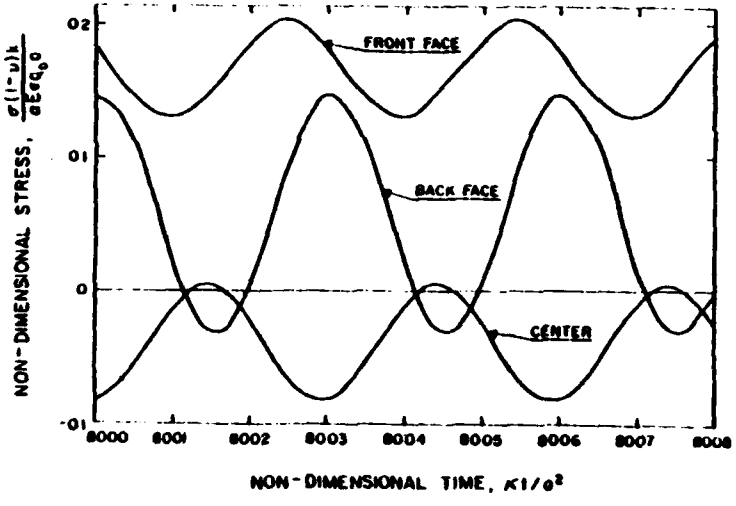

c.

Fig. 2. Transient thermal stresses in partially absorbing flat plate heated in front by normally incident cyclic thermal radiation and cooled by convection for time intervals and values of pertinent parameters identical to those of Fig. 1.

a.

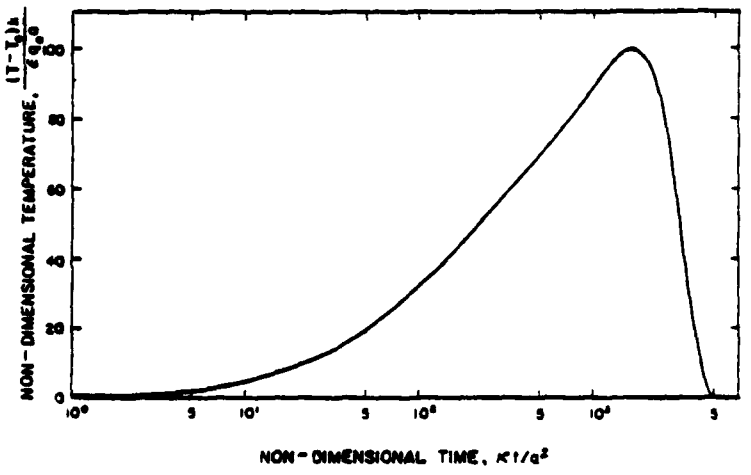

b.

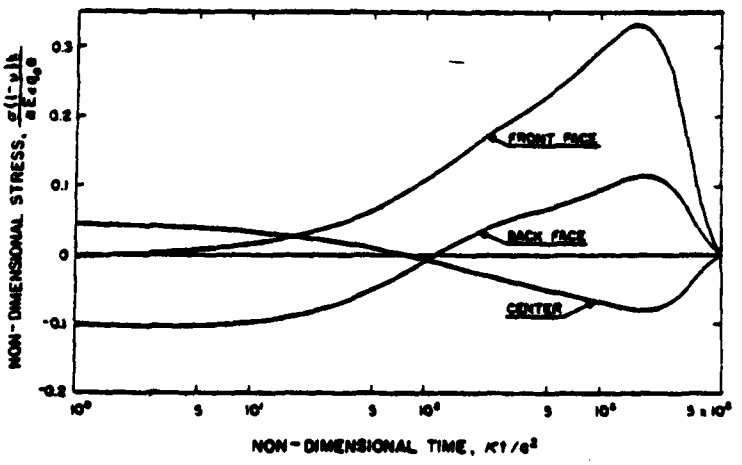

Fig. 3. Transient temperature (a) and thermal stresses (b) in partially absorbing flat plate heated in front by normally incident cyclic thermal radiation and cooled by convection for a value of angular frequency $\omega = 10^{-4}s^{-1}$ and values of pertinent parameters identical to those of Figs. 1 and 2. (Note, temperatures in the various positions in the plate were too close to be plotted separately for the scale used for Fig. 3a.)

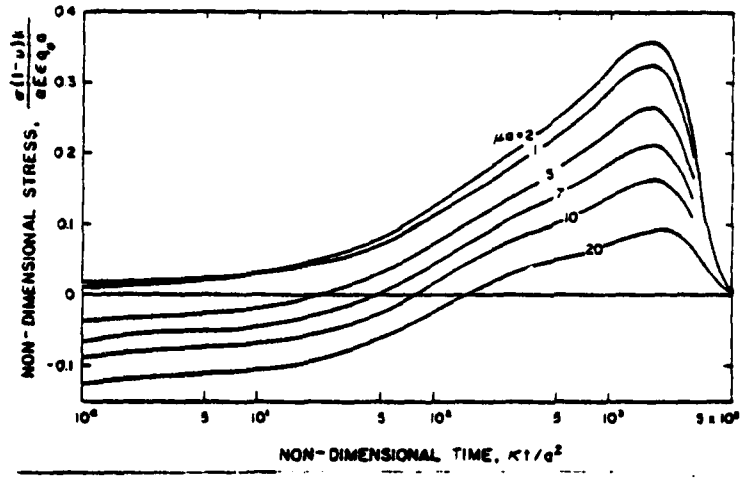

Fig. 4. Maximum thermal stresses in front surface of partially absorbing flat plate heated in front by normally incident cyclic thermal radiation and cooled by convection for an angular frequency $\omega = 10^{-4}s^{-1}$ and range of values of optical thickness and other parameters identical to those for Figs. 1, 2 and 3.

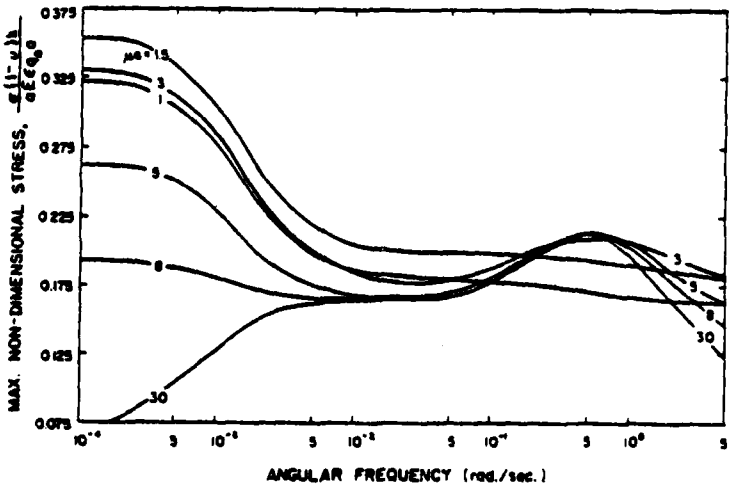

Fig. 5. Frequency dependence of maximum thermal stresses in front surface of partially absorbing flat plate heated in front by normally incident cyclic radiation and cooled by convection for range of optical thickness and other parameters identical to those of previous figures.

CHAPTER VI

THERMAL STRESSES IN PARTIALLY ABSORBING FLAT PLATE DUE TO SUDDEN INTERRUPTION OF STEADY-STATE ASYMMETRIC RADIATION, I: CONVECTIVE COOLING AT REAR SURFACE

by

J. I. Frankel, J. P. Singh, J. R. Thomas, Jr., D. P. H. Hasselman

Departments of Mechanical and Materials Engineering
Virginia Polytechnic Institute and State University
Blacksburg, Virginia 24061 USA

ABSTRACT

An analysis is presented for the thermal stresses in a partially absorbing flat plate due to sudden interruption of steady-state asymmetric thermal radiation on the front face with convection cooling at the rear face. Maximum transient tensile stresses occur in the rear surface and are almost independent of the heat transfer coefficient, h. For optical thickness $\mu a \geq 0.5$, the maximum tensile stress initially rises to reach a peak and then decreases with time. In contrast, for $\mu a \leq 0.5$, the stresses decrease monotonically. It is shown that a plot of non-dimensional stress as a function of non-dimensional time for a given value of μa and h does not result in a universal plot from which thermal stresses can be obtained for any value of plate thickness.

INTRODUCTION

Solutions for the transient temperatures and thermal stresses for heating frequently can be obtained from the corresponding solutions for cooling (or vice-versa) by a simple transformation and/or change in sign. This generally will be the case if the mode of heat transfer, such as convection, is the same for heating and cooling.

In practice, however, conditions are encountered for which the heat transfer conditions for heating and cooling are different. This will require separate solutions for the transient temperatures and corresponding thermal stresses. Such solutions are expected to be coupled, as the initial and boundary conditions for cooling following heating (or vice-versa) are governed by the magnitude and distribution of the temperatures and thermal stresses reached during heating.

The above situation is encountered in such installations as concentrated solar energy receivers or any other structures or components subject to simultaneous radiation heating and convective cooling. Such a structure may have reached a condition of steady-state temperature and thermal stress, when the radiation is suddenly decreased to zero, leaving the structure or component subject to rapid cooling by convection only. Such an event is expected to be a common occurrence for solar energy collectors under conditions of intermittent cloud cover.

The purpose of this paper is to illustrate such coupling between the thermal stresses encountered during heating and cooling. Specifically, thermal stresses will be analyzed for a semi-absorbing flat plate initially at steady-state conditions after being subjected to a long-term constant asymmetric radiation at the front face for which the temperature and

stresses were obtained in earlier studies [1,2]. The radiation is suddenly removed, subjecting the plate to cooling by convection at either the rear or front face. For convenience of the reader, Part I will concentrate on cooling at the rear face, with the solutions for front face cooling presented in Part II.

ANALYSIS

Initial and Boundary Conditions

The geometry selected for the analysis consisted of an infinite flat plate located in the y-z plane, with $-a \leq x \leq a$. The plate, initially at a uniform temperature T_o, is subjected to a normally incident uniform radiation q_o and cooled by convection at the rear surface ($x = a$). When the steady state conditions for temperatures and stresses inside the plate are reached, the radiation flux q_o is discontinued. The temperature solution for the above st dy-state conditions were obtained by the present authors [1]. By choosing the time $t = 0$ as the instant when the radiation flux q_o is cut off, the problem is reduced to finding the temperature and stress solutions for a plate with known initial temperature distribution cooled in the rear surface by Newtonian convection with heat transfer coefficient h. The optical properties of the material are assumed to be "gray", i.e., independent of wavelength. The surface reflectivity and thickness of the plate are assumed to be such that the effect of multiple internal reflections can be neglected. The material properties that affect the temperature distribution and thermal stresses, such as the emissivity (absorptivity), absorption coefficient, thermal conductivity and thermal diffusivity, coefficient of thermal expansion, Young's modulus and Poisson's ratio are assumed to be independent of temperature.

It is also assumed that the temperature of the plate, over the time period required for stresses to reach a value nearly equal to their maximum, remains sufficiently low so that the reemitted radiation is negligible in comparison to the incident radiation.

Solutions for the transient temperature T are obtained [3] by solving

$$\frac{\partial^2 T}{\partial x^2} = \frac{1}{\kappa}\frac{\partial T}{\partial t} \tag{1}$$

where κ is the thermal diffusivity.

The initial condition for the temperature distribution for the present problem is [1].

$$T(x,0) = T_o + \sum_{n=0}^{\infty} \frac{G_n}{\kappa \lambda_n^2} \cos\left[\lambda_n(a+x)\right] \tag{2a}$$

where the $\{\lambda_n\}$ are the roots of the transcendental equation

$$\lambda_n \tan(2\lambda_n a) = \frac{h}{k} \tag{2b}$$

and

$$G_n = \frac{\kappa q_o \varepsilon \mu}{N_n k}\left[\frac{\mu + e^{-2\mu a}\{\lambda_n \sin(2\lambda_n a) - \mu \cos(2\lambda_n a)\}}{\mu^2 + \lambda_n^2}\right] \tag{2c}$$

with

$$N_n = \frac{1}{2\lambda_n a}\left[\sin(2\lambda_n a)\cos(2\lambda_n a) + 2\lambda_n a\right] \tag{2d}$$

The boundary conditions are:

$$\frac{\partial T}{\partial x}(-a,t) = 0 \tag{3}$$

$$\frac{\partial T}{\partial x}(a,t) = -\frac{h}{k}\left[T(a,t) - T_o\right] \tag{4}$$

Transient Temperatures

The solution for the temperature was obtained by solving the differential equation (1) subject to the conditions given by Eqs. (2) - (4) and is found to be

$$T(x,t) = T_o + \sum_{n=0}^{\infty} B_n(t) \cos \lambda_n(x+a) \tag{5}$$

where

$$B_n(t) = \frac{G_n}{\kappa\lambda_n^2} e^{-\kappa\lambda_n^2 t} \tag{6}$$

with λ_n and G_n given by Eqs. (2b) and (2c).

Thermal Stresses

Thermal stresses are obtained by substitution for T from Eq. (5) in [4].

$$\sigma_{y,z} = \frac{\alpha E}{1-\nu} \left[-T + \frac{1}{2a}\int_{-a}^{a} T dx + \frac{3x}{2a^3}\int_{-a}^{a} Tx dx\right] \tag{7}$$

which results in

$$\begin{aligned}\sigma_{y,z} = {} & \frac{-\alpha E}{1-\nu} \sum_{n=0}^{\infty} B_n(t) \cos\left[\lambda_n(x+a)\right] \\ & + \frac{\alpha E}{2a(1-\nu)} \sum_{n=0}^{\infty} \frac{B_n(t)}{\lambda_n} \sin(2\lambda_n a) \\ & + \frac{3x\alpha E}{2a(1-\nu)} \sum_{n=0}^{\infty} B_n(t) \left[\frac{\sin(2\lambda_n a)}{a\lambda_n} + \frac{1}{a^2\lambda_n^2}\cos(2\lambda_n a) - \frac{1}{a^2\lambda_n^2}\right]\end{aligned} \tag{8}$$

For convenience, the numberical results are reported in terms of the non-dimensional temperature,

$$T^* = \frac{(T-T_o)k}{\varepsilon q_o a}$$

the non-dimensional stress,

$$\sigma^* = \frac{\sigma(1-\nu)k}{\alpha E q_o E a}$$

the non-dimensional time $t^* = \kappa t/a^2$, and the non-dimensional distance x/a.

NUMBERICAL RESULTS AND DISCUSSION

The analytical results presented above can be illustrated by a numerical example. Because of the relatively large number of independent variables, the numerical results to be presented will be limited to indicate a number of general results. The thermal conductivity of the plate was taken as K = 0.3 $W.cm^{-1}.{}^oC^{-1}$, a typical value for a dielectric material near room temperature. Also, the half-thickness of the plate, a, was taken as 1 cm, except where noted.

Figure 1a and 1b show the distributions of the temperatures and thermal stresses at a time immediately prior to the interruption of radiation at t = 0 for a value of the convective heat transfer coefficient h = 0.006 $W.cm.^{-2o}C^{-1}$. These temperatures and stresses, which represent the initial conditions for the present study, resulted from the combined effects of radiation heating and convective cooling of sufficiently long duration that the temperatures and stresses have reached steady-state conditions. For many of the details, the reader is referred to the earlier study of the temperature and thermal stresses [1] during the heat-up stage of the plate. The steady-state temperature at the rear-face is an inverse function of the heat transfer coefficient.

The temperature profile and the resulting thermal stresses in the plate were found to be independent of the value of the heat transfer coefficient. The maximum value of thermal stress was found to occur at a value of optical thickness $\mu a \simeq 2$. At $\mu a = 0$ the stresses are zero because no heat is absorbed. As $\mu a \to \infty$, the temperature distribution becomes linear which also results in a state of zero thermal stress. Due to the downward curvature of the temperature distribution, the thermal stresses are tensile at the hottest section of the plate ($x = -a$) [5].

Figures 2a and 2b, for a value of optical thickness $\mu a = 3$, show the transient temperatures and stresses following the interruption of the radiation at $t = 0$ for a number of values of time, τ, for the initial conditions shown in Fig. 1a and 1b. The stresses initially rise to a maximum followed by a decrease with time. The position of the maximum compressive stress within the plate shifts with increasing time.

The transient thermal stresses at both the front and rear faces of the plate are shown in Figs. 3a and 3b, respectively, for a number of values of the optical thickness for the initial conditions shown in Figs. 1a and 1b. It was found that for $\mu a \leq 0.5$, the stresses decreased with increasing time without passing through a maximum.

Figure 4 presents evidence for the coupled nature of the solutions for the temperature and thermal stress due to the interruption of the radiation and those for the heating stage of the plate prior to the radiation cut-off. For $\mu a = 3$, Fig. 4 shows the transient thermal stresses at the rear surface ($x = a = 1$ cm) for a range of values of the heat transfer coefficient. Even for a range in h of a factor of 15, the maximum values of the thermal stresses differ by only a few percent. At least qualitatively, this effect arises because the temperature rise of the plate above ambient at $t = 0$ is inversely proportional to the heat transfer coefficient. On subsequent cooling, the magnitude of the thermal stresses,

at least for small values of the Biot number $\beta = ah/k$, are directly proportional to the heat transfer coefficient as well as the total temperature range over which the plate is being cooled. This leads to the net effect that the peak stresses following the cut-off radiation, to a first approximation, are independent of the heat transfer coefficient.

The stresses in the front and rear surface for a plate half-thickness $a = 10$ cm and $\mu a = 3$ are shown in Figs. 5a and 5b, respectively. Comparison of the data of Figs. 5a and 5b and Figs. 3a and 3b shows that for plates of different thickness with identical values of optical thickness, non-dimensionalization of the numerical data does not result in a universal plot from which the thermal stresses can be obtained for any dimension. This can be explained by noting that for the same value of optical thickness μa, the total amount of heat absorbed at steady-state (t=0) is independent of the plate thickness. For this reason the temperature gradient within the plate at the rear surface is the same for all thicknesses. The temperature rise in the front of the plate, however, is not proportional to the plate thickness (unless $\mu a \to \infty$). For this reason the steady-state temperature distribution at t= 0 does not become normalized on a dimensionless basis. This can easily be seen by re-deriving Eq. (2a) in another form; i.e., if we solve the steady heat conduction equation with the same heat source used to derive Eq. (2a) instead of taking the limit of the transient solution, we find

$$\frac{[T(x)-T_o]k}{\varepsilon q_o a} = \frac{e^{-2\mu a}-e^{-\mu x}}{\mu a} + 2\left(1 - \frac{x}{2a}\right) + \frac{k}{ah}\left(1 - e^{-2\mu a}\right) \qquad (9)$$

in non-dimensional form. Clearly, if a is varied while μa is held constant, the non-dimensional temperature difference cannot remain constant.

A similar effect is noted in Part II of this study for front face cooling. This suggests that for plates of different thickness separate calculations of the temperatures and stresses will be required.

Acknowledgment

This study was conducted as part of a program on the thermo-mechanical behavior of brittle structural materials supported by the Office of Naval Research under Contract No. N00014-78-C-0431.

References

1. J. R. Thomas, Jr., J. P. Singh and D. P. H. Hasselman, Analysis of Thermal Stress Resistance of Partially Absorbing Ceramic Plate Subjected to Asymmetric Radiation, I: Convective Cooling at Rear Surface, J. Am. Ceram. Soc., Vol. 64, pp. 163-169, 1981.

2. J. P. Singh, K. Satyamurthy, J. R. Thomas, Jr., and D. P. H. Hasselman, Analysis of Thermal Stress Resistance of Partially Absorbing Ceramic Plate Subjected to Asymmetric Radiation, II: Convective Cooling at Front Surface, J. Am. Ceram. Soc., Vol. 64, pp. 169-173, 1981.

3. H. S. Carslaw and J. C. Jaeger, Conduction of Heat in Solids, 2nd ed., Clarendon Press, Oxford, 1960.

4. B. A. Boley and J. H. Wiener, Theory of Thermal Stresses, Wiley, New York, 1960.

5. K. Satyamurthy, D. P. H. Hasselman and J. P. Singh, Effect of Nature of Concavity of Temperature Distribution on Position and Sign of Maximum Thermal Stress: A Short Note, J. Thermal Stresses, Vol. 3, pp. 551-553, 1980.

Captions

Fig. 1. Distribution of steady state temperature (a) and thermal stress (b) in a partially absorbing flat plate heated in the front by normally incident radiation and cooled by convection at the rear surface for various values of μa with $k = 0.3$ W.cm.$^{-1}$°C.$^{-1}$, $h = 0.006$ W.cm.$^{-2}$°C.$^{-1}$, $\kappa = 0.1$ cm.^{2}s.$^{-1}$ and $a = 1$ cm.

Fig. 2. Distribution of temperature (a) and thermal stress (b) for various values of time following the interruption of the radiation at time $t = 0$ in a partially absorbing flat plate with originally steady state temperature and stress distributions due to normally incident radiation in the front face and cooling at the rear surface by convection for $k = 0.3$ W.cm.$^{-1}$°C.$^{-1}$, $h = 0.006$ W.cm.$^{-2}$°C.$^{-1}$, $\kappa = 0.1$ cm.^{2}s.$^{-1}$, $\mu a = 3$ and $a = 1$ cm.

Fig. 3. Transient thermal stresses in the front (a) and the rear face (b) following the interruption of the radiation at time $t = 0$ in a partially absorbing flat plate with originally steady state temperature and stress distribution due to normally incident radiation in the front face and cooling by convection at the rear surface for various values of μa with $k = 0.3$ W.cm.$^{-1}$°C.$^{-1}$, $h = 0.006$ W.cm.$^{-2}$°C.$^{-1}$, $\kappa = 0.1$ cm.^{2}s.$^{-1}$ and $a = 1$ cm.

Fig. 4. Transient thermal stress in the rear surface following the interruption of the radiation at time $t = 0$ in a partially absorbing flat plate with originally steady state temperature and stress distribution due to normally incident radiation in the front face and cooling by convection at the rear surface for various values of h with $k = 0.3$ W.cm.$^{-1}$°C.$^{-1}$, $\mu a = 3$, $\kappa = 0.1$ cm.^{2}s^{-1} and $a = 1$ cm.

Fig. 5. Transient thermal stresses in the front (a) and the rear face (b) following the interruption of the radiation at time $t = 0$ in a partially absorbing flat plate with originally steady state temperature and stress distribution due to a normally incident radiation in the front face and cooling by convection at the rear surface for various values of μa with $k = 0.3$ W.cm.$^{-1}$°C.$^{-1}$, $h = 0.006$ W.cm.$^{-2}$°C.$^{-1}$, $\kappa = 0.1$ cm.^{2}s.$^{-1}$ and $a = 10$ cms.

a.

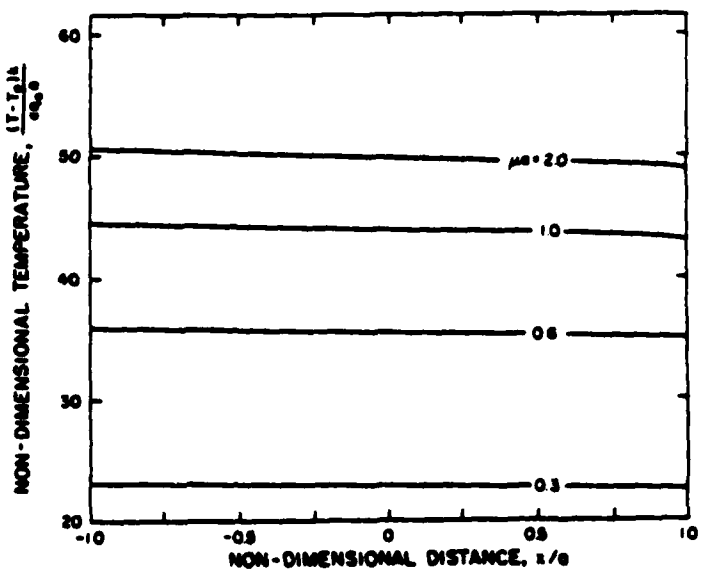

b.

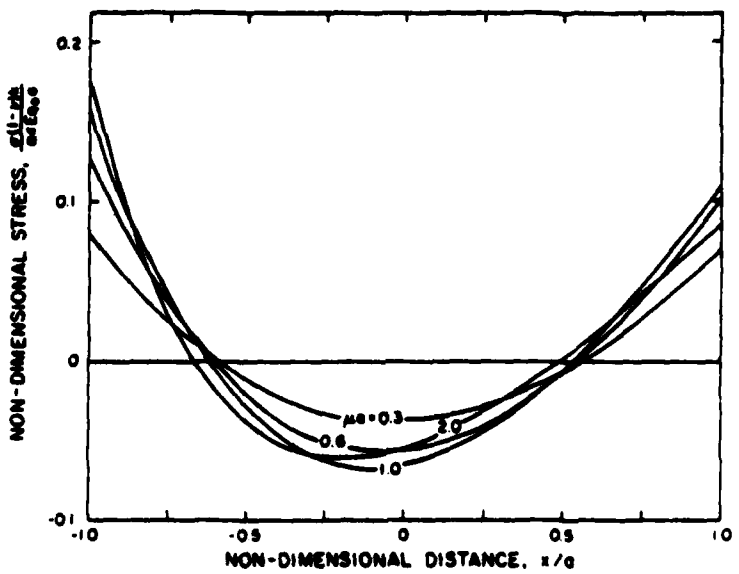

Fig. 1. Distribution of steady state temperature (a) and thermal stress (b) in a partially absorbing flat plate heated in the front by normally incident radiation and cooled by convection at the rear surface for various values of μa with k = 0.3 W.cm.$^{-1}$°C.$^{-1}$, h = 0.006 W.cm.$^{-2}$°C.$^{-1}$, κ = 0.1 cm.^{2}s.$^{-1}$ and a = 1 cm.

a.

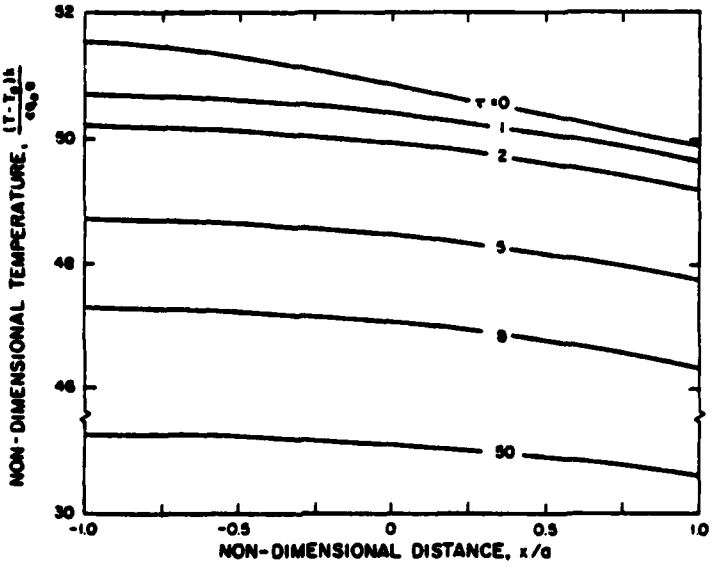

b.

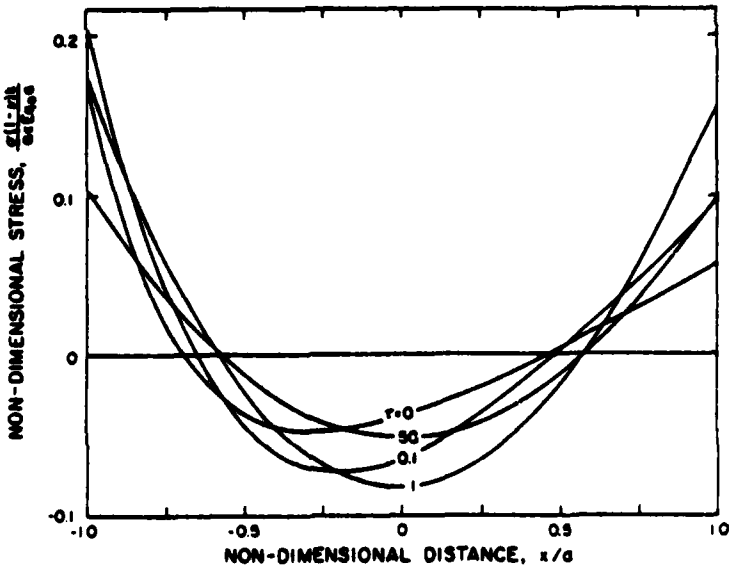

Fig. 2. Distribution of temperature (a) and thermal stress (b) for various values of time following the interruption of the radiation at time t = 0 in a partially absorbing flat plate with originally steady state temperature and stress distributions due to normally incident radiation in the front face and cooling at the rear surface by convection for k = 0.3 W.cm.$^{-1}$o C.$^{-1}$, h = 0.006 W.cm.$^{-2}$o C.$^{-1}$, κ = 0.1 cm.^{2}s.$^{-1}$, μa = 3 and a = 1 cm.

a.

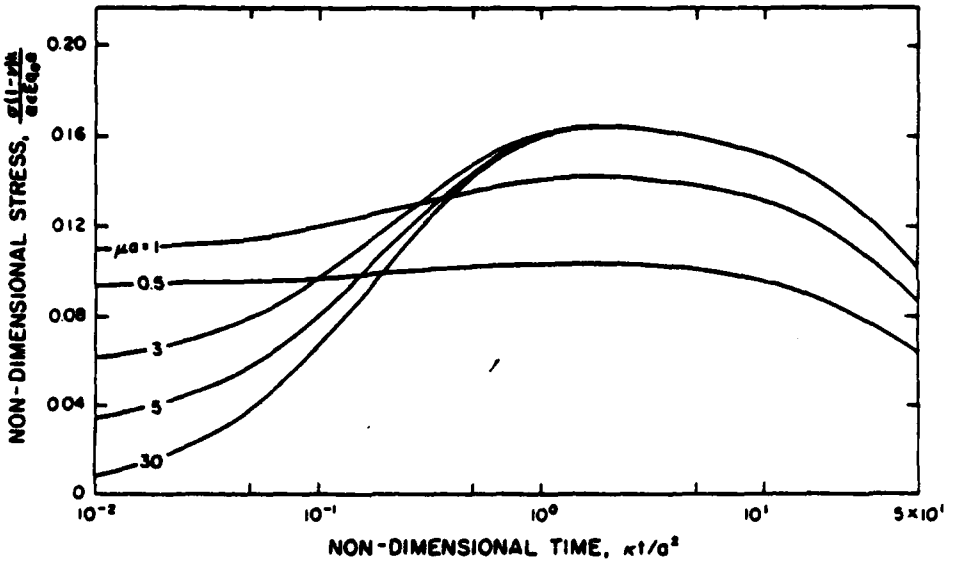

b.

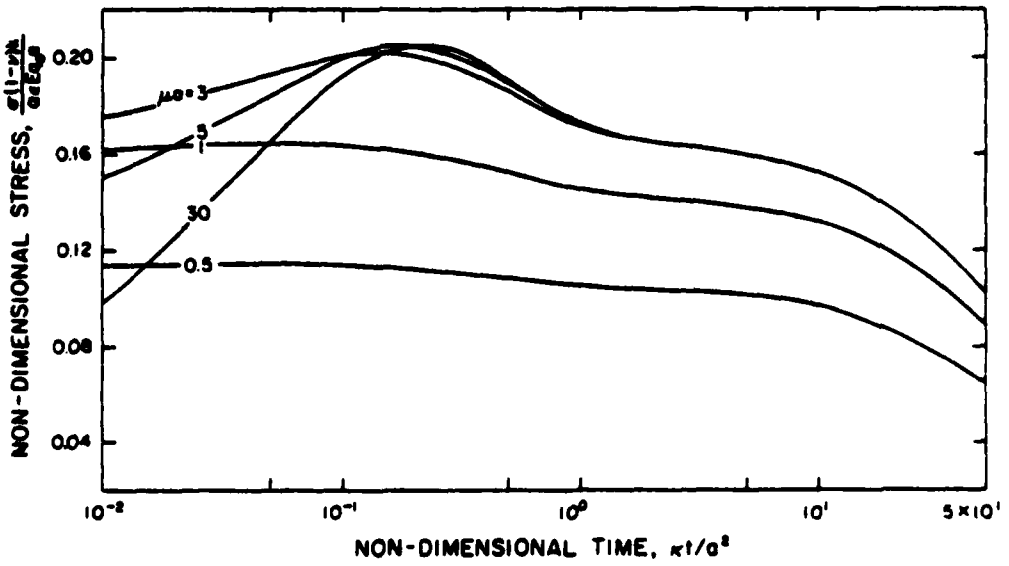

Fig. 3. Transient thermal stresses in the front (a) and the rear face (b) following the interruption of the radiation at time t = 0 in a partially absorbing flat plate with originally steady state temperature and stress distribution due to normally incident radiation in the front face and cooling by convection at the rear surface for various values of μa with k = 0.3 W.cm.$^{-1}$°C.$^{-1}$, h = 0.006 W.cm.$^{-2}$°C.$^{-1}$, κ = 0.1 cm.^{2}s.$^{-1}$ and a = 1 cm.

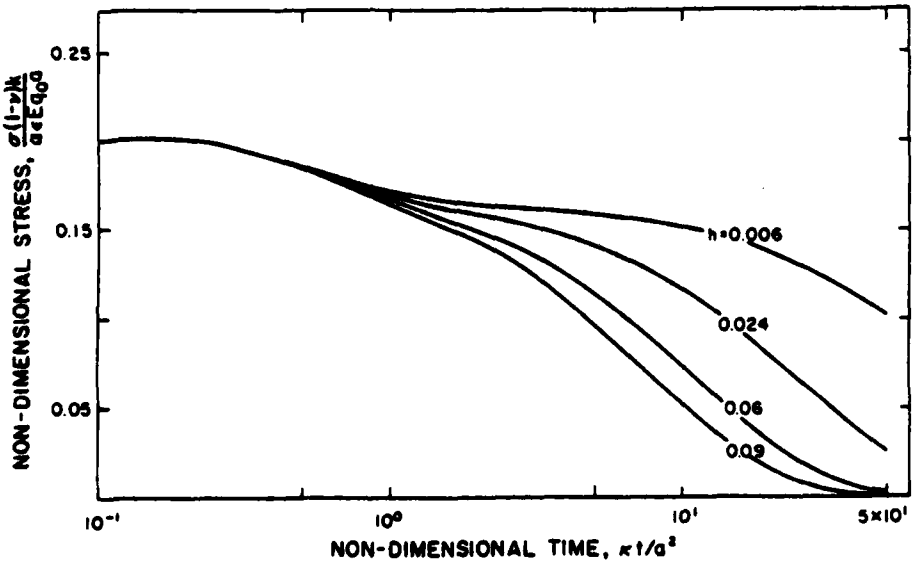

Fig. 4. Transient thermal stress in the rear surface following the interruption of the radiation at time t = 0 in a partially absorbing flat plate with originally steady state temperature and stress distribution due to normally incident radiation in the front face and cooling by convection at the rear surface for various values of h with k = 0.3 W.cm.$^{-1}$°C.$^{-1}$, μa = 3, κ = 0.1 cm.^{2}s^{-1} and a = 1 cm.

a.

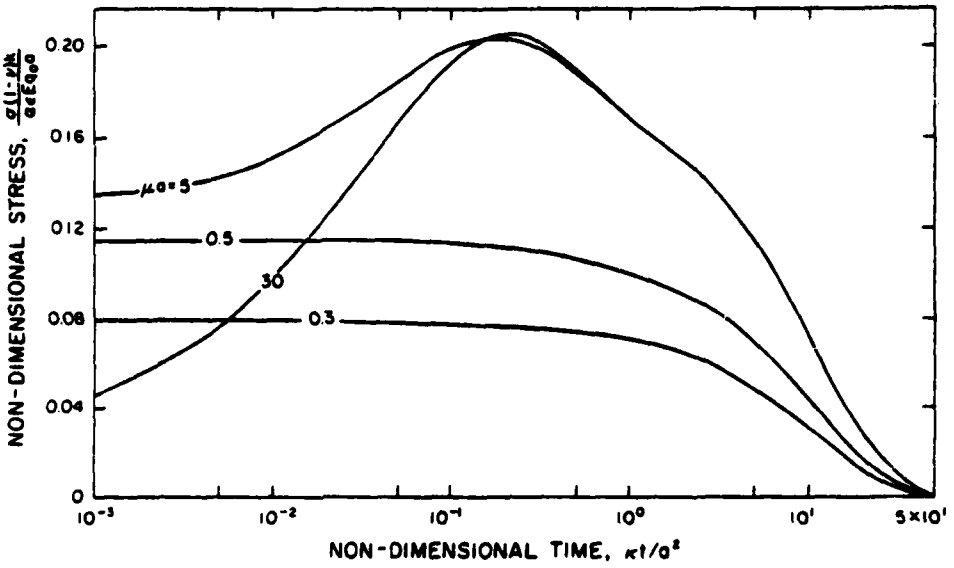

b.

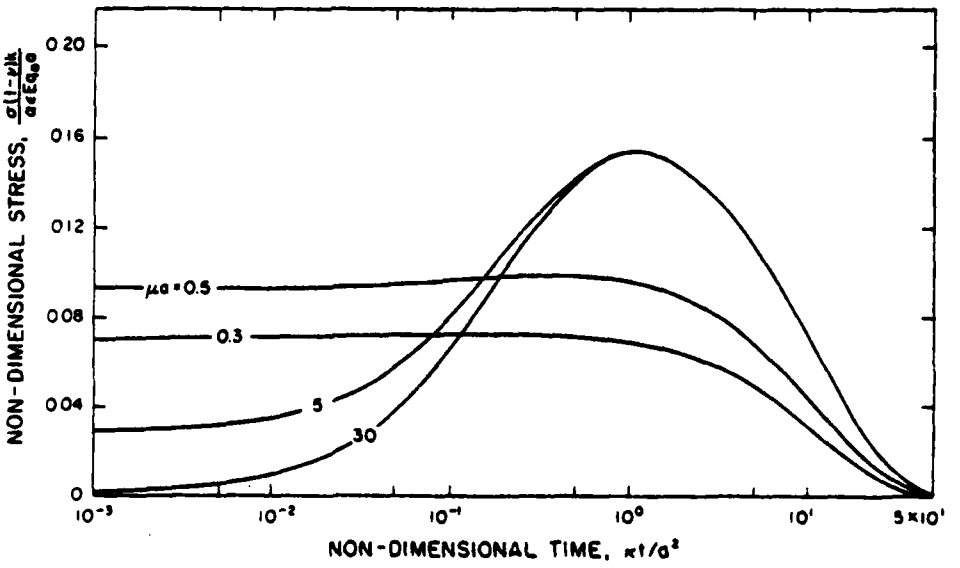

Fig. 5. Transient thermal stresses in the front (a) and the rear face (b) following the interruption of the radiation at time t = 0 in a partially absorbing flat plate with originally steady state temperature and stress distribution due to a normally incident radiation in the front face and cooling by convection at the rear surface for various values of μa with k = 0.2 W.cm.$^{-1}$°C.$^{-1}$, h = 0.006 W.cm.$^{-2}$°C.$^{-1}$, κ = 0.1 cm.^{2}s.$^{-1}$ and a = 10 cms.

a.

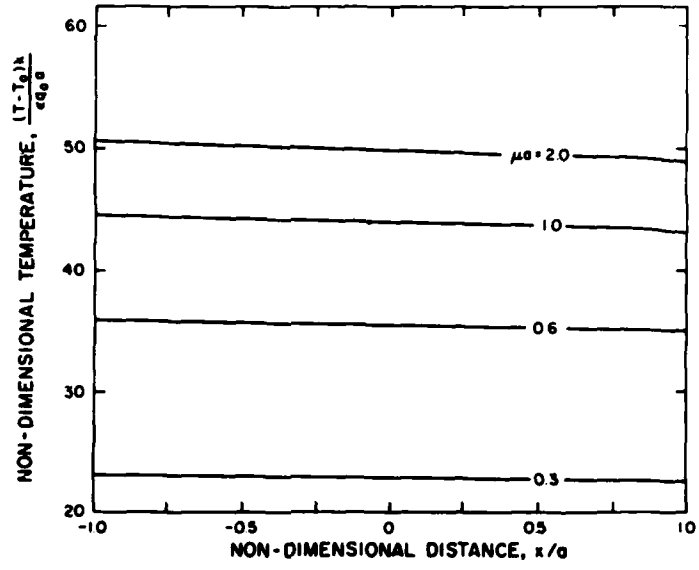

b.

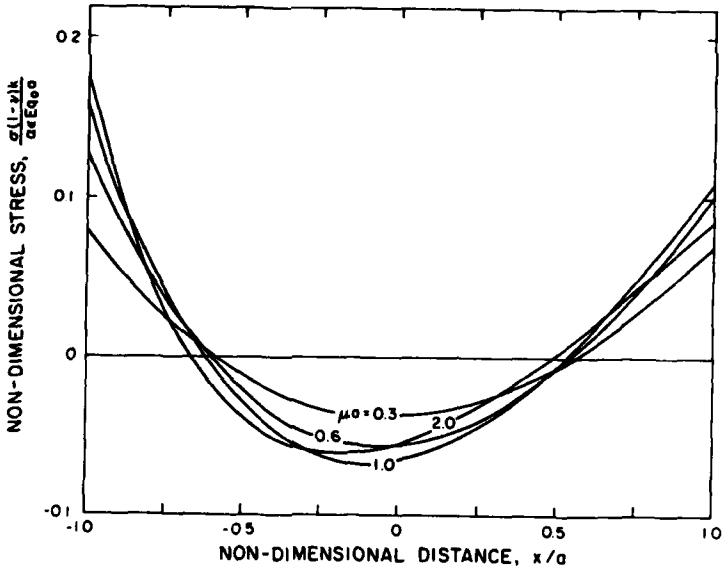

Fig. 1. Distribution of steady state temperature (a) and thermal stress (b) in a partially absorbing flat plate heated in the front by normally incident radiation and cooled by convection at the rear surface for various values of μa with k = 0.3 W.cm.$^{-1}$°C.$^{-1}$, h = 0.006 W.cm.$^{-2}$°C.$^{-1}$, κ = 0.1 cm.^{2}s.$^{-1}$ and a = 1 cm.

a.

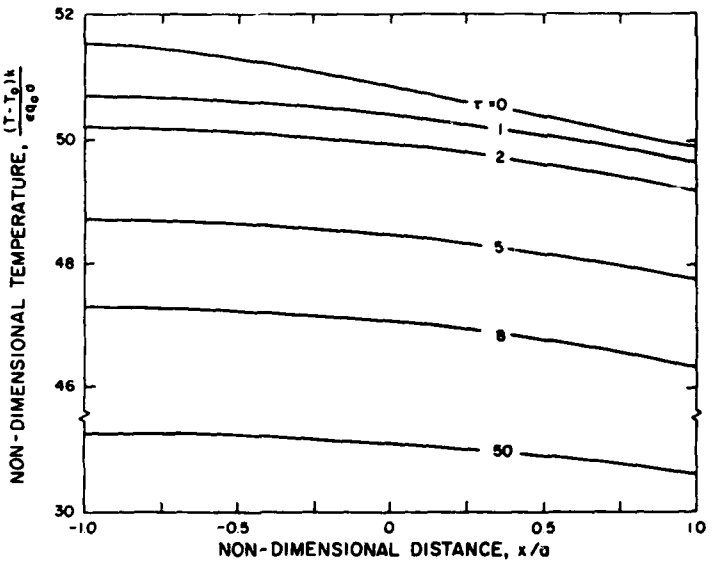

b.

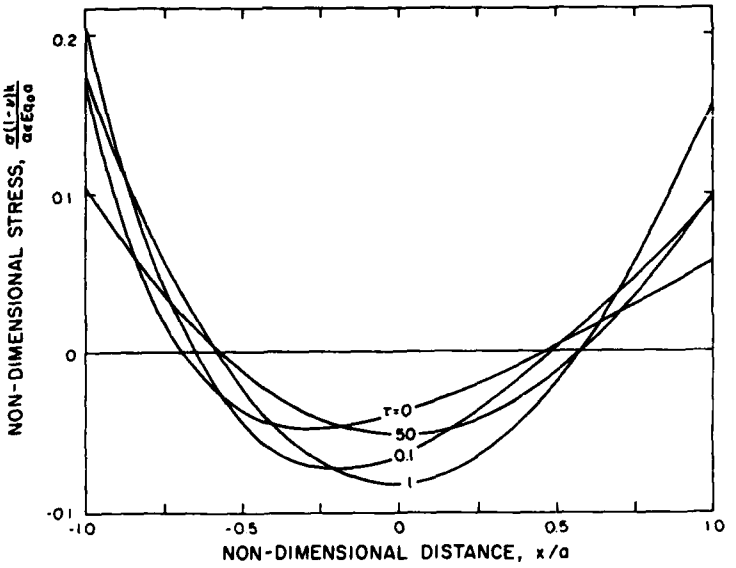

Fig. 2. Distribution of temperature (a) and thermal stress (b) for various values of time following the interruption of the radiation at time t = 0 in a partially absorbing flat plate with originally steady state temperature and stress distributions due to normally incident radiation in the front face and cooling at the rear surface by convection for k = 0.3 W.cm.$^{-1}$o$_C$.$^{-1}$, h = 0.006 W.cm.$^{-2}$o$_C$.$^{-1}$, κ = 0.1 cm.^{2}s.$^{-1}$, μa = 3 and a = 1 cm.

a.

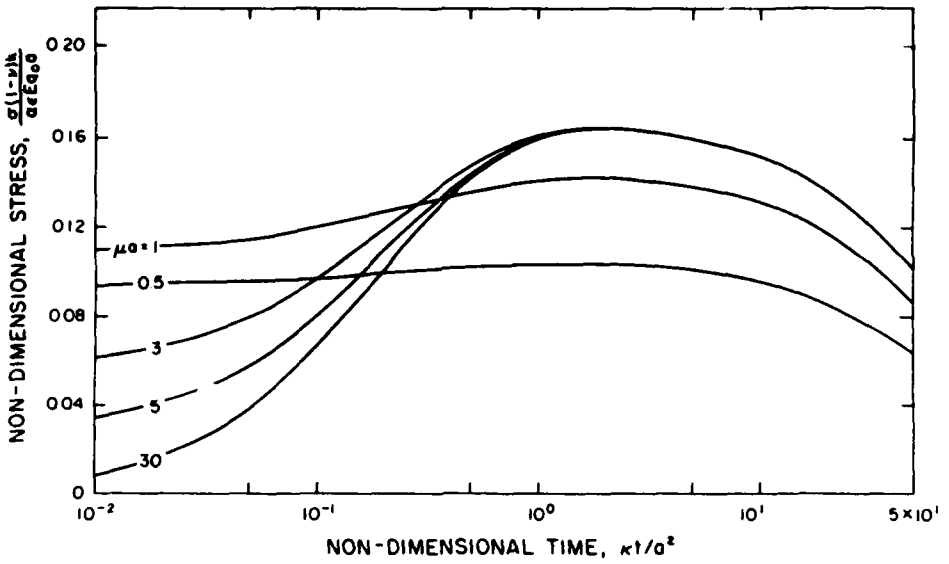

b.

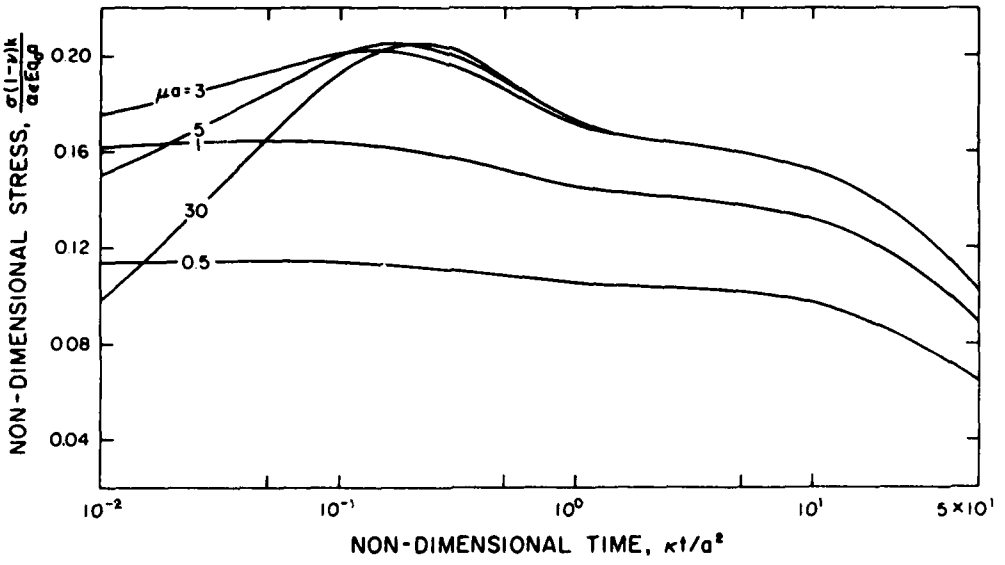

Fig. 3. Transient thermal stresses in the front (a) and the rear face (b) following the interruption of the radiation at time t = 0 in a partially absorbing flat plate with originally steady state temperature and stress distribution due to normally incident radiation in the front face and cooling by convection at the rear surface for various values of μa with k = 0.3 W.cm.$^{-1}$°C.$^{-1}$, h = 0.006 W.cm.$^{-2}$°C.$^{-1}$, κ = 0.1 cm.^{2}s.$^{-1}$ and a = 1 cm.

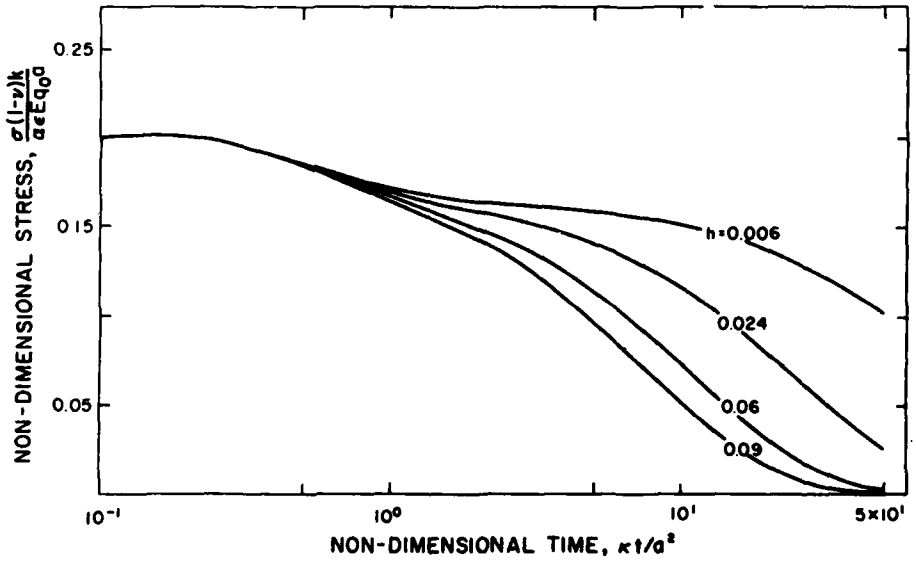

Fig. 4. Transient thermal stress in the rear surface following the interruption of the radiation at time t = 0 in a partially absorbing flat plate with originally steady state temperature and stress distribution due to normally incident radiation in the front face and cooling by convection at the rear surface for various values of h with k = 0.3 W.cm.$^{-1}$°C.$^{-1}$, μa = 3, ν = 0.1 cm.^{2}s^{-1} and a = 1 cm.

a.

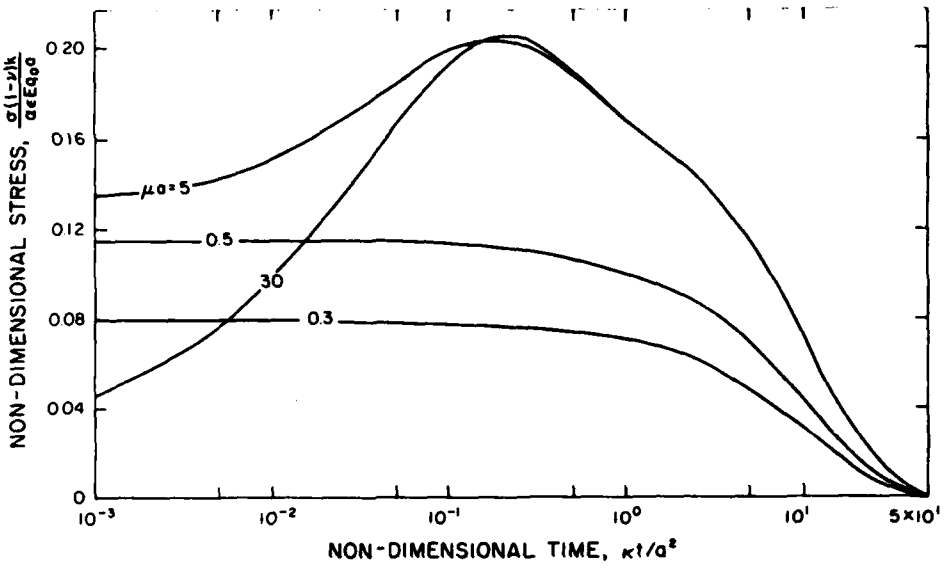

b.

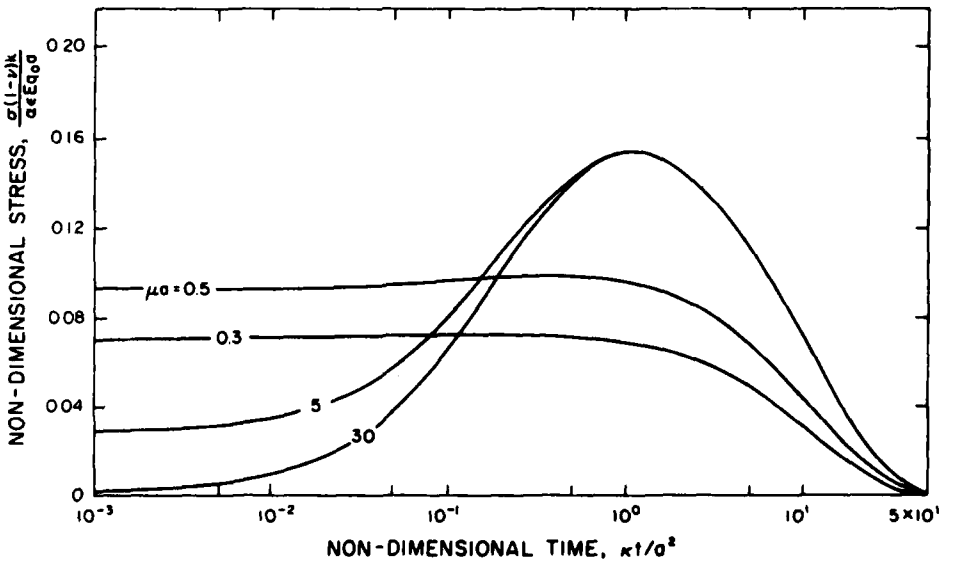

Fig. 5. Transient thermal stresses in the front (a) and the rear face (b) following the interruption of the radiation at time $t = 0$ in a partially absorbing flat plate with originally steady state temperature and stress distribution due to a normally incident radiation in the front face and cooling by convection at the rear surface for various values of μa with $k = 0.2$ W.cm.$^{-1}$°C.$^{-1}$, $h = 0.006$ W.cm.$^{-2}$°C.$^{-1}$, $\kappa = 0.1$ cm.^{2}s.$^{-1}$ and $a = 10$ cms.

CHAPTER VII

THERMAL STRESSES IN PARTIALLY ABSORBING FLAT PLATE DUE TO SUDDEN INTERRUPTION OF STEADY-STATE ASYMMETRIC RADIATION, II: CONVECTIVE COOLING AT FRONT SURFACE

by

J. P. Singh, J. I. Frankel, J. R. Thomas, Jr., D. P. H. Hasselman

Departments of Materials and Mechanical Engineering
Virginia Polytechnic Institute and State University
Blacksburg, Virginia 24061, USA

ABSTRACT

In Part II of this study the thermal stresses are analyzed in a partially absorbing flat plate, due to a sudden interruption of steady-state asymmetric radiation on the convectively cooled front face. As in the case of Part I, the maximum tensile stresses occur in the rear face. For the optical thickness $\mu a \geq 0.5$, the maximum tensile stress initially rises to a peak and then decreases with time. On the other hand, for $\mu a \leq 0.5$, the stresses decrease monotonically with time.

A comparison of the results for the front (Part II) and rear (Part I) cooling indicates that values of the maximum stress are numerically identical for small values of heat transfer coefficient, h, and plate thickness, a. Increasing difference in the magnitude of the stresses for the two cases is found with increasing h and a.

INTRODUCTION

In Part I of this study [1], solutions were presented for the temperatures and thermal stresses due to the sudden interruption of long-term steady-state asymmetric thermal radiation on the front surface of a partially absorbing flat plate cooled by Newtonian convection at the rear surface. In part II the same problem is considered, with the exception that the radiation heating and convection cooling both occur at the same (front) surface of the plate. The assumptions and notation for the present problem are identical to those of Part I.

ANALYSIS

Initial and Boundary Conditions

The initial condition for the temperature distribution for the present problem as obtained in an earlier study [2] is:

$$T(x,t) = T_o + \sum_{n=0}^{\infty} B_n(t)\cos\lambda_n(a - x) \tag{1a}$$

where

$$B_n(t) = \frac{G_n}{k\lambda_n^2}\left(1 - e^{-\kappa\lambda_n^2 t}\right) \tag{1b}$$

$$G_n = \frac{kq_o\mu\varepsilon}{N_n k}\left[\frac{\lambda_n\sin(2\lambda_n a)+\mu\cos(2\lambda_n a) - \mu e^{-2\mu a}}{\mu^2 + \lambda_n^2}\right] \tag{1c}$$

$$N_n = a + (h/2\lambda_n^2 k)\cos^2(2\lambda_n a) \tag{1d}$$

and λ_n is the root of the trancendental equation:

$$\lambda_n \tan(2\lambda_n a) = (h/k) \tag{1e}$$

Solutions for the transient temperature distribution are obtained by solving:

$$\frac{\partial^2 T}{\partial x^2} = \frac{1}{\kappa} \frac{\partial T}{\partial t} \tag{2}$$

subject to the boundary conditions:

$$\frac{\partial T}{\partial x}(a,t) = 0 \tag{3}$$

and

$$\frac{\partial T}{\partial x}(-a,t) = -\frac{h}{k}\,[T(-a,t)-T_o] \tag{4}$$

Transient Temperatures

Solution of Eq. 2 subject to the initial and boundary conditions given by Eqs. (1,3,4) yields:

$$T(x,t) = T_o + \sum_{n=1}^{\infty} B_n(t) \cos \lambda_n (a-x) \tag{5}$$

where

$$B_n(t) = \frac{G_n}{\kappa \lambda_n^2} e^{-\kappa \lambda_n^2 t} \tag{6}$$

with λ_n and G_n defined earlier.

Thermal Stresses

Following the procedure outlined in Part I the thermal stresses are:

$$\sigma_{y,z} = -\frac{\alpha E}{1-\nu} \sum_{n=0}^{\infty} B_n(t) \cos\,[\lambda_n(a-x)] + \frac{\alpha E}{2a(1-\nu)} \sum_{n=0}^{\infty} \frac{B_n(t)\sin(2\lambda_n a)}{\lambda_n} + \frac{3x\alpha E}{2a^3(1-\nu)} \sum_{n=0}^{\infty} B_n(t) \left[\frac{1-\cos(2\lambda_n a)}{\lambda_n^2} - \frac{a \sin(2\lambda_n a)}{\lambda_n}\right] \tag{7}$$

The numerical results will be presented in terms of the non-dimensional temperature, stress and time defined in Part I.

NUMERICAL RESULTS AND DISCUSSION

In order to facilitate comparison, the data presented will be for the identical values of the pertinent parameters chosen for Part I, namely $k = 0.3\ W.cm.^{-1}{}^{\circ}C^{-1}$ and $a = 1$ cm, except where noted. Furthermore, the sequence of the figures will be identical. For a range of values of optical thickness, μa, Figs. 1a and 1b show the distribution of the temperature and thermal stresses, respectively, in the plate at $t = 0$, immediately prior to the interruption of the radiation. Comparison of the temperature distribution (Fig. 1a) with the corresponding data in Part I shows that radiation heating and convective cooling at the same surface produces lower temperatures at the exposed surface than for radiation heating and convective cooling at opposite surfaces. As pointed out in earlier studies [2,3], this latter conclusion could be relevant to the design of components of high-intensity solar collectors subject to material degradation. Excessive surface temperatures can be avoided by providing the convective cooling at the same surface being irradiated.

The values of the thermal stresses reach their maximum for a value of optical thickness $\mu a \simeq 2$. Comparison of the values of the thermal stresses at $t = 0$, just prior to the interruption of the radiation as displayed in Fig. 1b of parts I and II, shows them to be almost independent of the surface at which the convective cooling takes place. However, comparison of the analytical expressions for the thermal stresses for the two modes of cooling show them not to be the same. Further detailed analysis reveals

that the numerical values for the thermal stresses for given values of the heat transfer coefficient, optical thickness, and thermal conductivity become equal only when the plate thickness $2a \to 0$.

Figures 2a and 2b, for $\mu a = 3$, show the distribution of the transient temperatures and stresses, respectively for a range of values of time, τ, following the interruption of the radiation using the same values of k, κ and h as in Figs. 1a and 1b. The data for the stress are almost identical to those given in Part I. However, slight differences necessitated choosing different values for τ in order to avoid too much overlap of the curves, for purposes of clarity.

Figures 3a and 3b show the values for the thermal stresses at the front and rear faces of the plate, respectively, as a function of time for a range of values of μa. As found in Part I, the stresses for $\mu a \geq 0.5$ initially increase to a maximum followed by a monotonic decrease with increasing time. The stresses in the rear face exceed those in the front face.

In Fig. 4, we compare the transient thermal stresses at the rear face for a range of values of the heat transfer coefficient for $\mu a = 3$. At thermal equilibrium, just prior to the cut-off of the radiation, the magnitude of stress is independent of the heat transfer coefficient [2]. This effect arises because the heat transfer coefficient controls the absolute temperature at the front face, but not the internal temperature distribution, which is responsible for the development of the thermal stresses. With increasing time, the stresses go through a maximum, with a peak value which is an inverse function of but strongly dependent on the magnitude of the heat transfer coefficient.

Comparison of the present data in Fig. 4 with the corresponding data for rear face cooling presented in Part I shows that for h = 0.006 cal. $cm.^{-2}{}^{\circ}C.^{-1}s^{-1}$, the numerical values for the stresses at any instant of time are almost identical. In contrast, at the highest value of the heat transfer coefficient (h = 0.09 cal.$cm.^{-2}{}^{\circ}C.^{-1}s^{-1}$), considerable difference exists in the magnitude of the stresses for front and rear face cooling. This difference was sufficiently large that a change in scale was required for presentation of the respective data shown in Fig. 4 in Parts I and II.

The difference in the effect of the heat transfer coefficient on the magnitude of thermal stress for front and rear face cooling can be explained qualitatively. It should be noted that the magnitude of the transient thermal stresses for both front and rear face cooling will be a function of both the magnitude of the initial temperature rise of the plate as well as the temperature non-uniformity within the plate. As noted earlier the initial temperature rise of the plate is inversely proportional to the value of the heat transfer coefficient. The non-uniformity of the internal temperature distribution is independent of the value of the heat transfer coefficient and is a function of the distribution of the internal absorption of the incident radiation. Two limiting cases can be considered, namely $h \to 0$ and $h \to \infty$. For $h \to 0$, the temperature non-uniformity within the plate will become very small relative to the initial total temperature rise. This latter quantity for front and rear face cooling will tend to become equal. With the magnitude of the transient thermal stresses being proportional to this initial temperature rise, the stresses will be equal for front and rear face cooling.

As $h \to \infty$, a completely different situation arises. For front face cooling, no temperature rise and temperature non-uniformity occurs which yields zero initial and transient thermal stress on cooling. Rear face cooling, however, will result in a temperature rise at the front face and accompanying non-uniform temperature distribution within the plate. In transient cooling after the cut-off of the radiation, transient thermal stresses will inevitably result. Obviously, the results for the present study ($0 \leq h \leq \infty$) will fall between the above mentioned two limits.

Figures 5a and 5b show the transient thermal stresses at the front and rear surface of the plate, respectively, for a = 10 cm for the same numerical values of the appropriate parameters for the data in Figs. 3a and 3b. Comparison with these latter data indicates that (as also noted in Part I) plotting the data for the present thermal problem on a dimensionless basis does not result in a universal plot for the same reasons as outlined in Part I.

Comparison of Figs. 5a and 5b in Part I and II shows that for a = 10 cm, the peak transient thermal stresses for front face cooling lie somewhat below the corresponding values for rear face cooling. As noted earlier, for a = 1 cm, these stresses are almost identical. It appears that the magnitudes of the peak tensile stresses for front and rear face cooling diverge with increasing plate thickness.

In summary, solutions and numerical values have been presented for the transient thermal stresses in a semi-absorbing flat plate initially at thermal equilibrium due to long-term radiation heating and convective cooling at the front surface, and subjected to an instantaneous cut-off

of the radiation. The transient stresses were found to be quantitatively almost identical to those for convective cooling at the rear surface, for small plate thicknesses and low heat transfer coefficient. However, the magnitude of the transient stresses for front and rear cooling diverge with increasing plate thickness and heat transfer coefficient.

ACKNOWLEDGMENT

This study was conducted as part of a program on the thermo-mechanical behavior of brittle structural materials supported by the Office of Naval Research under Contract No. N00014-78-C-0431.

REFERENCES

1. J. I. Frankel, J. P. Singh, J. R. Thomas, Jr., D. P. H. Hasselman, Thermal Stresses in Partially Absorbing Flat Plate Due to Sudden Interruption of Steady-State Asymmetric Radiation, I: Convective Cooling at Rear Surface, J. of Thermal Stresses (in review).

2. J. P. Singh, K. Satyamurthy, J. R. Thomas, Jr., D. P. H. Hasselman, Analysis of Thermal Stress Resistance of Partially Absorbing Ceramic Plate Subjected to Asymmetric Radiation, II: Convective Cooling at Front Surface, J. Amer. Ceram. Soc., Vol. 64, pp. 169-173, 1981.

3. J. R. Thomas, Jr., J. P. Singh and D. P. H. Hasselman, Analysis of Thermal Stress Resistance of Partially Absorbing Ceramic Plate Subjected To asymmetric Radiation, I: Convective Cooling at Rear Surface, J. Amer. Ceram. Soc., Vol. 64, pp. 163-169, 1981.

CAPTIONS

Fig. 1. Distribution of steady state temperature (a) and thermal stress (b) in a partially absorbing flat plate heated by normally incident radiation and cooled by convection in the front face for various values of μa with k = 0.3 $W.cm.^{-1}°C^{-1}$, h = 0.006 $W.cm.^{-2}°C.^{-1}$, κ = 0.1 $cm.s^{-1}$ and a = 1 cm.

Fig. 2. Distribution of temperature (a) and thermal stress (b) for various values of time folloiwng the interruption of the radiation at time t = 0 in a partially absorbing flat plate with originally steady state temperature and stress distributions due to normally incident radiation heating and convection cooling at the front face for k = 0.3 $w.cm.^{-1}°C^{-1}$, h = 0.006 $W.cm.^{-2}°C^{-1}$, κ = 0.1 $cm.^2s.^{-1}$, μa = 3 and a = 1 cm.

Fig. 3. Transient thermal stresses in the front (a) and the rear face (b) following the interruption of the radiation at time t = 0 in a partially absorbing flat plate with originally steady state temperature and stress distribution due to normally incident radiation heating and convection cooling at the front face for k = 0.3 $W.cm.^{-1}°C.^{-1}$, h = 0.006 $W.cm.^{-2}°C.^{-1}$, κ = 0.1 $cm.^2s.^{-1}$ and a = 1 cm.

Fig. 4. Transient thermal stresses in the rear surface following the interruption of the radiation at time t = 0 in a partially absorbing flat plate with originally steady state temperature and stress distribution due to normally incident radiation heating and convection cooling in the front face for various values of h with k = 0.3 $W.cm.^{-1}°C.^{-1}$, μa = 3, κ = 0.1 $cm.^2s.^{-1}$ and a = 1 cm.

Fig. 5. Transient thermal stresses in the front (a) and the rear face (b) following the interruption of the radiation at time t = 0 in a partially absorbing flat plate with originally steady-state temperature and stress distribution due to a normally incident radiation heating and convection cooling in the front face for various values of μa with k = 0.3 $W.cm.^{-1}°C.^{-1}$, h = 0.006 $W.cm.^{-2}°C^{-1}$, κ = 0.1 $cm.^2s.^{-1}$ and a = 10 cms.

a.

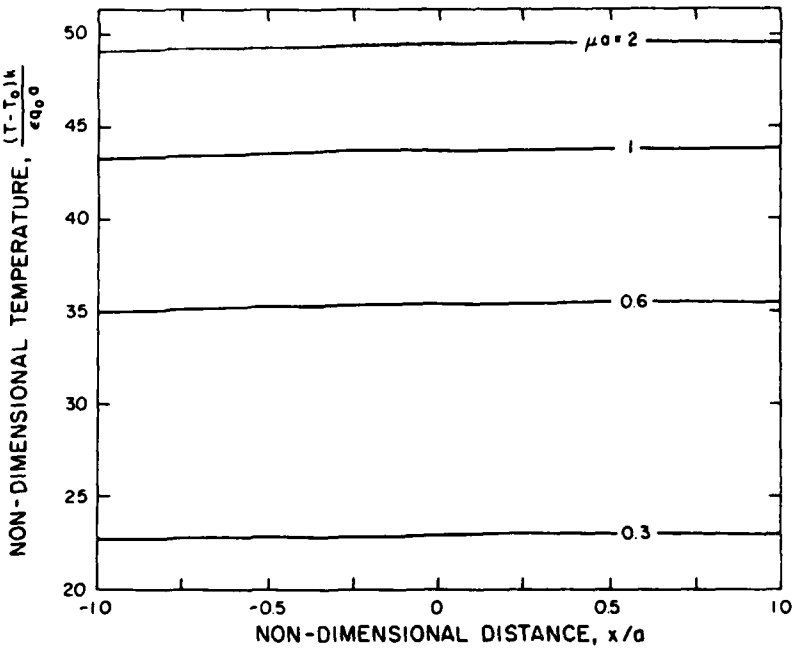

b.

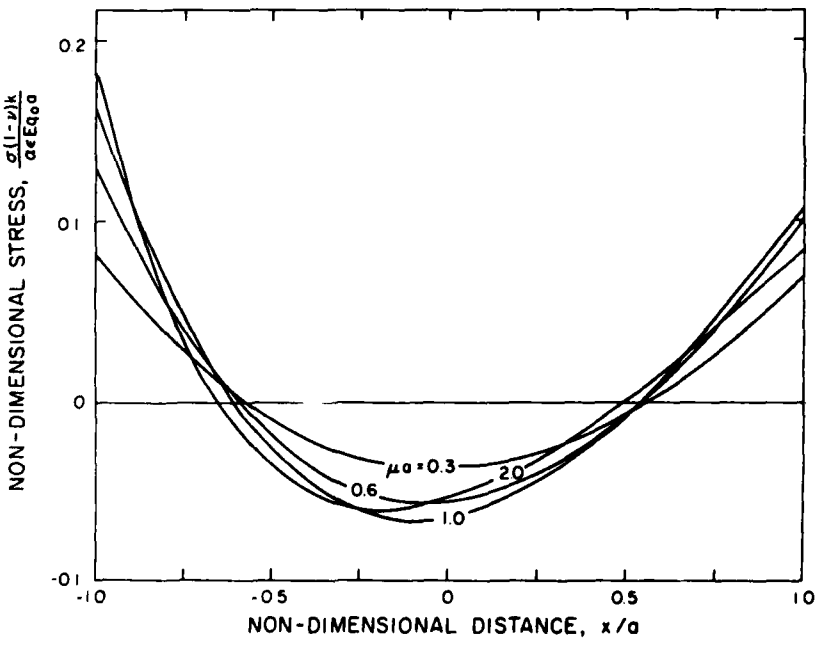

Fig. 1. Distribution of steady state temperature (a) and thermal stress (b) in a partially absorbing flat plate heated by normally incident radiation and cooled by convection in the front face for various values of μa with k = 0.3 W. $cm.^{-1}°C^{-1}$, h = 0.006 W. $cm.^{-2}°C^{-1}$, κ = 0.1 $cm.^2 s.^{-1}$ and a = 1 cm.

a.

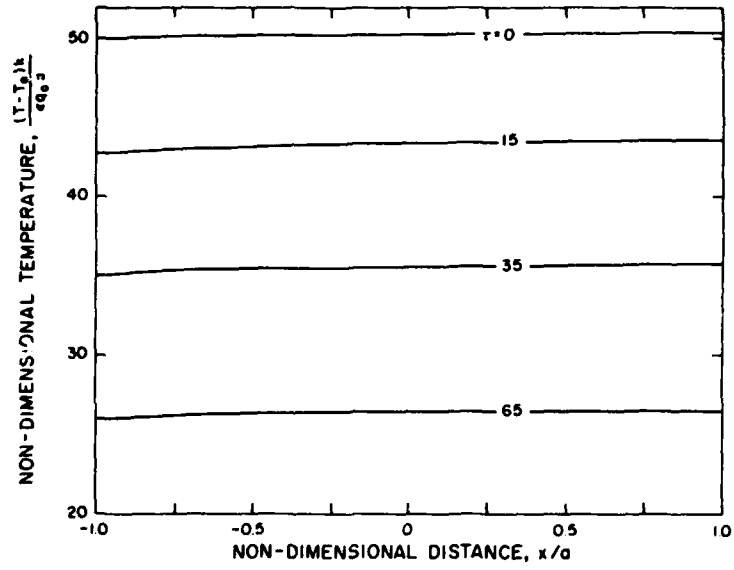

b.

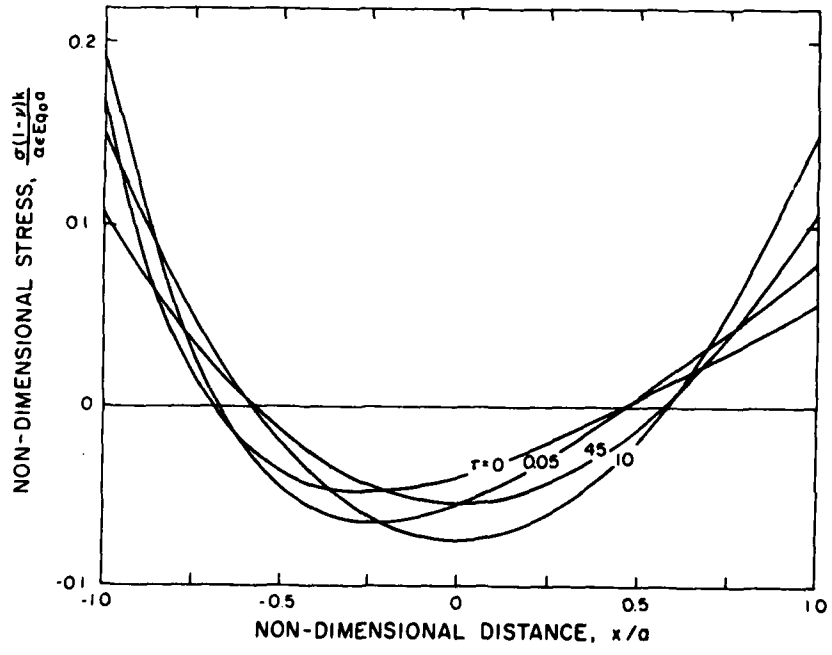

Fig. 2. Distribution of temperature (a) and thermal stress (b) for various values of time following the interruption of the radiation at time t = 0 in a partially absorbing flat plate with originally steady state temperature and stress distribution due to normally incident radiation heating and convection cooling at the front face for $k = 0.3$ W.cm.$^{-1}$°C.$^{-1}$, $h = 0.006$ W.cm.$^{-2}$°C^{-1}, $\kappa = 0,1$ cm.^{2} s.$^{-1}$, $\mu a = 3$ and $a = 1$ cm.

a.

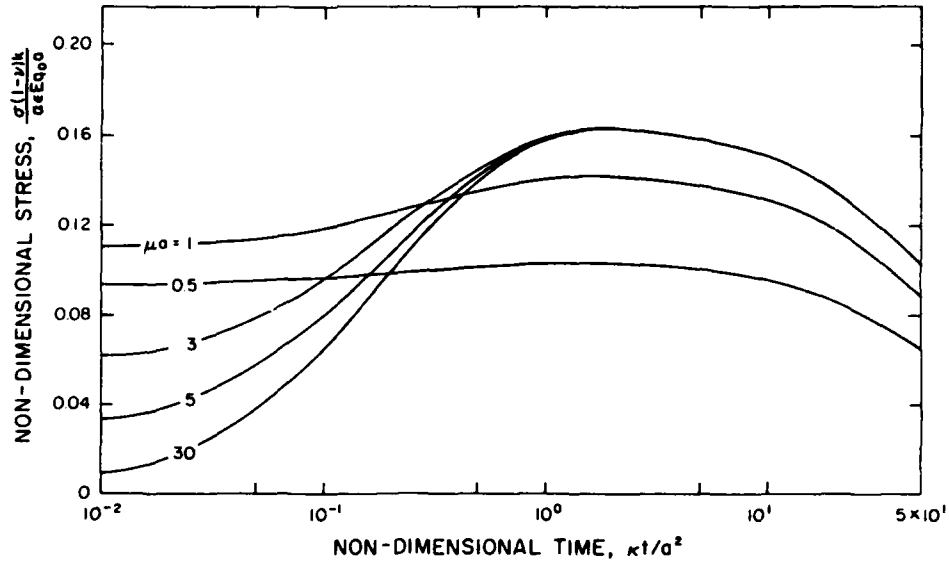

b.

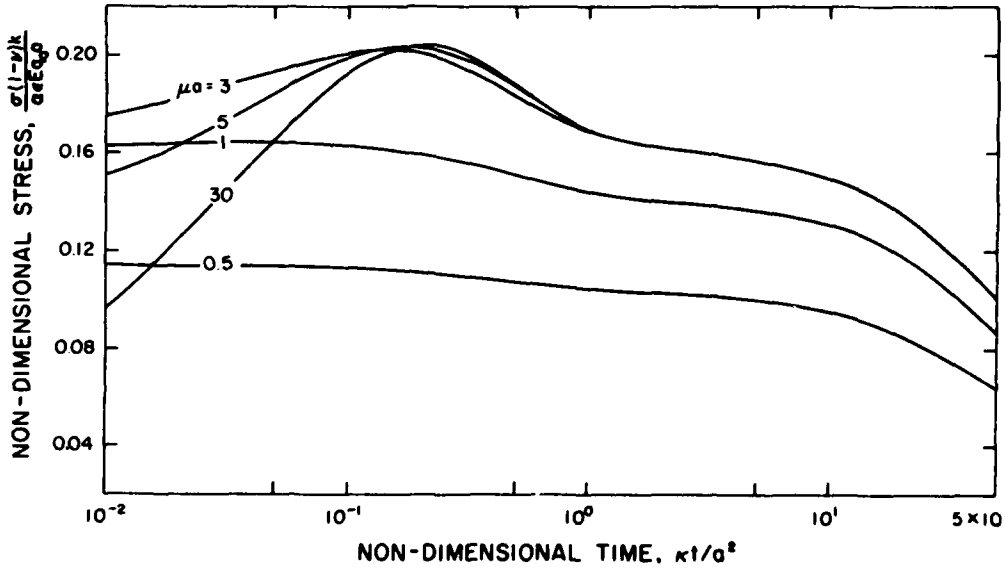

Fig. 3. Transient thermal stresses in the front (a) and the rear face (b) following the interruption of the radiation at time t = 0 in a partially absorbing flat plate with originally steady state temperature and stress distribution due to normally incident radiation heating and convection cooling at the front face for k = 0.3 W.cm.$^{-1}$°C^{-1}, h = 0.006 W.cm.$^{-2}$°C.$^{-1}$, κ = 0.1 cm.^{2}s.$^{-1}$ and a = 1 cm.

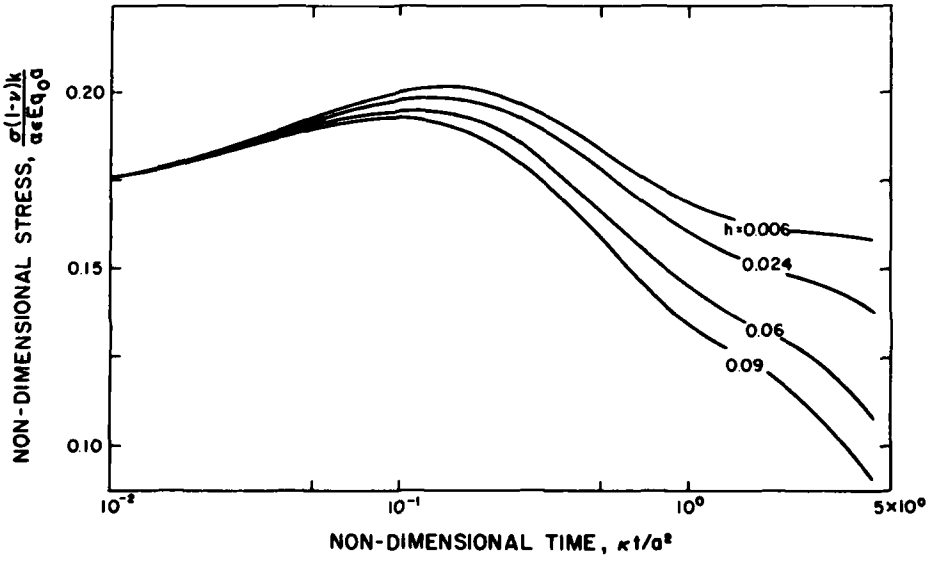

Fig. 4. Transient thermal stress in the rear surface following the interruption of the radiation at time t = 0 in a partially absorbing flat plate with orginally steady state temperature and stress distribution due to normally incident radiation heating and convection cooling in the front face for various values of h with k = 0.3 W.cm.$^{-1}$°C^{-1}, μa = 3, κ = 0.1 cm.^{2}s.$^{-1}$ and a = 1 cm.

a.

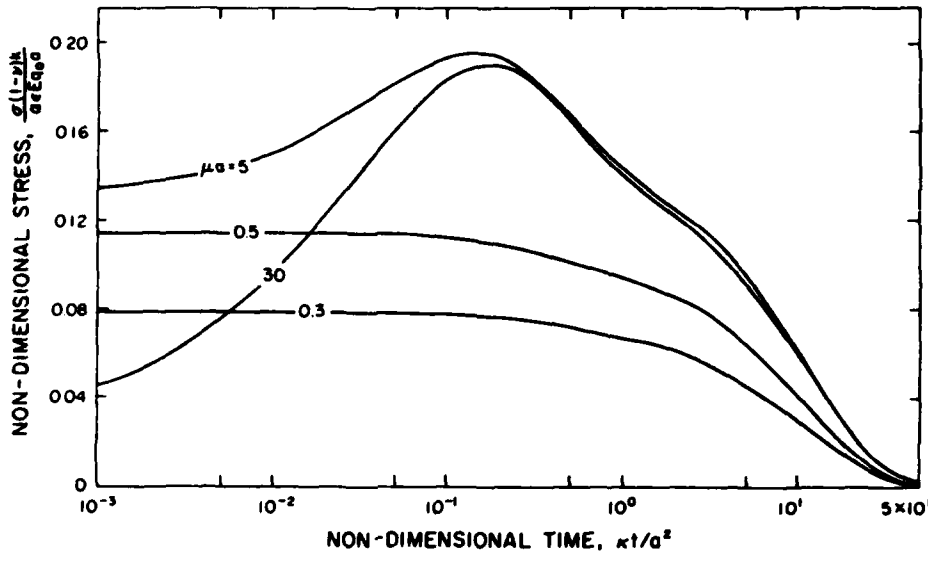

b.

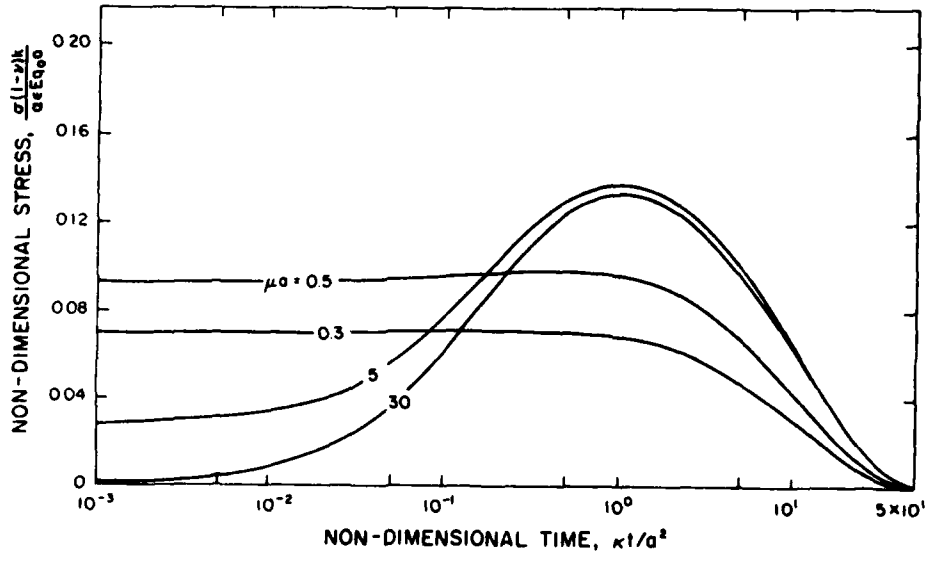

Fig. 5. Transient thermal stresses in the front (a) and the rear face (b) following the interruption of the radiation at time t = 0 in a partially absorbing flat plate with originally steady-state temperature and stress distribution due to a normally incident radiation heating and convection cooling in the front face for various values of μa with k = 0.3 W.cm.$^{-1}$°C^{-1}, h = 0.006 W.cm.$^{-2}$°C^{-1}, κ = 0.1 cm.^{2}s.$^{-1}$ and a = 10 cms.

CHAPTER VIII

THERMAL STRESSES IN A PARTIALLY ABSORBING FLAT PLATE ASYMMETRICALLY HEATED BY CYCLIC THERMAL RADIATION AND COOLED BY CONVECTION: ADDENDUM

J. P. Singh, J. R. Thomas, Jr., and D. P. H. Hasselman
Departments of Mechanical and Materials Engineering
Virginia Polytechnic Institute and State University
Blacksburg, VA 24061 USA

THERMAL STRESSES IN A PARTIALLY ABSORBING FLAT PLATE ASYMMETRICALLY HEATED BY CYCLIC THERMAL RADIATION AND COOLED BY CONVECTION: ADDENDUM

J. P. Singh, J. R. Thomas, Jr. and D. P. H. Hasselman
Departments of Mechanical and Materials Engineering
Virginia Polytechnic Institute and State University
Blacksburg, Virginia 24061 USA

In a recent study (1), the present authors presented an analysis of the frequency dependence of the thermal stresses in a partially absorbing flat plate due to the internal absorption of cyclic thermal radiation normally incident on one face, and cooling by convection at the opposite face. At higher frequencies, after an initial transient, the plate reaches a steady-state temperature profile and associated thermal stress distribution with a superposed cyclic variation of small amplitude relative to the total temperature rise and thermal stresses.

At very low frequencies, a different effect occurs. The mean temperature of the plate and associated thermal stresses cycle along with the intensity of the incident heat flux. As the frequency $\omega \rightarrow 0$, the plate is subjected to a quasi steady-state heat flux. This effect could not be included in the linear plots of the frequency dependence of the maximum thermal stresses encountered during the first cycle and after many cycles at which the plate has reached a constant time-averaged temperature given in Figs. 5a and 5b, respectively, of the original study (1). The purpose of this communication is to report these values. Material property values identical to those used for the data given in Fig. 5 of the original paper were used for the calculation, namely: heat transfer coefficient $h = 0.006\ W.cm^{2}.{}^{o}C^{-1}$, thermal diffusivity $\kappa = 0.1\ cm^{2}.s^{-1}$,

plate half-thickness a = 1 cm and absorption coefficient $\mu = 3\ cm^{-1}$.

Figures 1a and 1b show the values of the thermal stresses in the front face, center and back face(x = -a, 0, and a, respectively) as a function of the angular frequency encountered during the first cycle and after the plate has reached a quasi-static equilibrium when no cycle-to-cycle variation in temperature or stress is found. The results are presented in terms of the maximum and minimum stress encountered within a given cycle for the three positions in the plate.

Figure 1a shows that as $\omega \to o$, the mimimum value of tensile stress of 0.334 encountered during the first cycle is twice the value of 0.167 after long-term steady-state radiation of intensity q_o, found in an earlier study (2). It should be noted that for the specific cyclic variation chosen for this study with $q = q_o(1 + \sin \omega t)$, the maximum intensity of radiation within any one cycle reaches a value of $2q_o$. This indicates that indeed as $\omega \to o$ the plate can be considered to be subjected to a quasi-steady-state heat flux after an initial brief transient at t = 0 when the heat flux changes discontinuously from zero to q_o. The stresses due to this initial transient are identical to those found for sudden imposition of steady-state radiation with a constant flux q_o (2).

Figure 1b shows that after long-term radiation, as $\omega \to o$ the stresses in all three positions can become zero. This is expected since within the cycle the value of minimum heat flux is identically equal to zero. The other (non-zero) values of stress, as $\omega \to o$, corresponds to the maximum value of heat flux within the cycle, equal to $2q_o$.

Of interest to note is that, as indicated by both figures, the magnitude of the maximum stress, as well as the position within the plate at which it occurs, varies with frequency. When the frequency $\omega \to \infty$ the stresses correspond to those found for a constant heat flux q_o.

ACKNOWLEDGMENT

This study was supported by the Office of Naval Research under contract N00014-78-C-0431.

REFERENCES

1. J. R. Thomas, Jr., J. P. Singh and D. P. H. Hasselman, Thermal Stresses in a Partially Absorbing Flat Plate Asymmetrically Heated by Cyclic Thermal Radiation and Cooled by Convection, J. Thermal Stresses, (In press).
2. J. R. Thomas, Jr., J. P. Singh and D. P. H. Hasselman, Analysis of Thermal Stress Resistance of Partially Absorbing Ceramic Plate Subjected to Asymmetric Radiation, I: Convective Cooling at Rear Surface, J. Am. Ceram. Soc., 64, pp. 163-169, 1981.

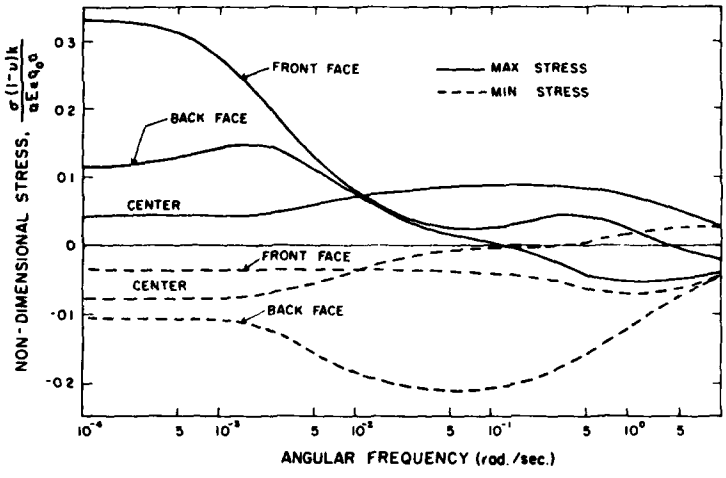

a.

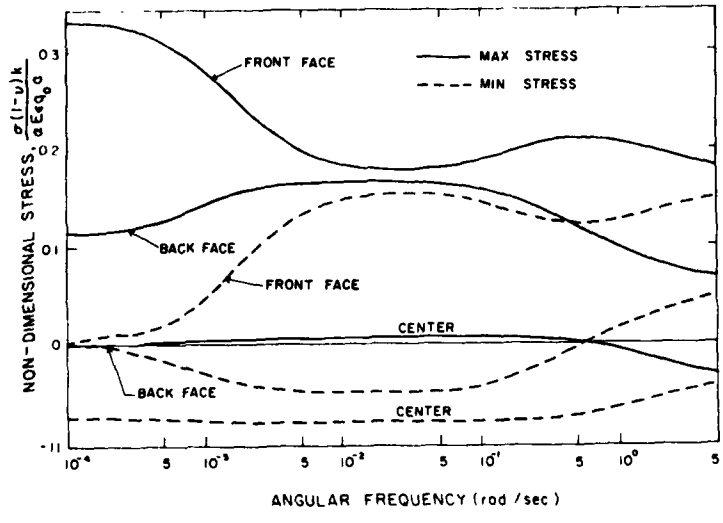

b.

Fig. 1. Frequency dependence of range of thermal stresses in front, center and rear in partially absorbing flat plate heated in front by cyclic thermal radiation and cooled by convection at the rear surface for: $h = 0.006$ W.cm.$^{-2}$°C^{-1}, $k = 0.3$ W.cm.$^{-1}$°C^{-1}, $\kappa = 0.1$ cm.^{2}s^{-1}, $\mu = 3$ cm^{-1} and $a = 1$ cm. (a) during first cycle and (b) for steady state.

CHAPTER IX

Analysis of Thermal Stress Failure of Segmented Thick-Walled Refractory Structures

by

W. S. Chang, C. E. Knight, D. P. H. Hasselman, and R. G. Mitchiner

Departments of Mechanical and Materials Engineering
Virginia Polytechnic Institute and State University
Blacksburg, Virginia 24061 USA

ABSTRACT

A finite-element-analysis was conducted of the thermal stresses in rectangularly shaped components of segmented thick-walled refractory structures with length in the direction of heat flow much larger than the height or width. Heating was assumed to occur uniformly at a linear rate over the front face defined by the smaller dimensions. Most calculations were carried out for two-dimensional conditions of plane stress, which assumes that the magnitude of stress is independent of height. A limited number of three-dimensional calculations permitted analyzing the effect of height.

For moderate values of heating rates, corresponding to those possibly encountered in practice, a biaxial tensile stress was found to exist some distance behind the hot face with the maximum value of stress along the centerline parallel to the component length in accordance with the fracture mode cbserved in practice. At high heating rates, however, the maximum tensile stress component was found to occur parallel tc the face being heated.

For conditions of plane stress under moderate heating rates, the magnitude of stress was found to be proportional to heating rate and an inverse function of the thermal diffusivity. Maximum values of stress were encountered for intermediate values of width. This latter result suggests that the incidence of thermal stress failure may be reduced by either reductions or increases in the values of width commonly used in practice. The three-dimensional calculations indicated that the magnitude of stress rises rapidly with height. This result suggests that

improvements in thermal stress resistance can be obtained by reductions in the values of height from the current values in practice.

By means of a fracture-mechanical analysis it is demonstrated that cracks oriented perpendicularly to the direction of heat flow formed as the result of the above stresses could be unstable and are expected to propagate across the total crossection to lead to total separation, in accordance with observations.

The stress values obtained in the present study were compared with those predicted by the Kienow theory. Reasonable agreement was found for the peak stresses at the lower values of time. However, with increasing duration and the higher values of height the Kienow theory underestimates the magnitude of stress considerably.

INTRODUCTION

Engineering structures or components which operate at elevated temperatures require materials of construction with high melting points, combined with excellent resistance to corrosion, deformation and fracture at high temperature. Many of these requirements are met by engineering ceramics or refractories. Unfortunately, these materials exhibit a high degree of brittleness.

In the majority of service requirements, involving elevated temperature, the structures or components inevitably are subjected to transient or steady-state heat flow. With few exceptions the corresponding spatially non-uniform temperature distribution within the structure or component can result in the formation of thermal stresses of high magnitude[1]. Because of the high brittleness of most ceramics or refractories, failure under the influence of these thermal stresses can involve extensive crack propagation[2]. Under these conditions failure can be near if not totally catastropic with an associated major adverse effect on the subsequent satisfactory performance of the structure or component in its intended application.

A number of different modes of failure and associated crack propagation in brittle ceramics and refractories can be identified. On heating, corners of angularly shaped components can be removed by spalling by what appears to be failure in shear. On heating or cooling, failure most commonly occurs in tension with the direction of crack propagation parallel to the direction of heat flow. This mode of failure is entirely in accordance with the fracture mode inferred from theoretical solutions[3] for the stresses in thin plates, tubes and other similar geometries

which indicate that the magnitude of the stresses in the direction of heat flow due to the presence of the free surfaces are small or even negligible compared to the stresses perpendicular to the heat flow. An exception to this general rule is found in the failure of thick-walled structures which consist of an assembly of sub-components with dimensions in the direction of heat flow larger than those in the perpendicular directions. Examples of such structures are linings of refractory process vessels used in the chemical and metal processing industries, coal-gasification systems, ship-board incinerators, air-preheaters for wind-tunnels, first walls in fusion reactors, and similar structures. The linings of the basic-oxygen-furnace (BOF) represent a particular case. The dimensions of the individual components of such linings typically have cross sections measuring some 8 by 15 cm with a length of as much as 75 cm, with the direction of heat flow along the length.

In such individual components due to the lack of structural interaction from component to component, thermal stresses perpendicular to the direction of heat flow cannot fully develop. In this case, failure is unlikely to occur with the plane of crack propagation parallel to the direction of heat flow. Instead, as identified by Kienow[4] and Ainsworth[5] failure occurs with the plane of crack propagation oriented perpendicularly to the direction of heat flow. In particular, this mode of failure occurs during too rapid heat-up of the refractory lining. The origin of failure appears to be located on the centerline of the refractory component and some 5-10 cm behind the face at which the heating occurs. Simultaneous failure of a number of adjacent components can result in the reduction in thickness of the refractory linings over a considerable

area. In turn this can have a major adverse effect on the total lifetime of the refractory structure. It should be noted that a similar mode of failure can occur on cooling[6], with the exception that the origin of failure appears to be located along the side of the component with the direction of crack propagation inward towards the center of the component. This study will concentrate on the mode of failure during heating.

For purposes of improved engineering design and assuring long-term structural reliability it is imperative that the fundamental variables which control the thermal stress failure on heating as described above are well understood. In an earlier study carried out for this purpose, Kienow[4] developed a theory which relates the tensile stress in the refractory component at any position along the center line to the curvature (i.e., the second derivative) of the temperature distribution at that position. Implicit in this relationship is that the thermal stresses at any position within the component are independent of the temperature distribution at other positions. This, however, is not likely to be correct in view of the coupled nature of thermal stresses and their general dependence on the temperature distribution and boundary conditions throughout a component or structure as evidenced by an extensive literature[3]. In the light of results obtained in this study, it should be noted also that the Kienow theory predicts that the magnitude of the stresses are a function of the width but not the height of the refractory component.

Because of the existence of corners and free surfaces parallel to the direction of heat flow analytical methods appropriate for geometries

such as infinite plates, hollow and solid cylinders etc., are inappropriate for a theoretical study of the mode of thermal fracture of components of finite size, as described above. In this respect, then, the objective of this study was to investigate the above problem by numerical means, specifically the finite element method.

II. Numerical Procedures and Boundary Conditions

The mechanical model selected for this study, shown schematically in Fig. 1, consisted of a rectangularly shaped solid located at $0 \leq x \leq L$, $-b/2 \leq y \leq b/2$, and $-d/2 \leq z \leq d/2$ where L, b, and d are the length, width, and height, respectively. These dimensions were such that $L >> b,d$. Heating was chosen to take place uniformly on the surface defined by the width, b, and height, d, located at $x = 0$. Because of its significance to industrial practice, this surface was assumed to be heated at a constant linear rate from an initial uniform temperature T_o at $t = 0$:

$$T(x = 0) = at + T_o(x = 0) \tag{1}$$

where a is the rate of change of temperature and t is the time. For simplicity T_o was taken equal to zero. The assumption of a linear rate of heating was also chosen for the study of Ainsworth[5]. Heat flow was assumed to be unidirectional along the x-axis only. As the segment is assembled with other segments surrounding it there is no heat transfer from the sides. The rear surface at $x = L$ was assumed to be insulated, that is:

$$\frac{dT}{dx}(x = L) = 0 \tag{2}$$

The assumption of an insulated back surface is not critical because as found in practice, fracture occurs during the initial stages of heating well before the rear surface (x = L) sees any perceptible increase in temperature.

A major simplification in the total computational effort was achieved by assuming that the thermal conductivity and thermal diffusivity were independent of temperature and position. By this assumption, the transient temperature distribution can be obtained from an analytical solution available from the literature, such that only the thermal stresses need to be evaluated numerically.

As presented by Carslaw and Jaeger[7] the transient temperature distribution for the geometry and boundary conditions described above is:

$$T(x,t) = at + \frac{a(x^2-2xL)}{2\kappa} + \frac{16aL^2}{\kappa\pi^3} \sum_{n=0}^{\infty} \left[\frac{(-1)^n}{(2n+1)^3}\right] \cdot \text{Cos} \left[\frac{(2n+1)\pi(L-x)}{2L}\right] \exp(-\beta t) \quad (3)$$

where

$$\beta = \kappa(2n+1)^2\pi^2/4L^2 \quad (4)$$

and κ is the thermal diffusivity.

The thermal stress field in the rectangular solid is three-dimensional even though the temperature distribution is one-dimensional. The stresses may be analyzed using three-dimensional finite element models, but for parametric studies such as the current one, such analyses become very time-consuming and expensive. For this reason, the stresses were calculated for a two-dimensional (plane stress) distribution by means of a finite element program used for a number of earlier studies[8-11]. A

limited number of three-dimensional cases were also run to investigate the effect of component height, d, using the SUPERB[12] finite element program.

The two-dimensional model consisted of a rectangular mesh with five elements across the half width by forty-nine elements along the length and heat flow direction. The half width model used prescribed boundary conditions on the center line edge to maintain the line of symmetry. For the two-dimensional model, a condition of plane stress were assumed throughout. This implies that the results obtained are appropriate for a plate with a height much less than its width.

Table 1 lists the property values (or range thereof) used for the calculations. The values listed are typical of those encountered in practice for magnesia-based refractories. The influence of the various parameters which affect the magnitude of thermal stresses, such as the thermal diffusivity or the structure dimensions, is not readily expressed in dimensionless form as is common practice in the analysis of thermal stresses. For this reason, the results obtained are reported in terms of absolute values of the stresses and other pertinent variables. Because the magnitude of the stresses is directly proportional to the values of the coefficient of thermal expansion and Young's modulus of elasticity, the stresses can be converted easily for other values for those two properties. In order to keep the total number of stress calculations within reasonable bounds the results to be reported will emphasize the general trend of the role of the various parameters on the magnitude of thermal stresses. Since brittle materials are most susceptible to thermal stress failure in tension, the magnitude of the tensile thermal stresses will receive major emphasis.

III. Results and Discussion

Figs. 2a, 2b, and 2c show typical distributions for the transient temperatures and components of thermal stress in the longitudinal (x) and transverse (y) directions, respectively, for numerical values of the thermal diffusivity, $\kappa = 12.9 \times 10^{-3}$ cm^2/s, heating rate, a = 300°C/hr, time, t = 3000 s, width, b = 15 cm and length, L = 60 cm. For the value of time chosen for this example, the back surface exhibits negligible increase in temperature. The surface being heated is in a state of transverse compression as expected. A biaxial tensile stress state is found in the interior some distance behind the face being heated with maximum values of stress on the centerline. For this specific numerical example the longitudinal stress parallel to the direction of heat flow exceeds the corresponding value perpendicular to the direction of heat flow. Such a stress distribution is expected to result in the mode of failure observed in practice in which the plane of crack propagation is parallel to and some distance behind the face being heated.

However, for shorter times and/or higher heating rates the tensile stress state can be such that the transverse tensile stresses exceed the longitudinal stresses as shown in Figs. 3a, 3b, and 3c, respectively, for a heating rate, a = 300°C/hr, time, t = 500 s, and values for the other pertinent variables identical to those used for the calculations of the data presented in Fig. 2. For this reason, a tensile failure mode with the plane of crack propagation parallel to the direction of heat flow can be anticipated for shorter time intervals and stresses of sufficient magnitude as may occur for the condition of very rapid heating rates well in excess of 300°C/hr. Calculations of the tensile thermal

stresses in the interior for other values of width and parameters for the data shown in Figs. 2 and 3 indicated that they always exhibited their maximum value along the centerline. Furthermore, observed in practice, failure always occurred parallel to the face being heated. For these latter two reasons, all further results to be presented will concentrate on the stress parallel to the direction of heat flow for heating rates and time intervals at which the longitudinal stresses exceed the transverse stresses.

Fig. 4 shows the distribution of the thermal stresses along the centerline for a range of values of heating rate and numerical values for the thermal diffusivity, $\kappa = 12.9 \times 10^{-3}$ cm^2/s, width, b = 10 cm, length, L = 60 cm at the instant of time, t = 1000 s. The magnitude of stress increases linearly with heating rate with the position of peak stress independent of heating rate. Nevertheless with increasing heating rate the position for any prescribed value of stress such as the tensile fracture strength moves towards the face being heated. For this reason, the location of tensile failure, if it occurs, is anticipated to be a function of heating rate.

Fig. 5 for a value of heating rate, a = 300°C/hr, thermal diffusivity, $\kappa = 12.9 \times 10^{-3}$cm^2/s, and width, b = 10 cm, shows the stress distribution along the centerline for a range of values of time. As expected, the magnitude of peak stress increases with increasing time. Furthermore, as time progresses the position of peak stress moves away from the face being heated. These results indicate that the position of failure at a given value of stress is expected to be a function of time. As an aside, it should be noted that at the highest value of time

indicated in Fig. 5 the front face temperature (417°C) for this particular value of heating rate has reached a value at which in many candidate materials, such as tar-bonded magnesite refractories, substantial softening and creep may occur. If so, considerable relaxation of the thermal stresses may occur which will reduce the magnitude of the thermal stresses and the probability of failure.

Fig. 6a indicates the effect of the magnitude of the thermal diffusivity on the peak value of longitudinal tensile thermal stress for three values of time and a heating rate a = 300°C/hr, width, 10cm, length, L = 60 cm. These data indicate that the magnitude of stress decreases with increasing thermal diffusivity. This effect arises because with increasing thermal diffusivity at a given time the temperature field has penetrated to a greater depth. This gives rise to a greater degree of temperature uniformity and associated lower magnitude of thermal stress. This suggests that for the same boundary conditions in practice as chosen for this study (linear heating of the front surface), candidate materials should have a thermal diffusivity as high as possible.

Fig. 6b shows the effect of the value of thermal diffusivity for t = 500 sec in greater detail for the values of heating rate, length and width identical to those for Fig. 6a. These results indicate that the stresses exhibit a maximum at an intermediate value of thermal diffusivity, also barely perceptible for t = 500 sec in Fig. 6a. This result should not be interpreted as suggesting that the magnitude of the stresses also can be reduced by choosing values of thermal diffusivity as low as possible. This would be true only for a value of thermal

diffusivity approaching zero, which is not realizable in practice. The decrease in stress with decreasing thermal diffusivity at the lower values of thermal diffusivity is because at the value of times for these data, the temperature field has not been able to penetrate deeply into the refractory. The stresses, however, will increase in magnitude with increasing time as clearly indicated in Fig. 6a, to values in excess of those found with the higher values of thermal diffusivity.

Fig. 7 shows the effect of width on the peak value of tensile thermal stress for a range of values of thermal diffusivity, length L = 60 cm, t = 500 s and heating rate, a = 300°C/hr. At this particular value of time the peak value of stress is almost independent of the thermal diffusivity as shown earlier in Fig. 6a. The stresses exhibit a maximum at an intermediate value of width. This latter result could be of practical interest as it would permit a reduction of stress in a material with a given value of thermal diffusivity by the simple expedient of increasing or decreasing the width, depending on other performance criteria. Additional calculations showed that the magnitude of the peak tensile stress is independent of the length for $40 < L < 80$ cm for the range of all values of time, width, and heating rate selected for this study. For this reason, it does not appear that design improvements to reduce the probability of thermal stress fracture can be made by changes in length.

All the results presented in Figs. 2 to 7 were based on the assumption of plane stress. This, in effect, treats the rectangular structure as a thin plate in which the stresses in the direction of the height are identically equal to zero. In practice, however, the dimensions of the

width and height are comparable so that a three-dimensional effect on the stress is anticipated.

A three-dimensional finite element model consisted of rectangular solid elements with five elements across the width, four elements across the height and twenty-five elements along the length. As in the plane stress model the cross section element dimensions were constant along the length, but the element length dimension was much smaller at the heated face gradually getting larger toward the cold face. This gives better accuracy where the stress gradients are highest near the heated face. The three-dimensional analysis was limited to evaluation of the effect of cross section height on a segment for the same numerical values of other parameters used for the plane-stress calculations: diffusivity, $\kappa = 12.9 \times 10^{-3}$ cm^2/s, width, b = 10 cm, length, L = 60 cm and heating rate, a = 300°C/hr at a time of 5000 s. The values of height ranged from h = 0 cm (plane stress) to 10 cm, which corresponds to a square cross section. Figure 8 shows the distribution of the stresses along the centerline. For any value of height the relative distribution of the stresses is similar to the plane-stress distribution. However, the peak stress magnitude, increases significantly with increasing height. In fact, for the height equal to the width of 10 cm the stress is more than double the corresponding value for plane-stress conditions. Fig. 9 shows the values of the peak stresses plotted as a function of height. The shape of the curve suggests the plane stress results are reasonably valid up to a height of about 2.5 cm. Beyond this value the magnitude of stress increases almost linearly with height. Of course, for any specific geometry encountered in practice

involving different values of width and height and the other relevant parameters, the effects will need to be established independently. In general, however, it appears that geometries approaching square cross sections should be avoided. In fact, it appears advisable that the value of height of some 5 cm currently encountered in practice should be reduced coupled with an increased width as pointed out before.

As a further comment, it should be noted that linear elastic stress-strain behavior was assumed throughout for all data presented above. However, varying Young's modulus effects are expected to be significant, especially in carbon-impregnated or tar-bonded magnesia refractories. Above about 100°C, Young's modulus undergoes a discontinous change from about 70 to 11 GPa as the direct result of the softening of the carbon phase. This effect on the numerical results of this study can be accounted for reducing the values of stress by the same ratio of the relative reduction of Young's modulus if the whole structure is above 100°C. In principle, this effect can be incorporated in the calculation by the finite element method regardless of the magnitude and distribution of temperature. Such calculations were judged beyond the scope of this parametric study, but should be carried out for any design of given geometry, dimensions and other pertinent variables.

Finally, the results obtained by the present numerical approach should be compared with those predicted by the theory of Kienow[4], which states that the stress, σ along the centerline parallel to the length is given by:

$$\sigma = \alpha E \, (d^2T/dx^2)b^2/(16 + 3b^3/x^3) \qquad (5)$$

where d^2T/dx^2 is the second derivative of the temperature distribution at the position x behind the face being heated and all other symbols having been defined earlier.

Figs. 10a and 10b compare the distributions of stresses along the centerline calculated by the Kienow theory and the present method for a value of thermal diffusivity, $\kappa = 12.9 \times 10^{-3}$ cm^2/s, two different widths, b = 7.5 and 15 cm, length, L = 60 cm, at the instant of time, t = 1000 s, for a heating rate of 300°C/hr. For both sets of data the magnitude of the peak stresses appear to be in reasonable agreement. At positions other than those for the peak stress, the agreement is less good. Such disagreement is expected to be particularly severe at the rear face at which the Kienow theory predicts a finite value of stress, whereas no such stress perpendicular to a free surface should exist. When the effect of height is considered the Kienow theory underestimates stresses by a large factor. For this reason, it is advised that caution be exercised in the use of the Kienow theory for geometries, dimensions, and values of the parameters other than those used for the data in Fig. 10.

The existence of the stresses calculated above, relies on the non-linear temperature distribution during transient heat-up. However, such stresses can exist also under conditions of steady-state heat flow if the thermal conductivity of the material of construction is strongly dependent on temperature. Indeed this is the case for the many materials in which heat conduction occurs primarily by phonon transport. The magnitude of these steady-state stresses probably will be less than those encountered during transient heat-up unless the rate of heat-up is

very low. Even if instantaneous fracture can be avoided, the steady-state stresses could lead to eventual failure by a fatigue process. If such failure is anticipated it could be worthwhile to select those materials which exhibit values of thermal conductivity which are as independent of temperature as possible.

The above calculations all have focused on the magnitude of thermal stress. The initiation of failure will occur when this value of thermal stress exceeds the tensile fracture stress. However, an additional effect needs to be considered. The initiation of failure will result in the formation of a crack within the interior of the segment. This crack is oriented perpendicularly to the direction of heat flow. The presence of this crack will disturb the original temperature distribution which leads to the formation of a localized thermal stress field in the immediate vicinity of the crack. This stress field can lead to crack-instability.

As shown by Nowinski[13], for a penny-shaped crack oriented in an infinite matrix and oriented perpendicular to the direction of heat flow, the mode II (shear) stress intensity factor (K_{II}) is:

$$K_{II} = \frac{1}{3\sqrt{\pi}} \quad \frac{\alpha E c^{3/2} \varepsilon}{(1-\nu)} \tag{6}$$

where c is the crack radius, ε is the temperature gradient, with α, E and ν having been defined earlier.

For a critical stress intensity factor K_{IIc}, the critical size, c_{cr} is:

$$c_{cr} = \{3\sqrt{\pi}\ K_{IIc}(1-\nu)/\alpha E\varepsilon\}^{2/3} \tag{7}$$

For a sample calculation of c_{cr} the following values will be assumed: $K_{IIc} = 2 \times 10^{6}$, $MN \cdot m^{-3/2}$, $\nu = 0.3$, $\alpha = 13 \times 10^{-6}\ °C^{-1}$, $E = 6 \times 10^{10} Nm^{-2}$ and $\varepsilon = 10^{4}\ °Cm^{-1}$. Substitution of these values into Eq. 7. yields:

$$c_{cr} \tilde{=} 0.01 \text{ m (1 cm)} \tag{8}$$

The formation of a crack of this radius following the initiation of fracture[2] is not unlikely especially in relatively dense refractory materials with the higher values of tensile fracture stress. Any crack larger than c_{cr} will be unstable and will propagate. This, in turn, increases the crack size even further, which enhances the degree of instability. Although Eq. 7 is strictly valid for a crack in an infinite solid, it is anticipated that in a segmented structure, the crack will propagate to the outer boundaries.

This phenomenon is offered to explain the observed total disintegration of such segmented refractory structures, which can involve the simultaneous fracture of a large number of neighboring segments, with disastrous consequences for the total structure as a whole. Possibly, this failure mode, at least in principle, may be suppressed by reducing the tensile fracture stress as much as possible and by promoting failure at as many fracture initiation sites as possible. As indicated theoretically[2] both these approaches tend to decrease the crack size which results following the initiation of failure. Clearly, this approach if practical, also will depend on other performance criteria imposed on the structure.

Even under conditions of steady-state heat flow with much lower values of temperature gradient than assumed, crack instability described

by Eq. 7 can exist. This can lead to fatigue failure by the sub-critical growth of cracks by stress-corrosion or diffusional mechanisms depending the environmental variables and magnitude of temperature. It is thought this failure mechanism may be responsible for the long-term failure of glass-tank refractories as the result of crack formation during initial heat-up as described in this paper.

In summary, this study has established the origin of the mode of thermal stress failure of segmented structures subject to rapid heat-up. The definition of the role of the various pertinent material and geometric variables hopefully will be of help in the improved design of such structures in engineering practice. Specifically, the results indicate that improvements in the resistance to thermal stress failure of segmented refractory structures can be brought about by increasing and decreasing the values of the width and height, respectively, from the values now commonly encountered in practice.

ACKNOWLEDGEMENT

This study was conducted as part of a research program on the thermo-mechanical and thermo-physical properties of brittle structural ceramics supported by the Office of Naval Research under contract N00014-78-C-0431.

REFERENCES

1. W. D. Kingery, "Factors Affecting Thermal Stress Resistance of Ceramic Materials", J. Amer. Ceram. Soc., 38 (1) 3-15 (1955)

2. D. P. H. Hasselman, "Unified Theory of Thermal Shock Fracture Initiation and Crack Propagation of Brittle Ceramics", J. Amer. Ceram. Soc. 52 (11) 600-04 (1969)

3. B. A. Boley and J. H. Weiner, Theory of Thermal Stresses, John Wiley, N.Y. 1960 (586 pp.)

4. S. Kienow, "Crack Formation in Fired Converter Bricks", Ber. Deut. Keram. Ges. 47(7) 426-30 (1970).

5. J. H. Ainsworth, "Calculation of Safe Heat-Up Rates for Steelplant Furnace Linings", Ceram. Bulletin, 58 (7) 676-78 (1979).

6. B. Brezny, "Crack Formation in BOF Refractories During Gunning", Ceramic Bulletin, 58 (7) 679-82 (1979).

7. H. S. Carslaw and J. C. Jaeger, Conduction of Heat in Solids, 2nd Ed. p. 104, Oxford University Press, London (1959).

8. K. Satyamurthy, J. P. Singh, M. P. Kamat and D. P. H. Hasselman, "Effect of Spatially Varying Porosity on Magnitude of Thermal

Stress During Steady-State Heat Flow", J. Amer. Ceram. Soc. 62 (7-8) 431-3 (1979).

9. K. Satyamurthy, M. P. Kamat, J. P. Singh and D. P. H. Hasselman, "Effect of Spatially Varying Thermal Conductivity on Magnitude of Thermal Stress in Brittle Ceramics Subjected to Convective Heating", J. Amer. Ceram. Soc., 63 (7-8) 063-67 (1980).

10. K. Satyamurthy, J. P. Singh, M. P. Kamat and D. P. H. Hasselman, "Transient Thermal Stresses in Cylinders with Square Cross-Section Under Conditions of Convective Heat Transfer", J. Amer. Ceram. Soc. 63 (11-12) 694-98 (1980).

11. T. Ozyener, K. Satyamurthy, C. E. Knight, G. Ziegler, J. P. Singh and D. P. H. Hasselman, "Effect of ΔT - and Spatially Varying Heat Transfer Coefficient on Thermal Stress Resistance of Brittle Ceramics Measured by the Quenching Method", J. Amer. Ceram. Soc. (in press).

12. SUPERB User's Manual, Version 5.2 Structural Dynamics Research Corp., Milford, Ohio, 1981, (300 pp.).

13. J. L. Nowinski, Theory of Thermoelasticity with Applications, Sijthoff and Noordhoff 1978 (836 pp.).

TABLE 1

Properties of Magnesia-Based Refractory and Parameter Values

Young's Modulus of elasticity (E):	70.0 GPa
Coefficient of thermal expansion (α)	12×10^{-6} °C^{-1}
Thermal diffusivity (κ):	$4.0 \times 10^{-3} - 4 \times 10^{-2}$ cm^2·s^{-1}
Poisson's ratio (ν):	0.3
Length (L):	40 - 80 cm
Width (b):	5 - 18 cm
Height (h):	2.5 - 10 cm
Heating rate (a):	100 - 900 °C/hr
Time (t):	500 - 15000 s

LIST OF FIGURES

8 Longitudinal stress distribution along the centerline from three-dimensional analysis for a range of heights, d, from plane stress to a square cross section with values of thermal diffusivity, $\kappa = 12.9 \times 10^{-3}$ cm^2 /s, length, L = 60 cm, width, b = 10 cm, heating rate, a = 300°C/hr at a time, t = 5000 s.

9 Peak longitudinal stress as a function of height, d, from plane stress to a square cross section with values of thermal diffusivity, $\kappa = 12.9 \times 10^{-3}$ cm^2/s, length, L = 60 cm, width, b = 10 cm, heating rate, a = 300°C/hr, at a time, t = 5000 s.

10 Longitudinal stress distributions calculated by the Kienow equation and finite element methods for a length, L = 60 cm, a thermal diffusivity, $\kappa = 12.9 \times 10^{-3}$ cm^2/s, a heating rate, a= 300°C/hr at a time, t = 1000 s, and segment widths: (a) b = 15 cm, (b) b = 7.5 cm.

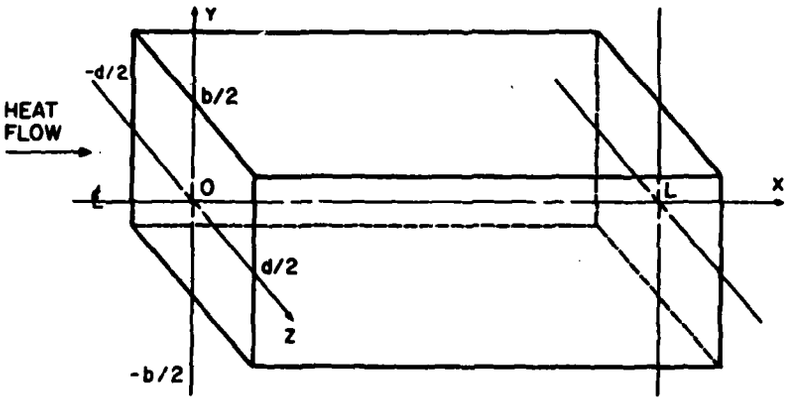

Fig. 1. Schematic illustration of the three-dimensional solid segment being heated on the x = 0 side and insulated on all other sides.

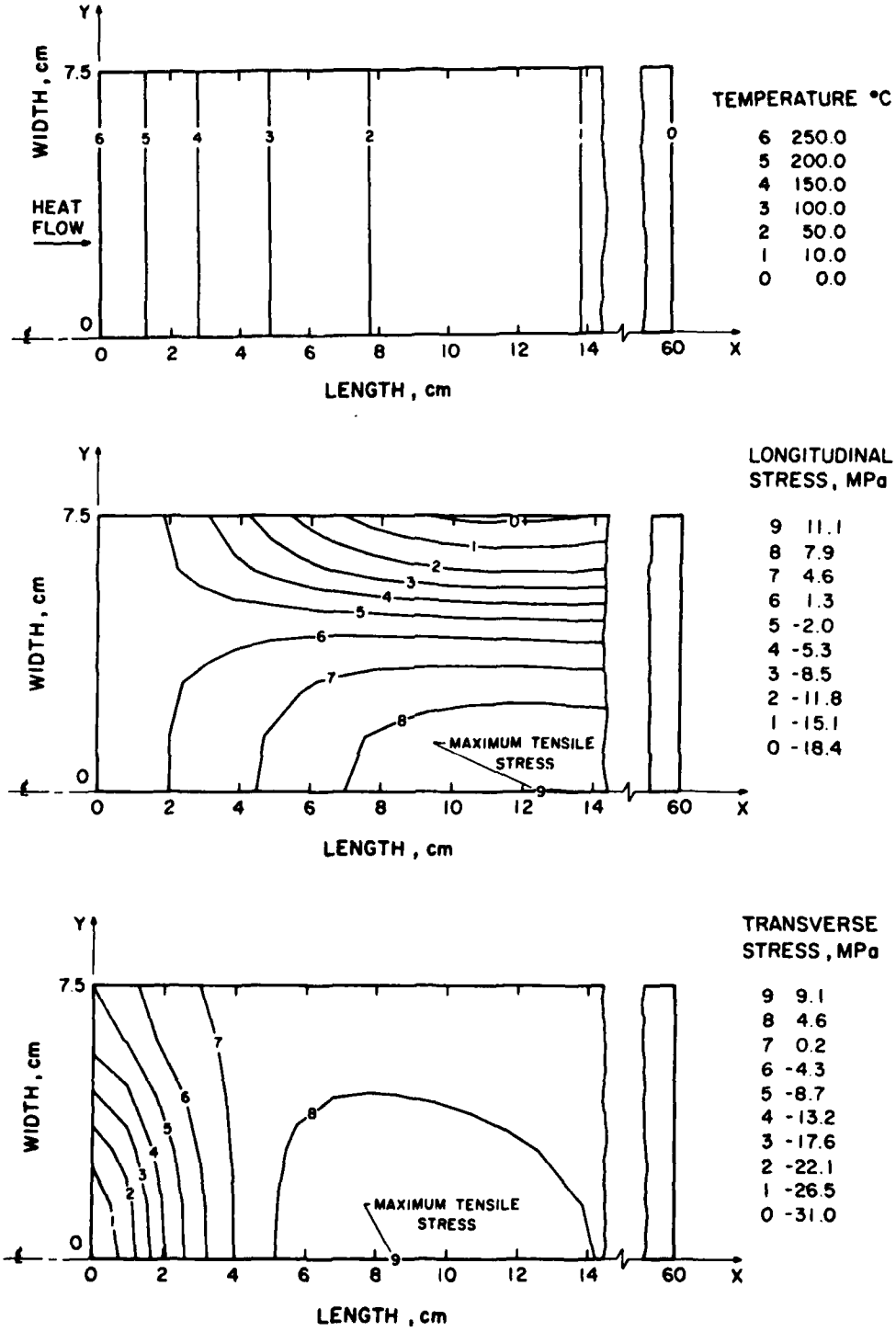

Fig. 2. Contour plots of (a) temperature, (b) longitudinal stress, and (c) transverse stress in a segment 60 cm long by 15 cm wide for a heating rate, a = 300°C/hr, a thermal diffusivity, $\kappa = 12.9 \times 10^{-3}$ cm^2/s, and other properties in Table 1 at a time t = 3000 s.

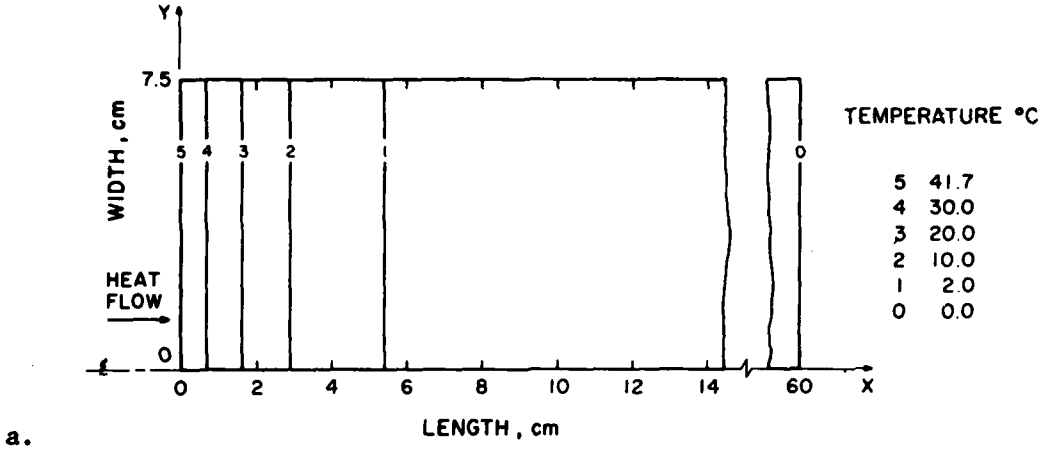

a.

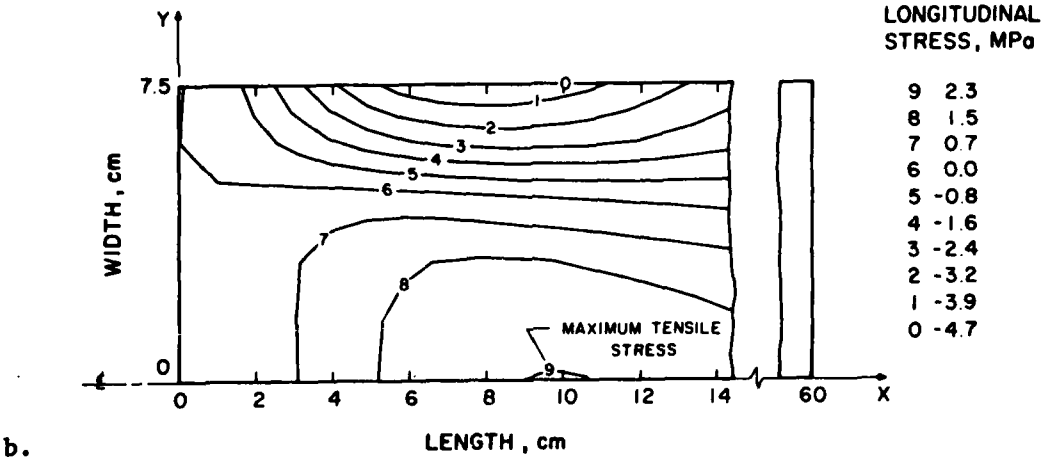

b.

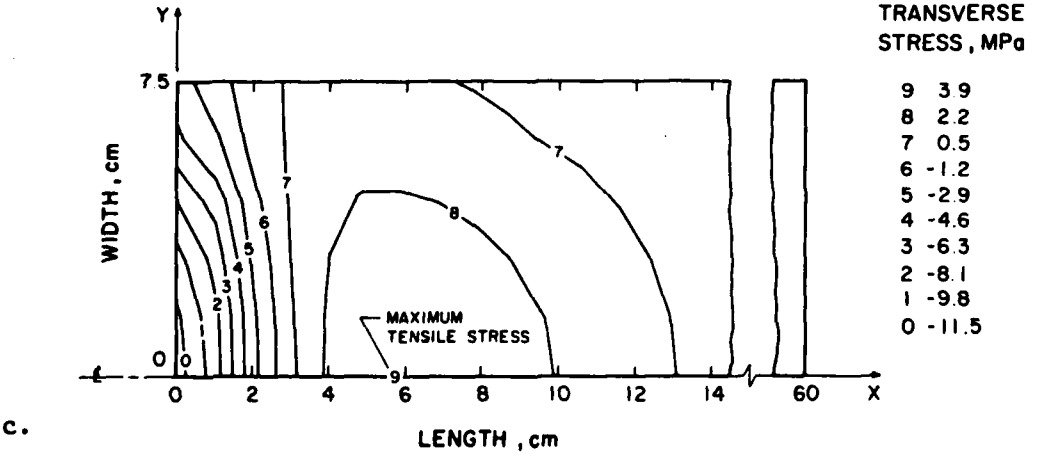

c.

Fig. 3. Contour plots of (a) temperature, (b) longitudinal stress, and (c) transverse stress in a segment 60 cm long by 15 cm wide for a heating rate, $a = 300°C/hr$, a thermal diffusivity, $\kappa = 12.9 \times 10^{-3}$ cm^2/s, and other properties in Table 1 at a time, $t = 500$ s.

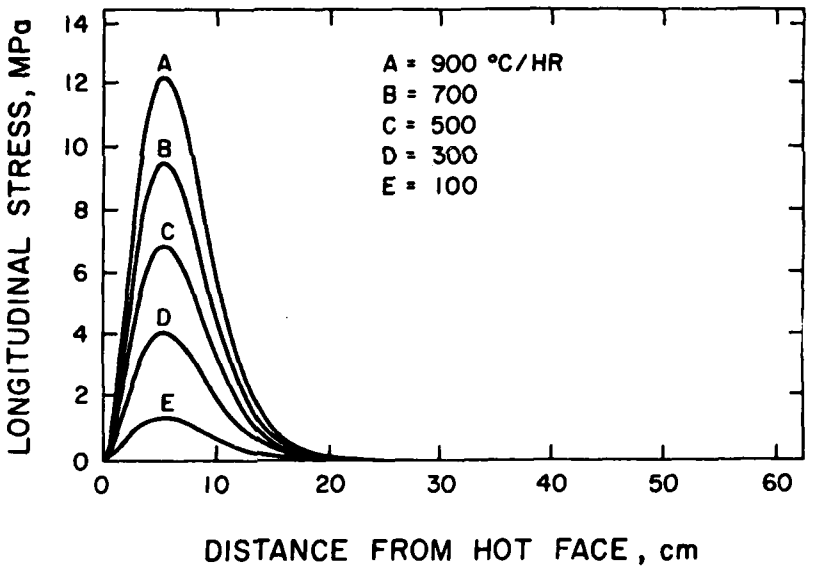

Fig. 4. Longitudinal stress distribution along the centerline for a range of heating rates using values of thermal diffusivity, $\kappa = 12.9 \times 10^{-3}$ cm^2/s, width, b = 10 cm, length, L = 60 cm at a time, t = 1000 s.

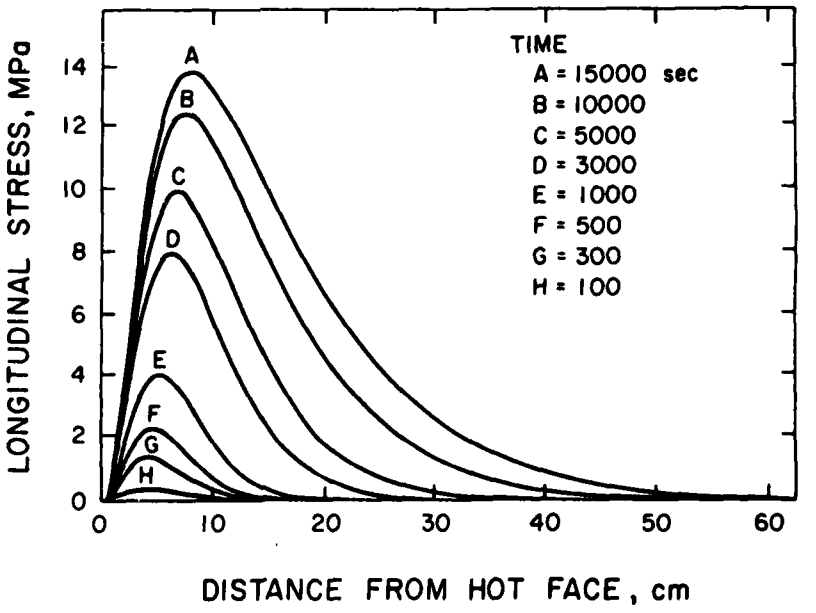

Fig. 5. Longitudinal stress distribution along the centerline for a range of times using values of thermal diffusivity, $\kappa = 12.9 \times 10^{-3}$ cm^2/s, heating rate, a = 300°C/hr, width, b = 10 cm, length, L = 60 cm.

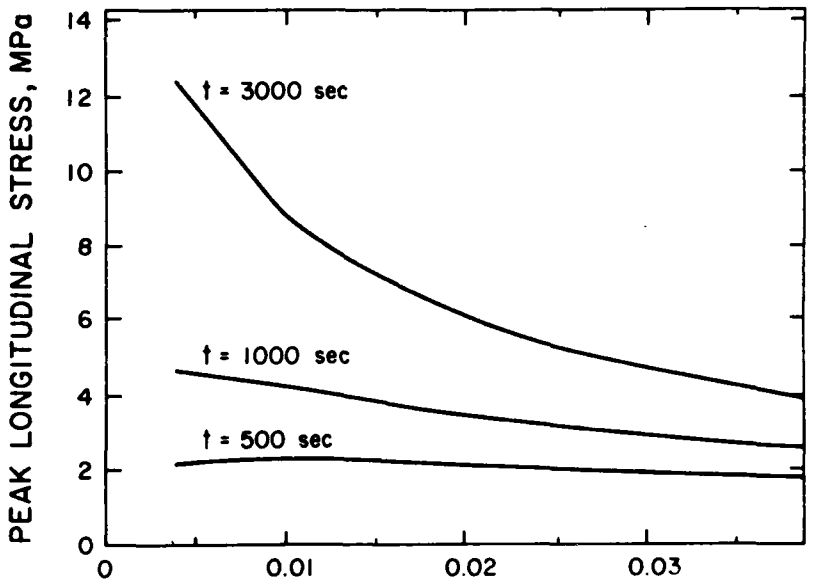

a.

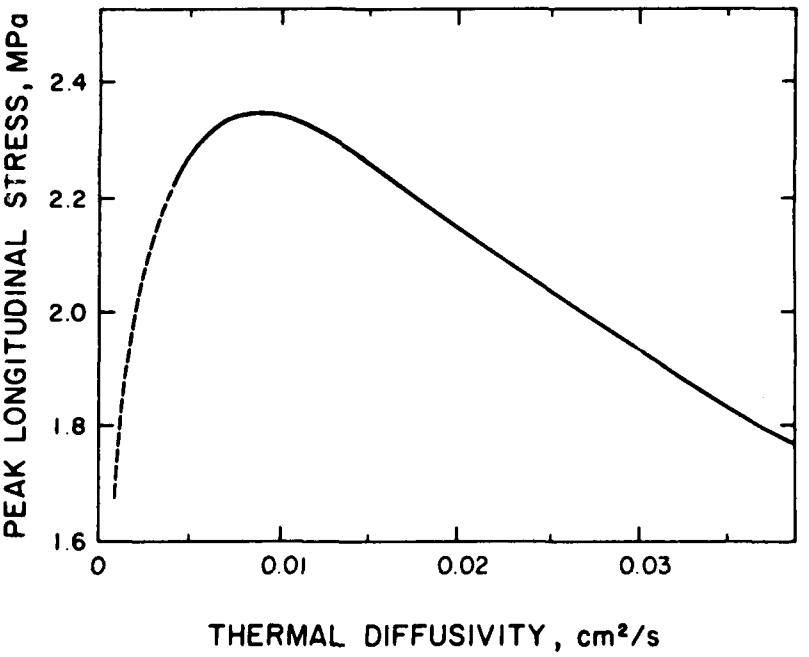

b.

Fig. 6. Peak longitudinal stress as a function of thermal diffusivity and values of heating rate, a = 300°C/hr, width, b = 10 cm, length, L = 60 cm: (a) range of values of time, and (b) expanded scale for t = 500 s.

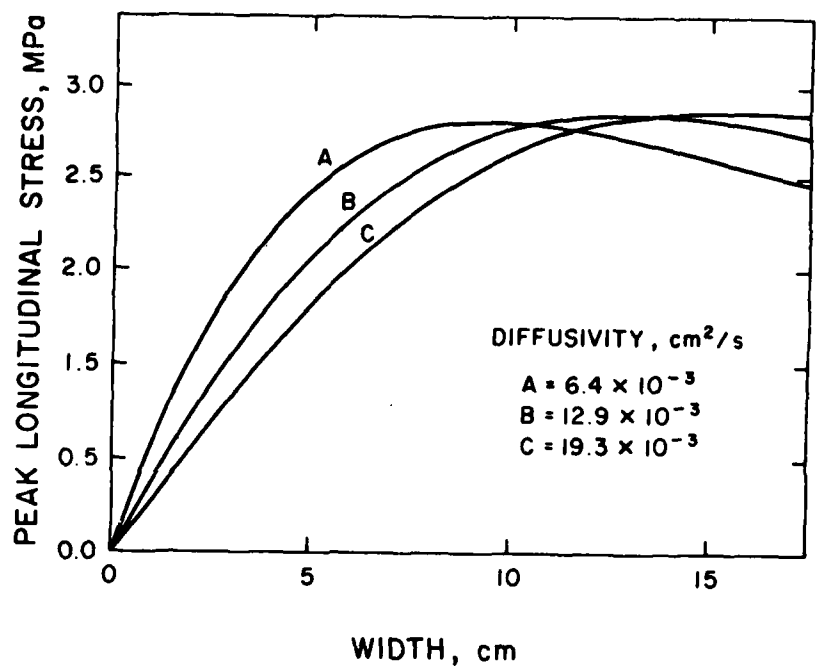

Fig. 7. Peak longitudinal stress as a function of segment width for three values of thermal diffusivity with a length, L = 60 cm, a heating rate, a = 300°C/hr at a time, t = 500 s.

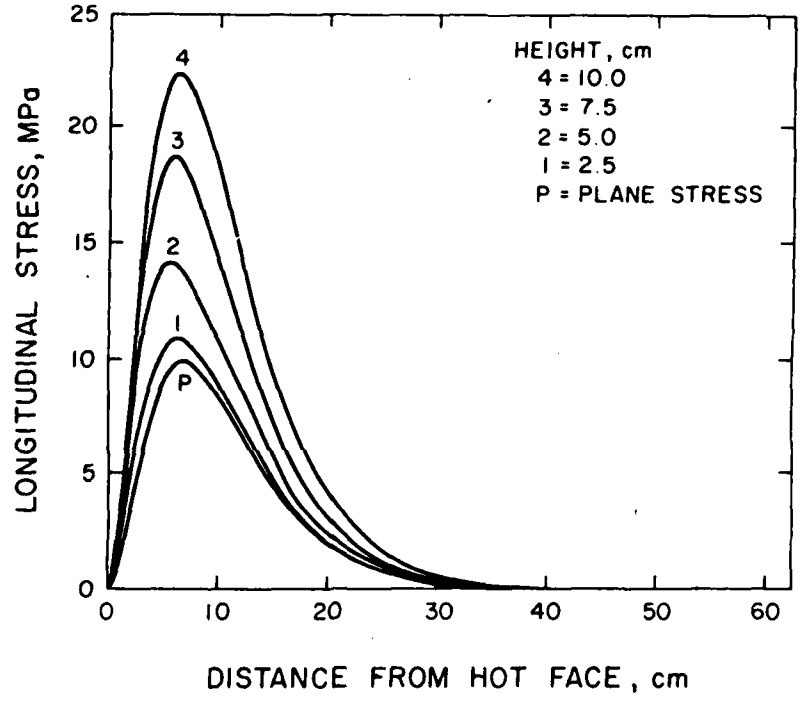

Fig. 8. Longitudinal stress distribution along the centerline from three-dimensional analysis for a range of heights, d, from plane stress to a square cross section with values of thermal diffusivity, $\kappa = 12.9 \times 10^{-3}$ cm^2 /s, length, L = 60 cm, width, b = 10 cm, heating rate, a = 300°C/hr at a time, t = 5000 s.

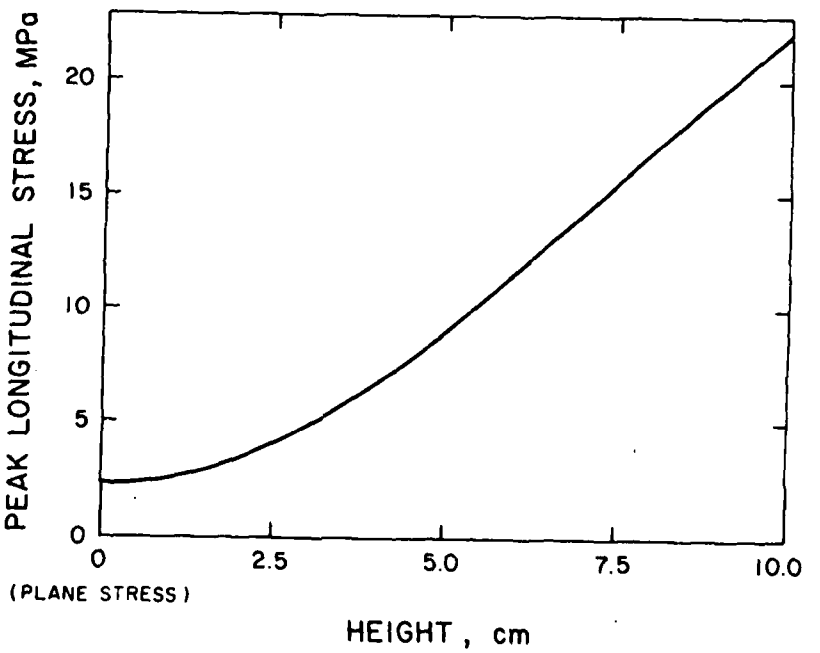

Fig. 9. Peak longitudinal stress as a function of height, d, from plane stress to a square cross section with values of thermal diffusivity, $\kappa = 12.9 \times 10^{-3}$ cm^2/s, length, L = 60 cm, width, b = 10 cm, heating rate, a = 300°C/hr, at a time, t = 5000 s.

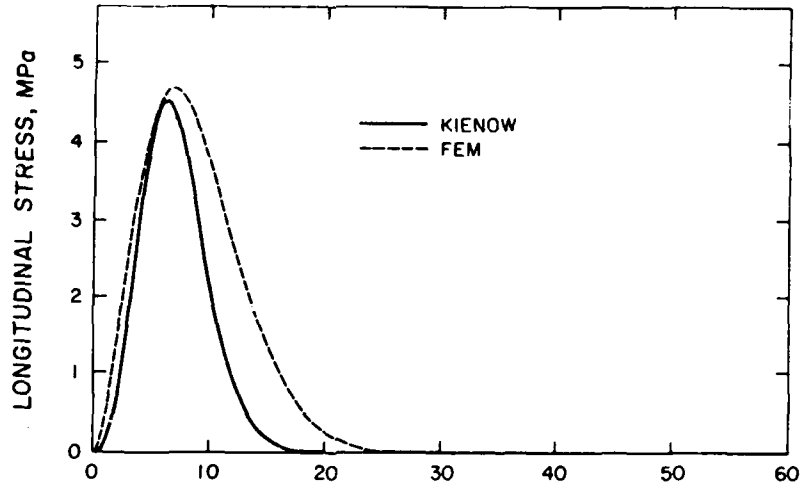

a.

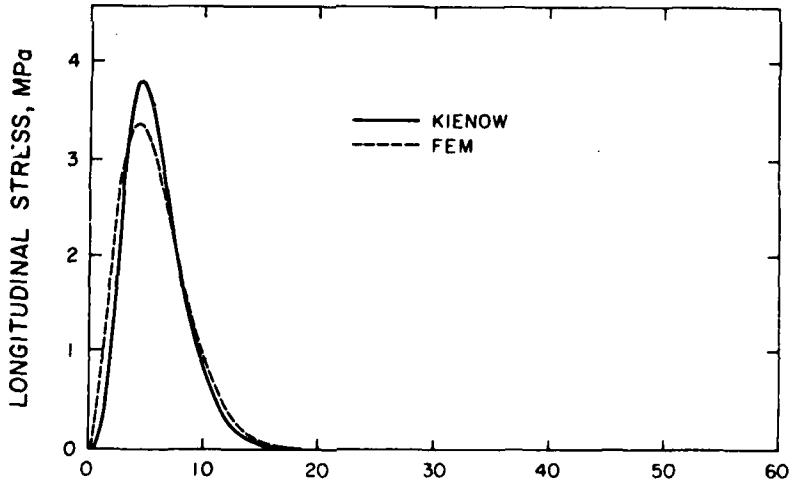

b.

Fig. 10. Longitudinal stress distributions calculated by the Kienow equation and finite element methods for a length, L = 60 cm, a thermal diffusivity, κ = 12.9 x 10^{-3} cm^2/s, a heating rate, a= 300°C/hr at a time, t = 1000 s, and segment widths: (a) b = 15 cm, (b) b = 7.5 cm.

CHAPTER X

EFFECT OF MICROSTRUCTURAL AND COMPOSITIONAL HETEROGENEITY ON THE CONDUCTION OF HEAT IN STRUCTURAL MATERIALS FOR HIGH-TEMPERATURE USE

BY

D. P. H. Hasselman and L. D. Bentsen

Department of Materials Engineering
Virginia Polytechnic Institute and State University
Blacksburg, VA 24061, USA

ABSTRACT

A review is presented of recent experimental data on the effect of microstructural and compositional heterogeneity on the thermal diffusivity/conductivity of structural materials for high-temperature applications. These materials include nitrides, carbides, oxides, and various composites. The microstructural and compositional variables include microcracking, solid solution alloying, densification aids, impurities, and the amount, type, distribution, and orientation of dispersed phases. Such variables can be used to tailor the heat transfer properties of a material for specific requirements.

INTRODUCTION

The increased performance requirements for many components of aerospace structures, energy-conversion systems, industrial process vessels, etc., has led to an increased demand for materials which exhibit superior mechanical and chemical behavior at high temperatures. Such materials frequently include the refractory nitrides, carbides, and oxides.

The in-service performance of such materials frequently also depends critically on their thermal properties such as thermal expansion, and thermal conductivity and diffusivity. Generally, values for the coefficient of thermal expansion should be as low as possible. Likewise, low values for the thermal conductivity and diffusivity are required for good thermal insulation; however, for heat exchangers, the thermal conductivity and diffusivity should be as high as possible. The latter requirement also is critical for those components which are subject to failure by thermal stresses, which are inevitably encountered during transient and steady-state non-isothermal conditions. Thermal stress failure is particularly critical for many refractory materials, which, because of their brittle nature, usually undergo totally catastrophic failure, rendering the component incapable of continued performance. Frequently, the service conditions for such materials may simultaneously require high thermal insulating ability and resistance to thermal stress failure. In such cases, appropriate trade-offs in materials properties need to be made, or alternatively, design modifications may be required.

Clearly, for the design and selection of materials for high-temperature service conditions, quantitative information for the values of the thermal conductivity and thermal diffusivity of candidate materials is required, together

with a detailed understanding of the intrinsic variables which may affect their magnitude.

Heat transport through solids occurs primarily by phonon, photon or electron transport. The heat flux which results from these mechanisms depends strongly on the associated specific heat, the temperature, and the existence of structural and chemical imperfections such as vacancies, dislocations, grain boundaries, foreign atoms, optical discontinuities and other variables which contribute to phonon, photon, and electron scattering (1,2). At the microstructural level, the conduction of heat is affected by the presence of pores, second-phase inclusions, cracks, grain boundary phases, texture, and other factors.

The purpose of this paper is to present an overview of experimental data obtained by the present writers and co-workers over the last few years which illustrates many of the above microstructural effects on heat conduction. The laser-flash diffusivity method was used for all studies (3). By multiplying the experimental values of the thermal diffusivity by the specific heat per unit volume, the corresponding values for the thermal conductivity, when required, were readily calculated. For many of the experimental details on the material preparation and characterization, the reader is referred to the original publications. For convenience, the data will be presented in terms of a number of phenomena observed for a given material such as silicon nitride, or else in terms of a given phenomenon, such as the effect of microcracking, observed for a number of different materials.

EXPERIMENTAL DATA

Silicon Nitride

Because of its relatively low coefficient of thermal expansion and other favorable properties, polycrystalline silicon nitride is a prime candidate material for such purposes as an all-ceramic turbine engine and components of an adiabatic diesel engine. Silicon nitride can be made by hot-pressing appropriate powders or by reaction sintering, which consists of nitriding silicon powders pressed into the appropriate shape.

Hot-pressed silicon nitride components are made using powders which consist initially of the α-crystallographic modification. To promote densification, a hot-pressing aid consisting of magnesium oxide, yttrium oxide or other oxide is added to the silicon nitride powder. By reacting with the silicon oxide layer on the silicon nitride particles, the hot-pressing aid exists in the form of a glassy silicate grain boundary phase. At the hot pressing temperature, the glassy phase promotes densification by viscous flow. The amount of hot-pressing aid can be varied in order to optimize the properties required for a given application. Since the sintering aid exists as a separate grain boundary phase, the heat conduction behavior of hot-pressed silicon nitride is a function of the relative amount of hot-pressing aid present.

Two additional effects occur during the hot-pressing of silicon nitride. First, the α-Si_3N_4 transforms into the β-phase by a time-dependent dissolution-precipitation process via the viscous grain boundary phase. Secondly, the β-particles become rod-shaped due to a preferred growth direction and become oriented such that the axis of the rod is perpendicular to the direction of hot-pressing (4,5). This latter effect introduces a texture which results in an anisotropy of those properties sensitive to grain geometry and/or crystallographic orientation.

Figures 1 and 2 present evidence for these three effects on the conduction of heat through hot-pressed silicon nitride as found by Ziegler and co-workers (6,7). Figure 1 shows the thermal diffusivity of hot-pressed silicon nitride with 5 wt.% MgO as a function of hot-pressing time, perpendicular and parallel to the hot-pressing direction. The increase in thermal diffusivity with hot-pressing time results from two causes. At the shorter values of time, the increase in density(i.e., reduction in relative pore content) has the major effect. At the longer hot-pressing time, the additional increases in the thermal diffusivity result from the α-to-β transformation, which is essentially complete at approximately 3 hours. It is believed that due to a zone-refining effect during its growth, the β-phase attains a higher level of purity and consequently a higher thermal diffusivity than the α-phase. Because of the preferred alignment of the axis of the rod-like β-particles, the thermal diffusivity perpendicular

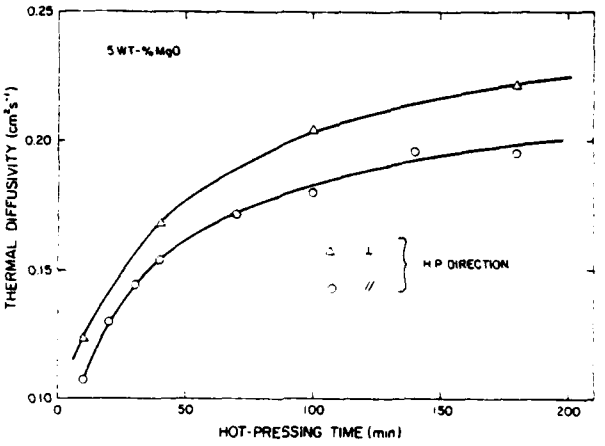

Fig. 1 Thermal diffusivity of hot-pressed silicon nitride at room temperature as a function of hot-pressing time and direction (after ref. 6).

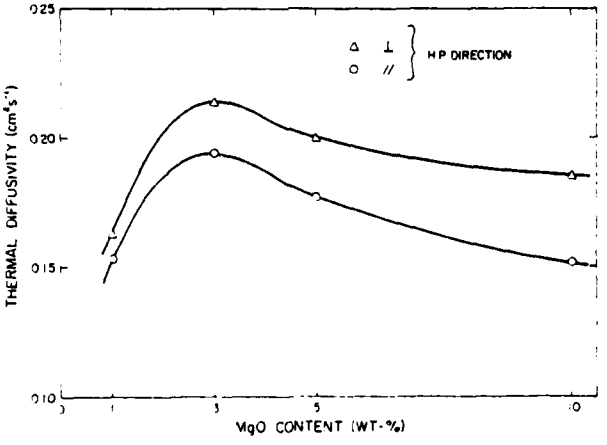

Fig. 2 Thermal diffusivity of hot-pressed silicon nitride at room temperature as a function of MgO content and hot-pressing direction (after ref. 6).

to the hot-pressing direction is higher than parallel to the hot-pressing direction.

Figure 2 shows the data for the thermal diffusivity as a function of MgO content of silicon nitride, hot-pressed for sufficient duration for the α-β transformation to be complete. At approximately 3% MgO the thermal diffusivity exhibits a maximum. Below 3% MgO, the increase in thermal diffusivity can be attributed primarily to the enhancement of density. Above 3% MgO, however, the increasing amount of glassy grain boundary phase, with low inherent thermal conductivity, leads to a decrease in thermal diffusivity with increasing MgO content.

A significant degree of anisotropy in heat conduction behavior of silicon nitride can be introduced by the addition of second phase particles such as boron nitride. Such Si_3N_4-BN composites have good resistance to catastrophic fracture by thermal shock. Due to its graphite-like hexagonal crystal structure, boron nitride is highly anisotropic in many of its properties. Furthermore, boron nitride powders exist in the shape of flat particles with the long dimension along the basal plane. During the powder orientation stage during the initial phases of hot-pressing, the BN particles take on a preferred orientation with the long dimension (i.e., the basal plane) perpendicular to the hot-pressing direction. Boron nitride exhibits the highest value of thermal conductivity within the basal plane. Thus, their preferred orientation within the silicon nitride leads to anisotropic thermal conductivity of the hot-pressed Si_3N_4-BN composites. Evidence for this effect was found by Niihara et. al. (8) and is shown in Figure 3. X-ray analysis revealed that the presence of the boron nitride reduces the degree of orientation of the β-Si_3N_4 grains which diminishes the anisotropy effect shown in Figure 1. For this reason, the pronounced anisotropy at the higher values of BN content, as indicated by the data in Figure 3, is primarily due to the preferred orientation of the boron nitride particles.

Solid-solution alloying is known to be very effective in reducing the phonon mean free path in dielectric materials, thus producing a significant decrease in the thermal diffusivity and conductivity. This effect is demonstrated by experimental data of Lange et. al. (9) in Figure 4, which shows the effect of alumina alloying on the thermal diffusivity of silicon nitride. As expected, the relative effect is larger at the lower levels of temperature than at the higher temperatures.

Silicon Carbide

SiC-based materials consisted of particulate composites of SiC-Si and SiC-fiber reinforced glass-ceramics. Composites of magnesium oxide and silicon carbide will be discussed in a later section on the effect of microcracking on thermal conductivity.

Silicon carbide-silicon composites are a new composite material for high-temperature turbine applications. Figure 5 shows experimental data for the thermal diffusivity of such SiC-Si composites at room temperature as a function of silicon content as reported by Srinivasan et. al. (10). Over the range of silicon content investigated, the thermal diffusivity, to a first approximation, is independent of silicon content. It is noteworthy that the thermal diffusivity of the SiC-Si composites is well below the corresponding value for the silicon carbide. From a practical viewpoint, these SiC-Si composites are much better thermal insulators than single-phase silicon carbide. This latter observation is of vital importance for turbine applications in order to minimize heat losses and thereby improve fuel efficiency.

Nevertheless, the much lower values for the thermal diffusivity of these composites than for SiC are unexpected since reported values for the thermal diffusivity of silicon metal (11) are comparable if not larger than those for silicon carbide. In this respect then, the data in Figure 5 appear not to be in accordance with composite theory which indicates that for materials with similar values for specific heat and density, the thermal diffusivity of composites should be intermediate to the values of the individual components. In order to resolve this apparent discrepancy, data were obtained for the thermal diffusivity of the industrial grade silicon metal used to fabricate these composites and compared with the data for a high purity zone-refined silicon. The results are shown in Figure 6. Clearly the industrial grade silicon has a much lower thermal diffusivity than the high-purity silicon. It is interesting to

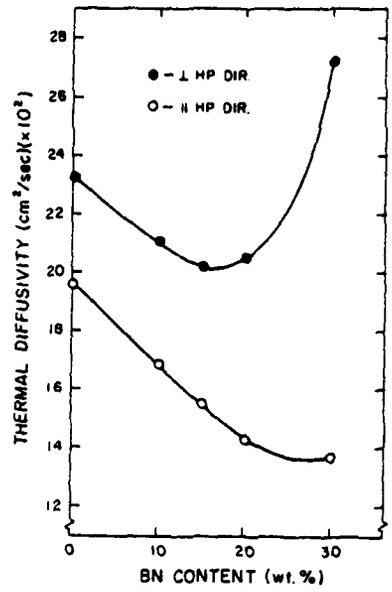

Fig. 3 Thermal diffusivity of silicon nitride-boron nitride composites at room temperature as a function of boron nitride content and hot-pressing direction (ref. 8).

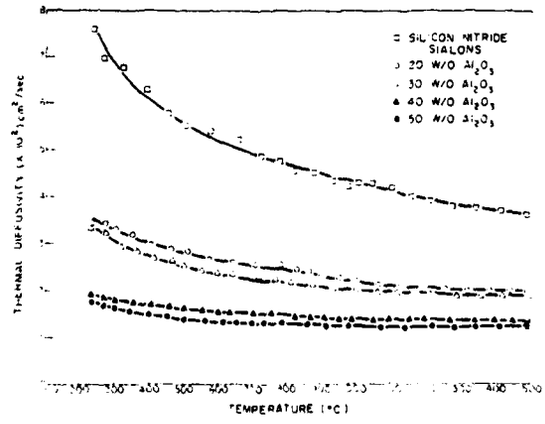

Fig. 4 Effect of alumina alloying on thermal diffusivity of silicon nitride (ref. 9).

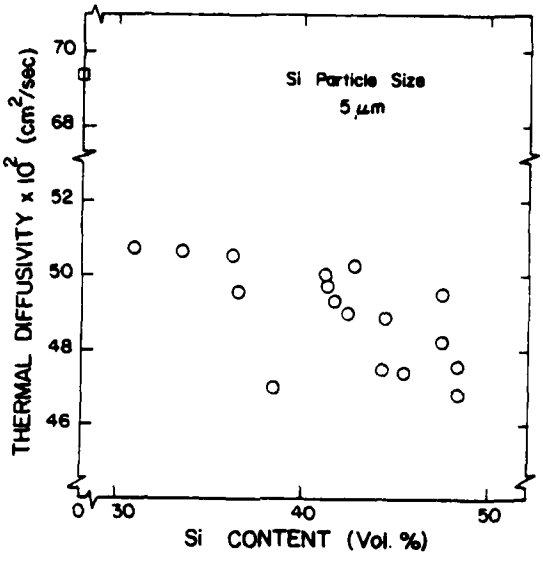

Fig. 5 Thermal diffusivity of silicon carbide-silicon composites at room temperature as a function of silicon content (ref. 10).

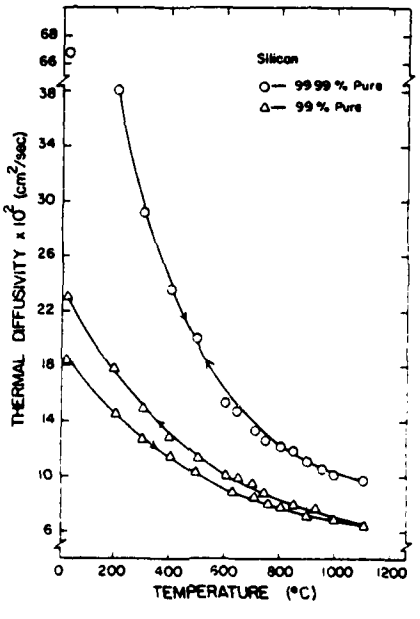

Fig. 6 Comparison of thermal diffusivity of industrial and zone-refined silicon (ref. 10).

note that the total impurity content in the industrial silicon was no more than 1%, with boron and iron as principal constituents. Thus, the apparent discrepancy of the composite data shown in Figure 5 is explained, and the critical role of impurities in governing the heat conduction behavior of these types of materials is clearly evident.

The SiC-fiber reinforced glass-ceramics consisted of a crystallized lithium aluminosilicate glass reinforced with fibers of an amorphous silicon carbide. These composites exhibit excellent mechanical behavior, such as high fracture toughness at elevated temperatures. Not only were the thermal transport properties of these composites of interest, but those of the individual silicon carbide fibers as well. At this time, no convenient method exists by which the thermal conductivity of non-conducting dielectric fibers can be measured. The approach taken to assess these latter values was to calculate the fiber conductivity from the experimental data for the fibrous composite and the single-phase matrix without fibers, by means of the theory for the thermal conductivity of composites (12).

Figure 7 shows the experimental data obtained by Brennan et. al. (13) for the thermal diffusivity of the glass-ceramic matrix without fibers and the composite with 49 vol.% fibers, oriented parallel and perpendicular to the direction of heat flow. The data for the composites do not differ appreciably from those of the matrix, which indicates that the values for the thermal conductivity of the glass-ceramic matrix and the fibers are comparable. Figure 8 shows the values for the thermal conductivity and diffusivity of the fibers calculated from the data given in Figure 7, and independently obtained values for the specific heat and density of the matrix and fibers.

Two noteworthy comments can be made. First, the fiber conductivity is comparable to that of amorphous glasses, with the value of thermal diffusivity some two orders of magnitude below the value for the thermal diffusivity of crystalline silicon carbide shown in Figure 5. Secondly, the thermal conductivity shows a positive temperature dependence, in contrast to the strongly negative temperature dependence exhibited by dielectric solids, especially near room temperature. Both these effects are related to the amorphous nature of the silicon carbide fibers, which also contain appreciable amounts of oxygen. The amorphous structure of the fibers limits the phonon mean free path to exceedingly small values, which results in very low thermal conductivity and thermal diffusivity. These values are reduced to such an extent that, as suggested by

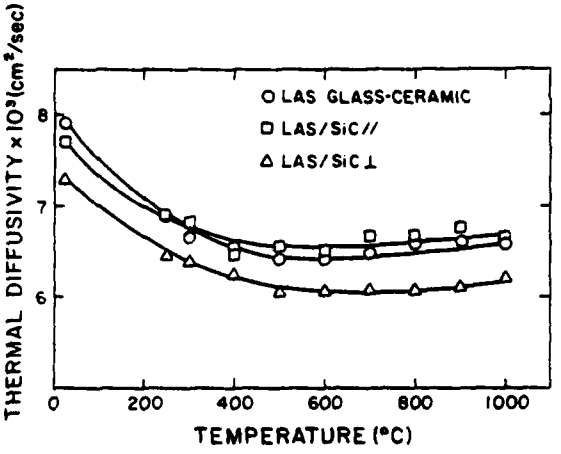

Fig. 7 Thermal diffusivity of lithium alumino-silicate (LAS) glass-ceramic and LAS-silicon carbide fiber composites parallel and perpendicular to fiber direction (ref. 13).

the positive temperature dependence of the thermal conductivity, radiation can make a significant contribution to the total conductivity. This latter conclusion implies that the thermal conductivity of these composites should increase with specimen thickness. In fact, this was found to be so. This effect should be taken into account in the design and performance analysis of structures or components made from these types of composites.

Microcracked Materials

Brittle materials with high densities of microcracks offer unique properties such as very low Young's modulus of elasticity (14,15), high fracture energy (15) coupled with a stable mode of crack propagation, high strain at fracture (16,17), ease of machinability, and excellent thermal shock resistance (18,19,20).

For randomly oriented equal sized penny-shaped cracks, the thermal conductivity (K) is given by (21):

$$K = K_o[1 + 8Nb^3/9]^{-1} \quad (1)$$

where K_o is the thermal conductivity of the crack-free solid, N is the number of cracks per unit volume, and b is the crack radius. Equation 1 indicates that microcracking will lead to a decrease in thermal conductivity, as expected, since in the absence of radiative heat transfer, the cracks act as barriers to heat flow. Because microcracking has little or no effect on the specific heat per unit volume, equation 1 is expected to describe the effect of microcracking on thermal diffusivity as well.

In polycrystalline single-phase materials microcracks can arise from the anisotropy in thermal expansion of the individual grains. In brittle composites, microcracks can result from mismatches in the coefficients of thermal expansion of the individual components. Brittle structural materials generally are made at high temperature. On cooling to room temperature, the non-uniform thermal expansion of the grains (or components in the case of composites) will result in the creation of internal stresses. If they are of sufficient magnitude, these stresses can lead to microcracking. This, however, requires precursors such as

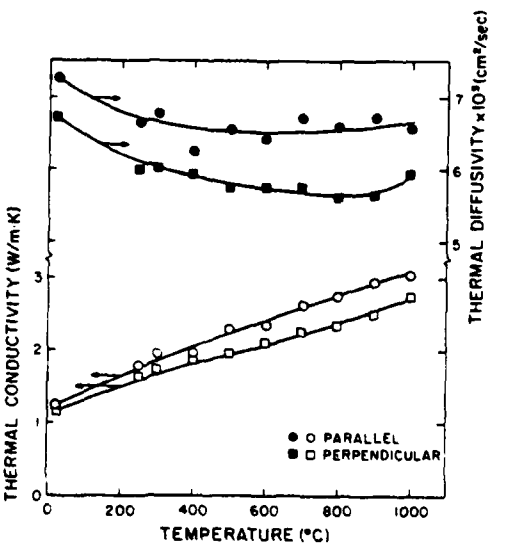

Fig. 8 Thermal conductivity and thermal diffusivity of amorphous silicon carbide fibers parallel and perpendicular to the fiber direction (ref. 13).

pores at grain boundaries, triple points, or areas of less than complete adhesion between the individual components. Fundamentally, microcracks will form if the combination of the magnitude of internal stress and the size of the crack precursors is such that the resulting stress intensity factor equals or exceeds the critical stress intensity factor. In polycrystalline materials, the size of residual pores which act as microcrack precursors generally exhibits a one-to-one correspondence with the size of the grains. For this reason, it is expected that the effect of microcracking on thermal conductivity or thermal diffusivity will show a pronounced dependence on grain size. Reheating microcracked materials back to the manufacturing temperature will be accompanied by crack closure and should lead to a positive temperature dependence of the thermal conductivity. At sufficiently high temperature, and if time permits, crack healing can occur by diffusional processes. This latter effect would lead to a thermal conductivity which is a function of thermal history. Evidence for these effects will be shown in the subsequent figures.

Figure 9a shows data measured by Siebeneck et. al. (22) for the temperature dependence of the thermal diffusivity of an as hot-pressed polycrystalline iron titanite with a mean grain size of approximately 1 μm. These data indicate the normal negative temperature dependence of a dielectric solid in which phonon conduction is the primary mechanism of heat transfer. Figure 9b shows the thermal diffusivity of an iron titanate sample which was given an annealing treatment following hot-pressing in order to promote grain growth. The resulting grain size distribution was bimodal with grains as large as 20-30 μm contained within the original fine grained matrix. Comparison of Figure 9a and 9b indicates that the thermal diffusivity of the large grained iron titanate has only about one third of the value of the fine grained material. This effect is due to the microcracking in the coarse-grained material. Figure 9b also indicates the existence of a pronounced hysteresis effect as the specimen is heated and cooled. During the heating part of the cycle the increase in the thermal diffusivity is attributed to crack closure. The higher values obtained during the cooling part are thought to be due to either irreversible crack closure due to frictional effects or to crack healing due to diffusional effects. Both these effects will

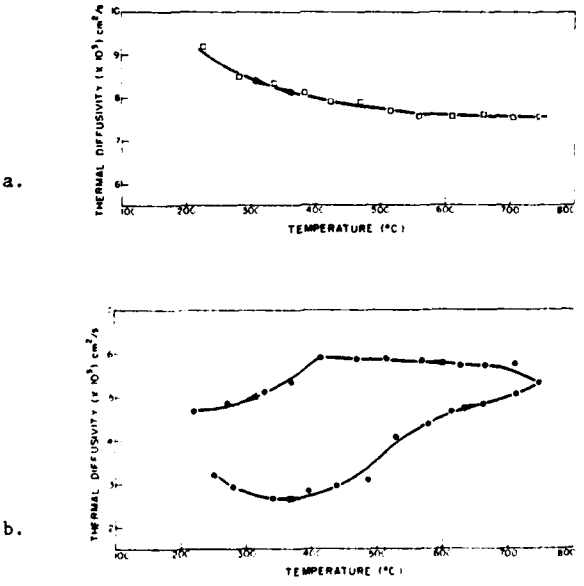

Fig. 9 Thermal diffusivity of polycrystalline iron titanate. a: grain size of ~ 1 μm; b: grain size up to 30 μm (ref. 22).

contribute to the observed hysteresis since a finite degree of cooling is required before healed microcracks will repropagate. As indicated by the discontinuity in slope in the cooling part of the curve, this recracking occurs at a temperature of approximately 400 C. Such crack healing and re-formation quite likely is accompanied by permanent microstructure changes, and the crack geometry and dimensions are not likely duplicated exactly from cycle to cycle. Regardless of whether this latter effect occurs or not, Figure 9b clearly indicates that the effect of microcracking on thermal conductivity or thermal diffusivity depends on prior thermal history.

Additional aspects related to the effect of microcracking on thermal diffusivity are shown in Figs. 10a and 10b for a fine and coarse grained magnesium dititanate, respectively, studied by Siebeneck et al. (23). In Figure 10a, the data for the thermal diffusivity during cooling are well below those obtained during heating. It is thought that this effect arises from the diffusional growth of the microcrack precursors, which, during the initial cooling from the hot-pressing temperature, were not of sufficient size to propagate into microcracks. The additional time at the higher temperatures during the measurement of the thermal diffusivity permitted sufficient growth so that on cooling, microcracks formed which were not present during the initial cooling.

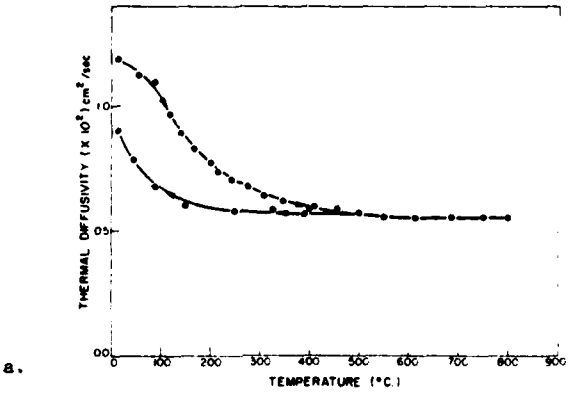

a.

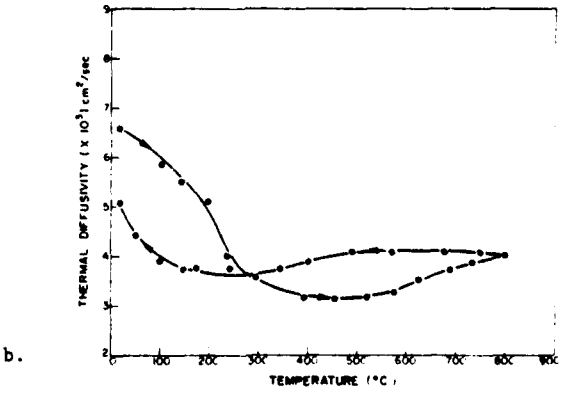

b.

Fig. 10 Thermal diffusivity of a. fine grained and b. coarse grained magnesium dititanate (ref. 23).

Figure 10b shows evidence of the combined effect of microcrack healing and precursor growth at the higher temperature for a coarser-grained (70 um) magesium dititanate (23), which results in a reversal in the direction of hysteresis at the lower and higher temperature changes. Again, the prior thermal history of the specimen can have a major influence on the effect of microcracking on heat conduction behavior. Clearly, for microcracked materials, no handbook values for thermal conductivity or diffusivity can be established.

Experimental data for microcracked composites permit a quantitative evaluation of the effect of microcracking on the thermal conductivity. Figure 11 compares the measured values for the thermal diffusivity of a microcracked composite which consists of a magnesium oxide matrix with a dispersed phase of silicon carbide (24), with values calculated from composite theory, which implicitly assumes that microcracks are absent (12). Due to the presence of the microcracks, the experimental data fall well below the composite data. The difference between these values increases with increasing SiC content. This is expected since the microcracks in the matrix are associated with the silicon carbide inclusions. At the highest values of SiC content, the microcracks have decreased the thermal diffusivity by nearly a factor of three.

The MgO-SiC composites also show evidence for crack healing at the higher temperatures and re-formation on cooling as shown in Figure 12 for a composite with 30 wt.% SiC. Crack re-formation appears to occur over the temperature range of about 850 to 600 C.

Other Materials

An interesting effect is shown by composites of a sodium borosilicate glass with Ni inclusions studied by Powell and co-workers (25). The composites were fabricated in order to study the composite behavior resulting from lack of adhesion between the glass matrix and Ni inclusions. These composites were made by hot-pressing mixtures of powders of the appropriate glass and spherical Ni

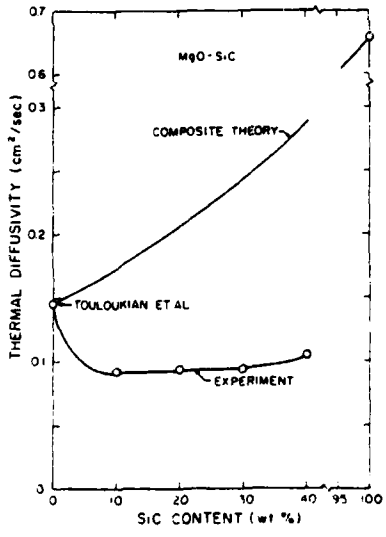

Fig. 11 Comparison of measured and calculated thermal diffusivity at room temperature of microcracked composites of magnesium oxide matrix containing silicon carbide (ref. 24).

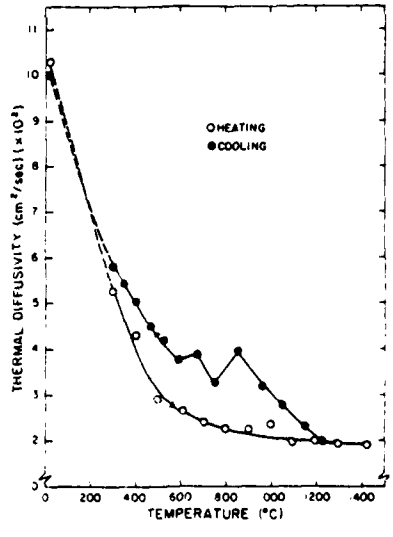

Fig. 12 Temperature dependence of thermal diffusivity of MgO-SiC composite with 30% SiC (ref. 24).

particles at a temperature of approximately 700 C. Since the coefficient of thermal expansion of the Ni is much higher than that of the glass, the Ni particles separate from the glass phase during cooling, which results in the formation of an interfacial gap. Such a gap prevents direct heat flow through the Ni particles, preventing them from contributing to the heat conduction process, with the exception of some heat flow through the points of contact between the Ni particles and the glass matrix.

Figure 13 compares the experimental data for the thermal diffusivity of these composites with a range of Ni contents with those calculated from composite theory (12). The data clearly indicate that near room temperature the interfacial gap lowers the thermal diffusivity appreciably. This effect is largest for the composite with the highest Ni content, as expected. However, evidence of the Curie point indicates that the nickel still contributes to the thermal diffusivity in spite of the interfacial gap. It is thought that this effect arises from the points of contact between the Ni and the glass, which still permit heat flow into the Ni. In this way the Ni contributes to the specific heat but not to the conduction of heat in this temperature range. At temperatures from about 300 C to 600 C the thermal diffusivity shows a rapid increase with temperature, attributable to gap closure and increased contact between the glass and nickel. Such a large positive temperature dependence is rather uncommon in most materials over this temperature range. The mechanism involved, at least in principle, permits the temperature dependence of the thermal conductivity or diffusivity to be tailored for specific purposes, if desired.

For design purposes, a thermal conductivity of dielectric materials which is independent of temperature may be required. For instance, this is the case in linear heat flow which, for a constant thermal conductivity, yields a linear temperature gradient and zero thermal stress. This aim can be achieved by synthesizing composites in which the negative temperature dependence of one component

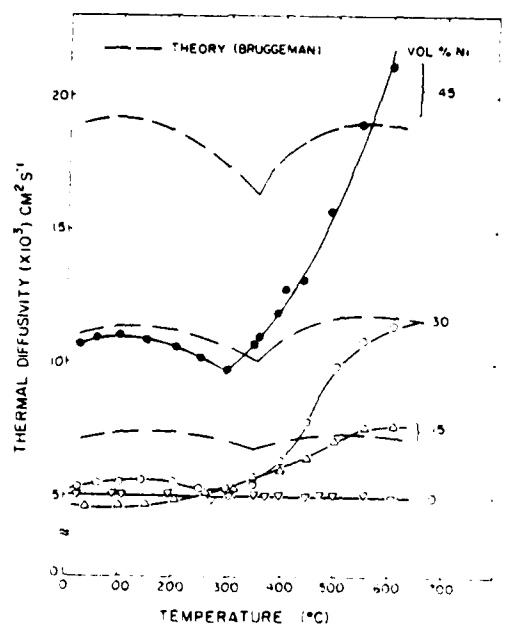

Fig. 13 Comparison of calculated and measured values of the thermal diffusivity of borosilicate glass with Ni inclusions (ref. 25).

is compensated by the positive temperature dependence of the other. A specific composite for which this aim was achieved consisted of a continuous sodium borosilicate glass matrix with a dispersed phase of crystalline aluminum oxide. Above room temperature the former material exhibits a thermal conductivity which increases with temperature, whereas for the aluminum oxide over the same temperature range, the thermal conductivity decreases rapidly with temperature.

Figures 14a and 14b show the experimental data for the thermal diffusivity and the calculated values for the thermal conductivity of this composite for a range of alumina contents as determined by Hasselman et.al.(26). At approximately 35 wt.% Al_2O_3 the thermal conductivity is virtually constant from room temperature to 600 C.

FINAL REMARKS

The data presented in this paper clearly indicate the important role of composition and microstructure in governing the heat transfer characteristics of brittle structural materials. In general, this will require that for each new

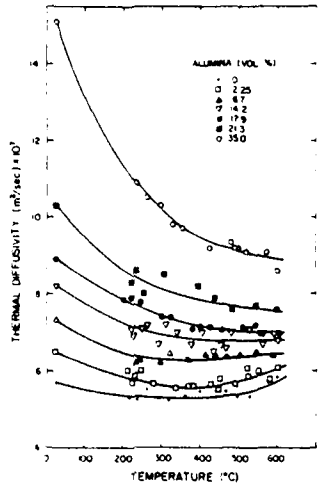

a.

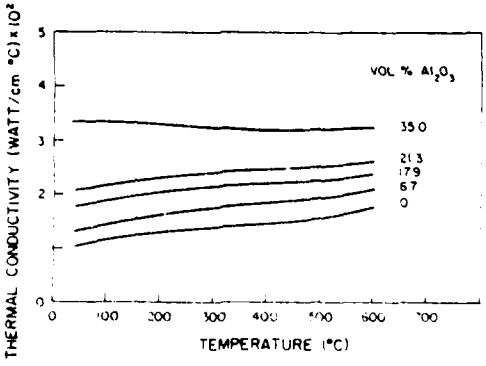

b.

Fig. 14 Heat conduction behavior of sodium borosilicate glass-alumina composites. a. Experimental values for the thermal diffusivity and b. data for the thermal conductivity calculated from the thermal diffusivity (ref. 26).

AD-A125 242 THERMO-MECHANICAL AND THERMAL BEHAVIOR OF HIGH-TEMPERATURE STRUCTURAL MAT..(U) VIRGINIA POLYTECHNIC INST AND STATE UNIV BLACKSBURG COLL OF E..

3/3

UNCLASSIFIED D P HASSELMAN ET AL. 31 DEC 82 F/G 11/2 NL

END

FILMED

DTIC

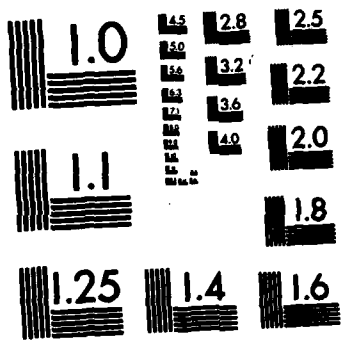

batch of materials the values for the thermal conductivity and diffusivity be measured, rather than relying on handbook values. On the other hand the high sensitivity of the thermal conductivity and diffusivity to a wide range of compositional and microstructural variables provides the materials technologist with a powerful tool to tailor these properties to meet specific design requirements.

ACKNOWLEDGEMENTS

This review was prepared as part of a research program on the thermal and thermomechanical behavior of structural materials for use at high temperature funded by the Office of Naval Research under contract N00014-78-C-0431.

REFERENCES

1. Berman, R., Thermal Conduction in Solids, Clarendon Press, Oxford, 1976.
2. Kingery, W. D., Bowen, H. K., and Uhlman, D. R., Introduction to Ceramics, 2nd ed., Wiley, New York, 1975, pp. 583-645.
3. Parker, W. J., Jenkins, R. J., Butler, C. P., and Abbott, G. L., "Flash Method of Determining Thermal Diffusivity, Heat Capacity, and Thermal Conductivity", Journal of Applied Physics, Vol. 32, No. 9, Sept. 1961, pp. 1679-1684.
4. Lange, F. F., "Relation Between Strength, Fracture Energy, and Microstructure of Hot-Pressed Si_3N_4," Journal of the American Ceramic Society, Vol. 56, No. 10, Oct. 1973, pp. 518-522.
5. Lange, F. F., "High Temperature Strength Behavior of Hot-Pressed Si_3N_4: Evidence for Subcritical Crack Growth," Journal of the American Ceramic Society, Vol. 57, No. 2, Feb. 1974, pp. 84-87.
6. Ziegler, G. and Hasselman, D.P.H., "Effect of Phase Composition and Microstructure on the Thermal Diffusivity of Silicon Nitride," Journal of Materials Science, Vol. 16, No. 2, Feb. 1981, pp. 495-503.
7. Ziegler, G., Bentsen, L. D., and Hasselman, D.P.H., "Orientation Effects on the Thermal Diffusivity of Hot-Pressed Silicon Nitride," Journal of the American Ceramic Society, Vol. 64, No. 2, Feb. 1981, pp. C-35-C-36.
8. Niihara, K., Bentsen, L. D., and Hasselman, D.P.H., "Anisotropy Effects in the Thermal Diffusivity of Si_3N_4-BN Composites," Journal of the American Ceramic Society, Vol. 64, No. 9, Sept. 1981, pp. C-117-C-118.
9. Lange, F. F., Siebeneck, J. H., and Hasselman, D.P.H., "Thermal Diffusivity of Four Si-Al-O-N Compositions," Journal of the American Ceramic Society, Vol. 59, No. 9-10, Sept-Oct. 1976, pp. 454-455.
10. Srinivasan, M., Bentsen, L. D., and Hasselman, D.P.H., "Thermal Diffusivity of Silicon Carbide-Silicon Composites," Proceedings of the 17th International Thermal Conductivity Conference, Plenum Press (in press).
11. Touloukian, Y. S., Powell, R. W., Ho. C. Y., and Nicolaou, M. C., Thermal Diffusivity, Vol. 10 of Thermophysical Properties of Matter, IFI/Plenum, New York, 1973, pp. 160-163.
12. Bruggeman, D.A.G., "Berechnung Verschiedener Physikalischer Konstanten von Heterogenen Substanzen, I. Dielektrizitatskonstanten und Leitfahigkeiten der Mischkorper aus Isotropen Substanzen," Annalen der Physik, Band 24, 5 Folge, Nov. 1935, pp. 636-664.
13. Brennan, J. J., Bentsen, L. D., and Hasselman, D.P.H., "Measurement of the Thermal Conductivity and Diffusivity of SiC Fibers by the Composite Method," Journal of Materials Science (in press).
14. Budiansky, B. and O'Connell, R. J., "Elastic Moduli of a Cracked Solid," International Journal of Solids and Structures, Vol. 12, No. 2, Feb. 1976, pp. 81-97.
15. Kuszyk, J. A. and Bradt, R. C., "Influence of Grain Size on Effects of Thermal Expansion Anisotropy in $MgTi_2O_5$," Journal of the American Ceramic Society, Vol. 56, No. 8, Aug. 1973, pp. 420-423.
16. Bush, E. A. and Hummel, F. A., "High-Temperature Mechanical Properties of Ceramic Materials: I," Journal of the American Ceramic Society, Vol. 41, No. 6, June 1958, pp. 189-195.
17. Bush, E. A. and Hummel, F. A., "High-Temperature Mechanical Properties of Ceramic Materials: II," Journal of the American Ceramic Society Vol. 42, No. 8, Aug. 1959, pp. 388-391.

18. Rossi, R. C., "Thermal-Shock-Resistant Ceramic Composites," American Ceramic Society Bulletin, Vol. 48, No. 7, July 1969, pp. 736-737.

19. Hasselman, D.P.H., "Unified Theory of Thermal Shock Fracture Initiation and Crack Propagation in Brittle Ceramics," Journal of the American Ceramic Society, Vol. 52, No. 11, Nov. 1969, pp. 600-604.

20. Hasselman, D.P.H. and Singh, J.P., "Analysis of Thermal Stress Resistance of Microcracked Brittle Ceramics," American Ceramic Society Bulletin, Vol. 58, No. 9, Sept. 1979, pp. 856-860.

21. Hasselman, D.P.H., "Effect of Cracks on Thermal Conductivity," Journal of Composite Materials, Vol. 12, Oct. 1978, pp. 403-407.

22. Siebeneck, H. J., Hasselman, D.P.H., Cleveland, J. J., and Bradt, R. C., "Effect of Microcracking on the Thermal Diffusivity of Fe_2TiO_5," Journal of the American Ceramic Society, Vol. 59, No. 5-6, May-June 1976, pp. 241-244.

23. Siebeneck, H. J., Cleveland, J. J., Hasselman, D.P.H., and Bradt, R. C., "Effect of Grain Size and Microcracking on the Thermal Diffusivity of $MgTi_2O_5$," Journal of the American Ceramic Society, Vol. 60, No. 7-8, July-Aug. 1977, pp. 336-338.

24. Bentsen, L. D., Hasselman, D.P.H., and Claussen, N., "Effect of Microcracking on the Conduction of Heat in Brittle Composites," Proceedings of the Conference on Environmental Degradation of Engineering Materials, VPI Press, 1981, pp. 369-382.

25. Powell, B. R., Jr., Youngblood, G. E., Hasselman, D.P.H., and Bentsen, L. D., "Effect of Thermal Expansion Mismatch on the Thermal Diffusivity of Glass-Ni Composites," American Ceramic Society Bulletin, Vol. 63, No. 9-10, Sept.-Oct. 1980, pp. 581-586.

26. Hasselman, D.P.H., Zdaniewski, W. A., Swearengen, J. C., and Beauchamp, E. K., "Effect of Alumina Dispersions on the Thermal Conductivity/Diffusivity and Thermal Stress Resistance of a Borosilicate Glass," Journal of Materials Science, Vol. 15, No. 2, Feb. 1980, pp. 518-520.

December 1981

BASIC DISTRIBUTION LIST

Technical and Summary Reports

Organization	No. of Copies
Defense Documentation Center Cameron Station Alexandria, Virginia 22314	(12)
Office of Naval Research Department of the Navy	
Attn: Code 471	(1)
Code 102	(1)
Code 470	(1)
Commanding Officer Office of Naval Research Branch Office 495 Summer Street Boston, Massachusetts 02210	(1)
Commanding Officer Office of Naval Research Branch Office 536 South Clark Street Chicago, Illinois 60605	(1)
Office of Naval Research San Francisco Area Office One Hallidie Plaza, Suite 601 San Francisco, California 94102	(1)
Naval Research Laboratory Washington, D.C. 20390	
Attn: Code 6000	(1)
Code 6100	(1)
Code 6300	(1)
Code 6400	(1)
Code 2627	(1)
Naval Air Development Center Code 302 Warminster, Pennsylvania 18974 Attn: Mr. F. S. Williams	(1)
Naval Air Propulsion Test Center Trenton, New Jersey 08628 Attn: Library	(1)
Naval Construction Batallion Civil Engineering Laboratory Port Hueneme, California 93043 Attn: Materials Division	(1)
Naval Electronics Laboratory Center San Diego, California 92152 Attn: Electron Materials Science Division	(1)
Naval Missile Center Materials Consultant Code 3312-1 Point Mugu, California 93041	(1)
Commanding Officer Naval Surface Weapons Center White Oak Laboratory Silver Spring, Maryland 20910 Attn: Library	(1)
David W. Taylor Naval Ship R&D Center Materials Department Annapolis, Maryland 21402	(1)
Naval Undersea Center San Diego, California 92132 Attn: Library	(1)
Naval Underwater System Center Newport, Rhode Island 02840 Attn: Library	(1)
Naval Weapons Center China Lake, California 93555 Attn: Library	(1)
Naval Postgraduate School Monterey, California 93940 Attn: Mechanical Engineering Dept.	(1)
Naval Air Systems Command Washington, D.C. 20360	
Attn: Code 52031	(1)
Code 52032	(1)

BASIC DISTRIBUTION LIST (Cont'd)

Organization	No. of Copies
Naval Sea System Command Washington, D. C. 20362 Attn: Code 035	(1)
Naval Facilities Engineering Command Alexandria, Virginia 22331	(1)
Scientific Advisor Commandant of the Marine Corps Washington, D.C. 20380 Attn: Code AX	(1)
Naval Ship Engineering Center Department of the Navy Washington, D.C. 20360 Attn: Code 6101	(1)
Army Research Office P.O. Box 12211 Triangle Park, N.C. 27709 Attn: Metallurgy & Ceramics Program	(1)
Army Materials and Mechanics Research Center Watertown, Massachusetts 02172 Attn: Research Programs Office	(1)
Air Force Office of Scientific Research Bldg. 410 Bolling Air Force Base Washington, D.C. 20332 Attn: Chemical Science Directorate	(1)
Electronics and Solid State Science Directorate	(1)
Air Force Materials Lab (LA) Wright-Patterson AFB Dayton, Ohio 45433	(1)
Library, Bldg 50, Rm 134 Lawrence Radiation Laboratory Berkeley, CA 94720	(1)

Organization	No. of Copies
NASA Headquarters Washington, D. C. 20546 Attn: Code RRM	(1)
NASA Lewis Research Center 21000 Brookpark Road Cleveland, Ohio 44135 Attn: Library	(1)
National Bureau of Standards Washington, D.C. 20234 Attn: Metallurgy Division	(1)
Inorganic Materials Division	(1)
Defense Metals and Ceramics Information Center Battelle Memorial Institute 505 King Avenue Columbus, Ohio 43201	(1)
Office of Naval Research, Branch Office 1030 East Green Street Pasadena, CA. 91106	(1)
Metals and Ceramics Division Oak Ridge National Laboratory P.O. Box X Oak Ridge, Tennessee 37380	(1)
Los Alamos Scientific Laboratory P.O. Box 1663 Los Alamos, New Mexico 87544 Attn. Report Librarian	(1)
Argonne National Laboratory Metallurgy Division P.O. Box 229 Lemont, Illinois 60439	(1)
Brookhaven National Laboratory Technical Information Division Upton, Long Island New York 11973 Attn: Research Library	(1)

BASIC DISTRIBUTION LIST (Cont'd)

Organization	No. of Copies
Director Applied Physics Laboratory University of Washington 1013 Northeast Fortieth Street Seattle, Washington 98105	(1)

SUPPLEMENTARY DISTRIBUTION LIST

Advanced Research Project Agency
Materials Science Director
1400 Wilson Boulevard
Arlington, VA 22209

Mr. George Boyer
Sensor Systems Program
Office of Naval Research
Code 222
Arlington, VA 22217

Professor R. Bradt
Ceramics Section
Materials Sciences Department
The Pennsylvania State University
University Park, PA 16802

Professor L. E. Cross
The Pennsylvania State University
Materials Research Laboratory
University Park, PA 16802

Dr. A. G. Evans
Department Materials Science
and Engineering
Hearst Mining Building
University of California
Berkeley, CA 94720

Dr. Gene Haertling
Motorola Corporation
3434 Vassar, NE
Albuquerque, NM 87107

Dr. L. L. Hench
Department of Metallurgy
University of Florida
Gainesville, FL 32603

Dr. A. A. Heuer
Professor of Ceramics
Case Western Reserve University
University Circle
Cleveland, OH 44106

Dr. Paul Jorgensen
Stanford Research Institute
333 Ravenswood Avenue
Menlo Park, CA 94025

Dr. R. N. Katz
Army Materials and Mechanics
Research Center
Watertown, MA 02172

Dr. H. Kirchner
Ceramic Finishing Company
P.O. Box 498
State College, PA 16801

Dr. B. G. Koepke
Honeywell, Inc.
Corporate Research Center
10701 Lyndale Avenue South
Bloomington, MN 55420

Mr. Frank Koubek
Naval Surface Weapons Center
White Oak Laboratory
Silver Spring, MD 20910

Dr. J. Lankford
Southwest Research Institute
8500 Culebra Road
San Antonio, TX 78284

Professor P. B. Macedo
The Catholic University of America
Washington, DC 20017

Dr. N. Perrone
Code 474
Office of Naval Research
800 N. Quincy Street
Arlington, VA 22217

Dr. R. Rice
Naval Research Laboratory
Code 6360
Washington, DC 20375

SUPPLEMENTARY DISTRIBUTION LIST (Cont'd)

Mr. R. T. Swann
Md-Materials Research Branch
Mail Stop 396
NASA Langley Research Center
Hampton, VA 23665

Dr. K. H. Holko, Manager
Materials Applications
General Atomic Company
P. O. Box 81608
San Diego, CA 92138

Dr. W. Bakker
EPRI
3412 Hillview Avenue
P. O. Box 10412
Palo Alto, CA 94303

Dr. P. A. Miles, Research
Raytheon Company
28 Seyon Str.
Waltham, MA 02154

Dr. J. Ritter
University of Massachusetts
Dept. of Mech. Engr.
Amherst, MA 01002

Professor T. J. Rocket
University of Rhode Island
Kingston, RI 02881

Dr. G. E. Youngblood
MERDI
Butte, MT 59701

Dr. E. G. Kobetich
Experimental Station, Bldg. 302
E. I. DuPont Company
Wilmington, DE 19898

Dr. M. A. Adams
Jet Propulsion Laboratory
California Institute of Technology
4800 Oak Grove Drive
Pasadena, CA 91103

Dr. Clifford Astill
Solid Mechanics Program
National Science Foundation
Washington, DC 20550

Dr. R. J. Gottschall
U. S. Dept. of Energy
Div. of Materials Science
Mail Stop J309
Washington, DC 20545

Prof. R. Roy
Pennsylvania State Univ.
Materials Research Lab.
University Park, PA 16802

Dr. M. P. Borom
Research and Development
General Electric Company
Box 8
Schenectady, NY 12301

Hague International
3 Adams Street
South Portland, ME 04106

Mr. J. D. Walton
Engineering Exp. Station
Georgia Inst. of Technology
Atlanta, GA 30332

Dr. W. F. Adler
Effects Technology, Inc.
5383 Hollister Avenue
P. O. Box 30400
Santa Barbara, CA 92105

Dr. L. R. Hettche
Metallurgy Division
Naval Research Laboratory
Washington, D. C. 20375

Mr. W. B. Harrison
Honeywell Ceramics Center
1885 Douglas Drive
Golden Valley, MN 55422

SUPPLEMENTARY DISTRIBUTION LIST (Cont'd)

Dr. J. Rosolowski
General Electric Company
Research and Development Center
P. O. Box 8
Schenectady, NY 02301

Dr. J. H. Simmons
Catholic University of America
Washington, DC 20064

Dr. P. L. Smith
Naval Research Laboratory
Code 6361
Washington, DC 20375

Dr. R. W. Timme
Naval Research Laboratory
Code 8275
Underwater Sound Reference Division
P. O. Box 8337
Orlando, FL 32806

Dr. Charles C. Walker
Naval Sea Systems Command
National Center #3
2531 Jefferson Davis Highway
Arlington, VA 20390

Dr. Paul D. Wilcox
Sandia Laboratories
Division 2521
Albuquerque, NM 87115

Dr. Murray Gillen
Australian Embassy
Washington, DC 33801

Mr. J. D. Sibold
Coor Porcelain Company
17750 W. 32nd Avenue
Golden, CO 80401

Dr. S. M. Wiederhorn
Physical Properties Section
Bldg. 223, Rm. A355
National Bureau of Standards
Washington, DC 20234

Dr. P. F. Becher
Metals and Ceramics Division
Oak Ridge National Laboratories
Box X, Oak Ridge, TN 37830

Dr. R. Jaffee
Electric Power Research Institute
3412 Hillview Avenue
P. O. Box 10412
Palo Alto, CA 94303

Dr. B. A. Wilcox
Metallurgy and Materials Division
National Science Foundation
Washington, DC 20550

Dr. H. E. Bennett
Naval Surface Weapons Center
Research Department Code 601
China Lake, CA 93555

Dr. R. J. Charles
General Electric Company
Research and Development Center
Schenectady, NY 12301

Dr. A. R. C. Westwood
Martin-Marietta Laboratories
1450 South Rolling Road
Baltimore, MD 21227

Dr. N. S. Corney
Ministry of Defense
(Procurement Executive)
The Adelphi
John Adam Street
London WC2N 6BB
UNITED KINGDOM

Dr. D. E. Niesz
Battelle Memorial Institute
505 King Avenue
Columbus, OH 43201

Dr. R. E. Engdahl
Deposits and Composites, Inc.
318 Victory Drive
Herndon, VA 22070

Professor W. D. Kingery
Ceramics Div. Rm. 13-4090
MIT
77 Mass. Avenue
Cambridge, MA 02139

SUPPLEMENTARY DISTRIBUTION LIST (Cont'd)

Dr. J. J. Petrovic
Los Alamos National Lab
MST-5
Los Alamos, NM 87545

Dr. W. H. Rhodes
GTE Laboratories Inc.
40 Sylvan Rd.
Waltham, MA 02154

Dr. D. C. Larson
IIT Research Inst.
10 W. 35th Street
Chicago, IL 60616

Dr. B. Butler, Chief
Materials Branch
Solar Energy Research Institute
1536 Cole Blvd.
Golden, CO 80501

Dr. S. Greenberg
Materials Science Division
Argonne National Laboratory
Argonne, IL 60439

Dr. F. E. Kennedy
Thayer School of Engineering
Dartmouth School of Engineering
Hanover, NH 03755

Dr. R. J. Bratton
R&D Center
Westinghouse Electric Corp.
Pittsburgh, PA 15235

Mr. B. North
Kennametal Inc.
1011 Old Salem Rd.
P. O. Box 639
Greensburg, VA 15601

Dr. D. J. Godfrey
Admiralty Materials Laboratory
Ministry of Defense
(Procurement Executive)
Holton Heath
Poole, Dorset
BH 16 6 JU
UNITED KINGDOM

Dr. Wm. Kessler
AFML
Wright-Patterson Air Force Base
OH 45433

Dr. S. F. Galasso
United Aircraft Research Laboratories
East Hartford, CN 06108

Dr. M. Srinivasan
The Carborundum Comp.
P. O. Box 1054
Niagara Falls, NY 14302

Dr. W. D. Tuohig
Bendix Research Laboratories
Southfield, MI 48076

Dr. Robert Ruh
AFML/LLM
Wright-Patterson AFB
OH 45433

Mr. J. Schuldies
Airesearch Manufacturing Company
P. O. Box 5217
Phoenix, AZ 85010

Dr. S. Musikant
General Electric Company
3198 Chestnut Street
Philadelphia, PA 19101

Dr. D. W. Richerson Comp. Code 503-44
Garrett Corp.
111 S. 34th Str., Box 5217
Phoenix, AZ 85034

Dr. R. Baumgartner
PPG Industries
P. O. Box 31
Barberton OH 44203

Globe-Union, Inc.
5757 North Green Bay Avenue
Milwaukee, WI 53201
Attn: G. Goodman

SUPPLEMENTARY DISTRIBUTION LIST (Cont'd)

Mr. J. F. McDowell
Sullivan Park
Corning Glass Works
Corning, NY 14830

Dr. E. K. Beauchamp, Div. 5846
Sandia Laboratories
Albuquerque, NM 87185

Dr. J. A. Rubin
Kyocera International, Inc.
8611 Balboa Avenue
San Diego, CA 92123

Dr. W. V. Kotlensky
Materials Technology Department
TRW, Inc.
One Space Park
Redondo Beach, CA 90278

Dr. N. N. Ault
NORTON Comp.
One New Bond Street
Worcester, MA 01606

Dr. Hayne Palmour III
Engineering Research Division
N. C. State University
P. O. Box 5995
Raleigh, NC 27650

Dr. D. Ulrich
AFOSR, Code NC
Chemical Sciences Div.
1400 Wilson Blvd.
Arlington, VA 22209

Dr. V. J. Tennery
Oak Ridge Nat. Lab.
Oak Ridge, TN 38730

Dr. D. R. Petrak
Lynchburg Research Center
Babcock and Wilcox Co.
Box 1260
Lynchburg, VA 24505

Dr. S. C. Dixon
SDD-Thermal Structure Branch
Mail Stop 395
NASA Langley Research Center
Hampton, VA 23665

Dr. F. W. Clinard, Jr.
Los Alamos Scientific Lab.
MS 546
P. O. Box 1663
Los Alamos, NM 87544

Dr. D. DeCoursin
Fluidyne Eng.
5900 Olson Memorial Hwy.
Minneapolis, MN 55422

Dr. F. F. Lange
Rockwell International
P. O. Box 1085
1049 Camino Dos Rios
Thousand Oaks, CA 91360

Dr. T. Vasilos
AVCO Corporation
Research and Advanced Development
Division
201 Lowell Str.
Wilmington, MA 01887

Dr. R. E. Rondeau
AFML-LDJ
Wright-Patterson AFB
OH 45433

Dr. S. Dutta
NASA-Lewis Research Center
Mail Stop 49-3
21000 Brookpark Rd.
Cleveland, OH 44135

Mr. B. Probst
NASA-Lewis Research Center
21000 Brookpark Rd.
Cleveland, OH 44135

Dr. S. W. Freiman
Deformation and Fracture Group
Physical Properties Section, Bldg. 223
National Bureau of Standards
Washington, DC 20234

Mr. W. Trombley
Garrett Corporation
1625 I Str. NW
Suite 515
Washington, D.C. 20006

SUPPLEMENTARY DISTRIBUTION LIST (Cont'd)

Dr. P. Heitman
Detroit-Diesel Allison
Mail Stop W5
P. O. Box 894
Indianapolis, IN 46206

Mr. Charles P. Blankenship
Chief, Materials Division
Mail Stop 188M
NASA-Langley Research Center
Hampton, VA 23665

Dr. R. J. Palicka
CERADYNE, Inc.
3030 South Red Hill Avenue
Santa Ana, CA 92705

Dr. W. R. Prindle
Research and Development
Corning Glass Works
Corning, NY 14830

Dr. K. H. Styhr
AiResearch Casting Co.
2525 W. 190th St.
Torrance, CA 90509

Dr. Donald M. Curry, ES32
Thermal Technology Br.
National Aeronautics and
Space Administration
Lyndon B. Johnson Space Center
Houston, TX 77058

Dr. F. L. Kennard III
A. C. Spark Plug Division
General Motors Corp.
1300 N. Dort Hwy.
Flint, MI 48556

Dr. M. E. Gulden
INESCO
11077 N. Torrey Pines Rd.
La Jolla, CA 92037

Dr. J. J. Brennan
United Technologies Research Center
East Hartford, CT 06108

Dr. C. O. Hulse
United Technollgies Research Center
East Hartford, CT 06108

Dr. S. Rangaswamy
METCO, Inc.
1101 Prospect Avenue
Westbury, NY 11590

Dr. E. M. Anderson
Research and Engineering
Exxon Corporation
P. O. Box 101
Florham Park, NJ 07923

Dr. Fred Schmidt
E. I. DuPont
Engineering Dept. E-304
Experimental Station
Wilmington, DE 19898